THE COUPLING BETWEEN FOLDING, ZINC BINDING, AND DISULFIDE BOND STATUS OF HUMAN CU, ZN SUPEROXIDE DISMUTASE

A Dissertation Presented

By

CAN KAYATEKIN

Submitted to the Faculty of the

University of Massachusetts Graduate School of Biomedical Sciences, Worcester

in partial fulfillment of the requirements for the degree of

DOCTOR OF PHILOSOPHY

June 15, 2010

Biochemistry and Molecular Pharmacology

THE COUPLING BETWEEN FOLDING, ZINC BINDING, AND DISULFIDE-BOND STATUS OF HUMAN CU, ZN SUPEROXIDE DISMUTASE

A Dissertation Presented

By

CAN KAYATEKIN

The signatures of the Dissertation Defense Committee signifies completion and approval as to style and content of the Dissertation

C. Robert Matthews, Ph.D.

Lawrence Hayward, Ph.D.

Dan Bolon, Ph.D.

Gregory Petsko, Ph.D.

The signature of the Chair of the Committee signifies that the written dissertation meets the requirements of the Dissertation Committee.

Kendall Knight, Ph.D.

The signature of the Dean of the Graduate School of Biomedical Sciences signifies that the student has met all graduation requirements of the school.

Anthony Carruthers, Ph.D.

Program in Biochemistry and Molecular Pharmacology

June 15, 2010

Acknowledgements

Above all I would like to acknowledge the incredible guidance and support of my mentor, Bob Matthews. His enthusiasm for research and his qualities as a mentor have been instrumental in my development as a scientist. I can't imagine a better environment to earn a PhD. Thank you Bob for encouraging me when I had difficult times and keeping me going when things were on a roll.

A big thank you to my entire family, especially my parents. Our lives haven't been the most straightforward, and despite their declarations to the contrary, I'm sure it was harder on them than my brother and I. Thank you for being there for us, providing guidance, and always pushing us to exceed expectations. I would also like to thank my friends, who have made the last six years socially, as well as intellectually, so interesting. It would have been an exhausting journey without them.

Many people have been instrumental in the science reported in this thesis. Osman Bilsel first introduced me to the world of protein folding when I was a naïve undergrad, and Jill Zitzewitz has been an incredible SOD1 teammate. Special thanks to the UMass Mass Spectroscopy core, specifically Jim Evans, Barbara Evans, and Karin Green, who have been instrumental in the acquisition and analysis of the MS data. Thank you to Elena Kondrashkina and Liang Guo, who were collaborators for all of the x-ray scattering work performed at the Advanced Photon Source.

Finally, I would like to thank the members of the Matthews lab both past and present for their support in the lab and their friendship. Rarely does such a professional, friendly, kind and helpful group of people come together. Graduate school was some of the best years in my life and I am very happy to have shared it with such fine people.

Copyright Notice

Portions of this dissertation are represented in the following publications.

Kayatekin C, Zitzewitz JA, Matthews CR. 2010. “Disulfide-Reduced ALS Variants of Cu, Zn Superoxide Dismutase Exhibit Increased Populations of Unfolded Species” *J. Mol. Biol.* 398(2): 320-31.

Kayatekin C, Zitzewitz JA, Matthews CR. 2008. “Zinc binding modulates the entire folding free energy surface of human Cu,Zn superoxide dismutase.” *J. Mol. Biol*. 384(2):540-55.

The following figures were modified or added:

Figure 2.6

The materials and methods were expanded.

Abbreviations

ACO: Absolute contact order

ALS: Amyotrophic lateral sclerosis

AS-SOD1: C6A/C111S SOD1

CCS: Copper chaperone of SOD1

CD: Circular Dichroism

DHFR: Dihydrofolate reductase from *E. coli*

EDANS: 5 - [(2 - aminoethyl)amino]naphthalene - 1 - sulfonic acid

EDTA: ethylenediaminetetraacetic acid

ESI-MS: Electrospray ionization mass spectrometry

FRET: Förster resonance energy transfer

Gdn-HCl: Guanidine hydrochloride

HEPES: 4-(2-hydroxyethyl)-1-piperazineethanesulfonic acid

HPLC: High pressure liquid chromatography

HX: Hydrogen exchange

MALDI-TOF MS: Matrix assisted laser desorption ionization, time-of-flight mass spectrometry

mAS-SOD1: C6A/F50E/G51E/C111S SOD1

NATA: N-acetyl tryptophanamide

NMR: Nuclear magnetic resonance

SAXS: Small angle x-ray scattering

SOD1: Human Cu, Zn superoxide dismutase

TCEP: tris(2-carboxyethyl)phospine

TFA: Trifluoroacetic acid

TSE: Transition state ensemble

WT: Wild type

Abstract

Cu, Zn superoxide dismutase (SOD1) is a dimeric, β-sandwich, metalloenzyme responsible for the dismutation of superoxide. Mutations covering nearly 50% of the amino acid sequence of SOD1 have been found to acquire a toxic gain-of-function leading to amyotrophic lateral sclerosis. A hallmark of this disease is the presence of insoluble aggregates containing SOD1 found in the brain and spinal cord. While it is unclear how these aggregates or smaller, precursor oligomeric species may be the source of the toxicity, mutations leading to increased populations of unstable, partially folded species along the folding pathway of SOD1 may be responsible for seeding and propagating aggregation.

In an effort to determine the responsible species, we have systematically characterized the stability and folding kinetics of five well studied ALS variants: A4V, L38V, G93A, L106V and S134N. The effect of the amino acid substitutions was determined on a variety of different constructs characterizing the various post-translational maturation steps of SOD1: folding, disulfide bond formation and Zn binding. Zn was found to bind progressively tighter along the folding pathway of SOD1, minimizing populations of monomeric species. In contrast, ALS variants were found to have the greatest perturbation in the equilibrium populations of the folded and unfolded state for the most

immature, disulfide-reduced metal-free SOD1. In this species, at physiological temperature, four out of five ALS variants were >50% unfolded.

Finally the energetic barriers in the folding and unfolding reaction were studied to investigate the unusually slow folding of SOD1. These results reveal that both unfolding and refolding are dominated by enthalpic barriers which may be explained by the desolvation of the chain and provide insights into the role of sequence in governing the folding pathway and rate.

Table of Contents

List of Figures

List of Tables

Chapter I. Cu, Zn Superoxide Dismutase Mediated Amyotrophic Lateral Sclerosis

Introduction

The ability for proteins to fold correctly in the cell is a critical component of human health. Mutations in genes and/or environmental stresses can lead to defects in the sequence of proteins or the cellular environment leading to the expression of misfolded proteins. Non-native interactions between these misfolded proteins are thought to be the underlying cause of protein aggregation diseases including, Alzheimer's disease, Parkinson's disease, Huntington's disease and amyotrophic lateral sclerosis.[1; 2] While the natural proteostatis machinery exists in the cell to deal with such lesions, the loss of efficacy of these mechanisms with age is consistent with the late-onset of these diseases.[3; 4]

With a lifetime risk of 1 in 2000, amyotrophic lateral sclerosis (ALS) is the most common motor neuron disease and the fourth most common neurodegenerative disease behind Alzheimer's, Pick's and Parkinson's disease.[5;6] ALS, more commonly known as Lou Gehrig's disease in North America, is characterized by the death of motor neurons in the brain and spinal cord, leaving the patient paralyzed and eventually leading to death by asphyxiation. It is a late-onset disease, with patients exhibiting initial symptoms at 45-55 years of age. Regardless of the age of onset, most cases of ALS progress very rapidly. Typical survival time of patients after diagnosis is 3-4 years.[7] This rapid progression was classically displayed by Lou Gehrig himself, who was a star baseball player for the

Yankees in 1937. His skill began to rapidly deteriorate due to ALS in 1938, forcing him to retire the next year and ultimately leading to his death in 1941.

Mutations in the Cu, Zn Superoxide Dismutase Cause ALS

A hallmark of ALS, as well as other protein misfolding diseases, is the incidence of visible, protein based, inclusions found in tissue sections extracted from the brain and spinal cord of patients.[8] Approximately 90% of ALS cases have no apparent pattern of genetic inheritance and are termed sporadic ALS (sALS). In the remaining ~10% of cases, a variety of heritable factors have been determined (Table 1.1)[9; 10; 11; 12; 13; 14; 15; 16] and are collectively termed familial ALS cases (fALS). The most prevalent of these fALS cases are caused by mutations in the gene encoding for the Cu, Zn superoxide dismutase (SOD1), which were discovered by the Brown lab in 1993,[14] and account for ~20% of all cases of fALS. Mutant SOD1 mediated neurodegeneration may even be a universal phenomenon as presence of mutant SOD1 in mice, the G86R variant,[17; 18] and dogs, the E40K variant,[19] has also been linked with ALS-like symptoms in these animals.

The SOD1 gene is located on chromosome 21 and consists of 5 exons which are spliced to produce a single species of SOD1 protein. To date, there are no known natural alternative splicing isoforms of SOD1. The mRNA encodes for a 154 amino acid protein,

Table 1.1. List of confirmed fALS genes

Gene	Protein	Inheritance	Clinical Features	Protein Function
SOD1	Superoxide dismutase I	AD	Typical ALS	Superoxide dismutase
ALS2	Alsin	AR	Juvenile onset, slowly progressive, predominantly corticospinal	Guanine exchange factor for Rab5a
SETX	Senataxin	AD	Adult onset, slowly progressive, early vocal cord paralysis	DNA/RNA helicase
VAPB	VAMP-associated protein B	AD	Typical ALS	Vesicle transport regulation
Dynactin	Dynactin	AD	Adult onset, slowly progressive, early vocal cord paralysis	Component of retrograde axonal transport motor dynein
TDP-43	Tar DNA Binding Protein 43	AD	Typical ALS	Transcription and splicing
FUS/TLS	Fused in sarcoma/Translated in liposarcoma	AD	Typical ALS	DNA/RNA metabolism

which is post-translationally modified by the cleavage of the N-terminal methionine residue, follow by N-terminal acetylation. Across species, the sequence of SOD1 is highly conserved, with 112 of 153 residues conserved in mammals and 70 residues which are invariant across eukaryotes.[20]

The function of SOD1 was first identified by McCord and Fridovich in 1969.[21] Its catalytic activity is to facilitate the disproportionation reaction of superoxide (O_2^-) into molecular oxygen and hydrogen peroxide, which is then further converted by catalase into water and oxygen. Superoxide is generated primarily in the mitochondria as a byproduct of aerobic respiration. This highly reactive radical species can react with and damage many cellular structures, proteins, and nucleic acids. The enzyme functions through the cyclical oxidation and reduction of the copper cation.

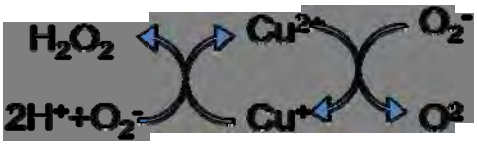

To date, over 140 mutations have been identified in SOD1 from patients with fALS. A comprehensive list of mutations can be found at http://alsod.iop.kcl.ac.uk/Als/Index.aspx. The known missense mutations are listed in Figure 1.1, and a subset of these is the primary focus of this thesis. The overwhelming majority of SOD1 mutations are autosomal dominant, with 61 of these mutations occurring at partially conserved residues,

Figure 1.1. The sequence, secondary structure and missense mutations in SOD1.

The sequence, secondary structure and missense mutations found in SOD1. The β-strands that form each of the two sheets are separated by color. The five exons which encode for the sequence of SOD1 are separated by color.

Figure 1.1. The sequence, secondary structure and missense mutations in SOD1.

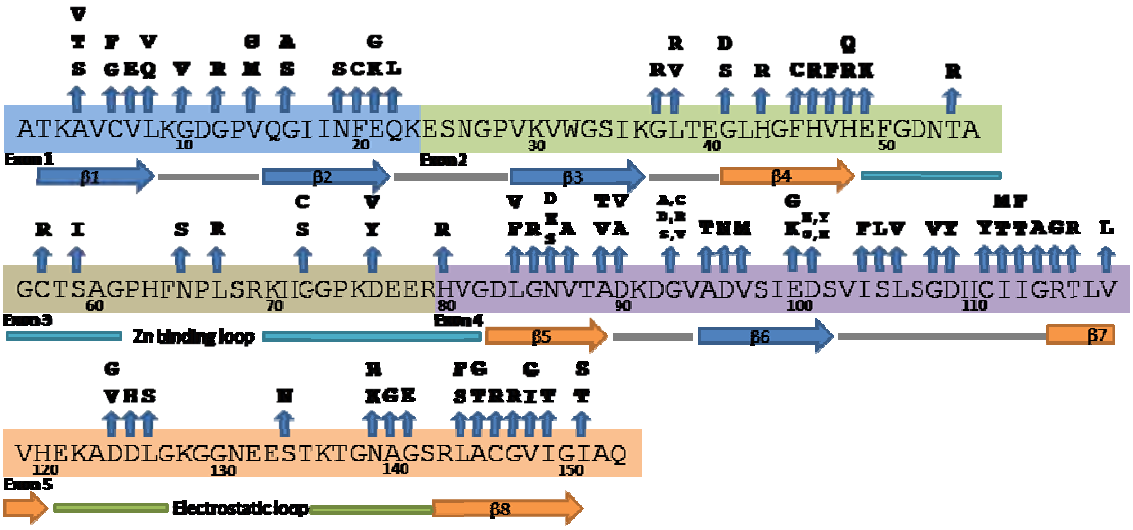

and 49 occurring at highly conserved residues in mammals.[22] The high sequence conservation combined with the dispersal of mutations throughout the sequence (Figure 1.1) suggests that SOD1 is not a protein which is particularly tolerant of mutations. Interestingly, even though all aerobically respiring organisms have some version of a superoxide dismutase, SOD1 is not an essential gene in humans or mice.[23] Humans and mice have a complementary manganese superoxide dismutase, SOD2, which is localized directly in the innermembrane space of mitochondria where much of the superoxide anion is produced. It is likely SOD2 actually performs much of the dismutation activity necessary for cellular survival. This idea is supported by the observation that SOD2 knockout mice suffer early postnatal death,[24] whereas SOD1 knockout mice display subtle motor neuron dysfunction,[25] and impaired fertility,[26] but no symptoms of ALS.

The Structural Features of SOD1

SOD1 is a diffusion-limited enzyme, and several structural characteristics of the protein, such as the sterically limited active site channel, the high stability, or the absence of easily oxidizable methionine residues, would indicate that evolution has selected for features that can withstand dealing with highly reactive species such as superoxide or copper. SOD1 is present at high concentrations in the cell, ranging from 10 – 100 μM in different tissues.[27; 28] However, the inability to isolate only motor neurons from brain and spinal cord samples, without contamination from glia, makes an accurate estimate of

SOD1 concentration in motor neurons difficult. SOD1 is primarily located in the cytosol, but is also found in the intermembrane space of mitochondria,[29; 30] the nucleus and in peroxisomes.[31] It is also one of the most stable proteins in the human proteome. The fully-metalated protein has a melting point over 90 °C and is enzymatically active in 8 M urea.[32; 33; 34]

SOD1 is functional as a 32 kDa homodimer, with one copper and one zinc binding site in each 153 amino acid monomer (Figure 1.2). Each monomer binds a catalytic copper and a structural zinc ion and contains eight anti-parallel β-strands, supporting two large, structurally important loops. Each chain also contains an intramolecular disulfide bond between C57 and C146. The fold of SOD1 is similar to the immunoglobulin-like family of proteins, characterized by two anti-parallel β-sheets and a Greek key motif. Each β-sheet is formed by four anti-parallel β-strands. The first sheet is mostly local in sequence, consisting of β1-3 and β6 which is part of the Greek key motif (Figure 1.3). The more C-terminal β-sheet contains the disulfide bond as well as the two long loops, the Zn-binding loop between β4 and β5, and the electrostatic loop between β7 and β8. These loops are critical in binding the Zn cation and facilitating the electrostatic guidance of the superoxide anion to the active site, respectively. In the absence of metals, especially Zn, these loops appear largely disordered by NMR and x-ray crystallography.[35; 36]

Figure 1.2. Crystal structure of SOD1.

SOD1 is a 153 amino acid, β-sandwich protein with eight anti-parallel β-strands organized in two sheets, and supported by two large catalytic loops (PDB: 2C9V). These are the Zn binding loop, loop IV shown in cyan, and the electrostatic loop, loop VII shown in green. The Cu ion is responsible for catalyzing the disproportionation reaction of the superoxide anion, while the Zn serves a structural role. These metals are depicted as orange and blue spheres respectively. Primarily a cytosolic enzyme, SOD1 nevertheless has an intramolecular disulfide bond between C57-C146, shown here in yellow. For the studies in this thesis, the free cysteines C6 and C111, shown in red, have been mutated to alanine and serine respectively.

Figure 1.2. Crystal structure of SOD1.

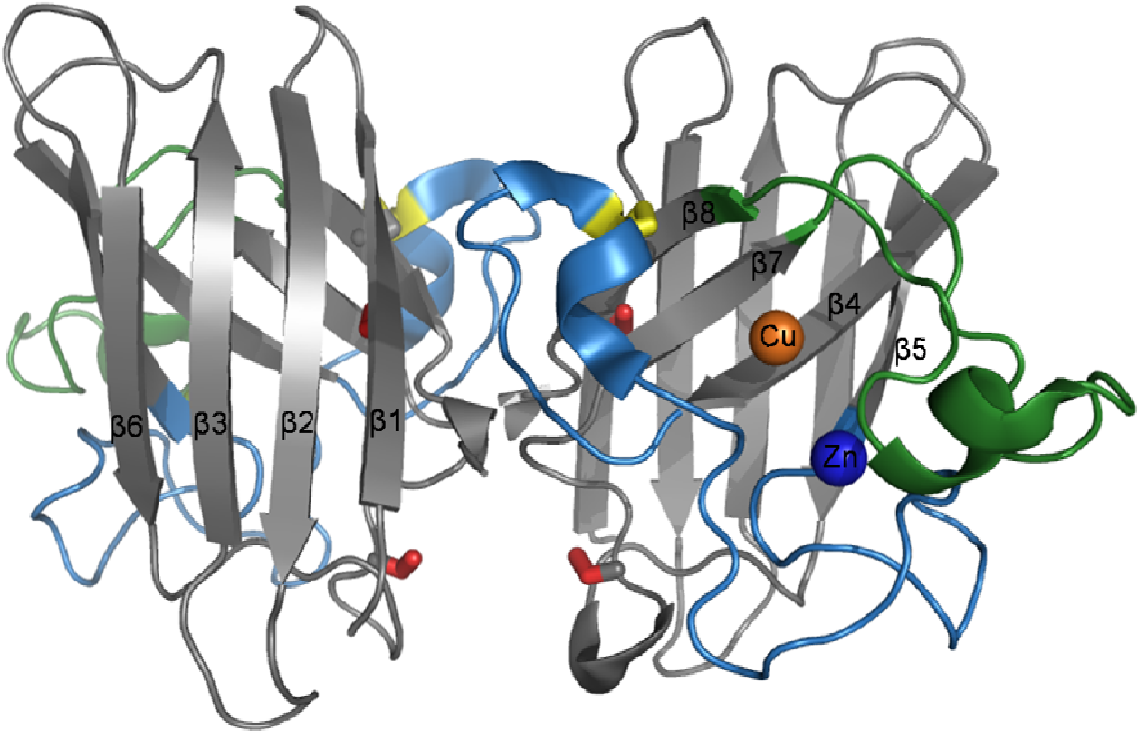

Figure 1.3. The topology of SOD1.

The eight anti-parallel β-strands of SOD1 are organized in two β-sheets formed by β1-3+β6 and β4+ β5+ β7+ β8. The β-strands β3- β6 form a Greek-key motif, disrupting the sequence local structure of the β-sandwich. The seven loops of SOD1 are labeled with roman numerals. Both structurally distinct loops of SOD1, the Zn-binding (blue) and electrostatic loops (green), are located in the second β-sheet, as well as the intramolecular disulfide bond between C57 and C146, depicted by the orange dotted line.

Figure 1.3. The topology of SOD1.

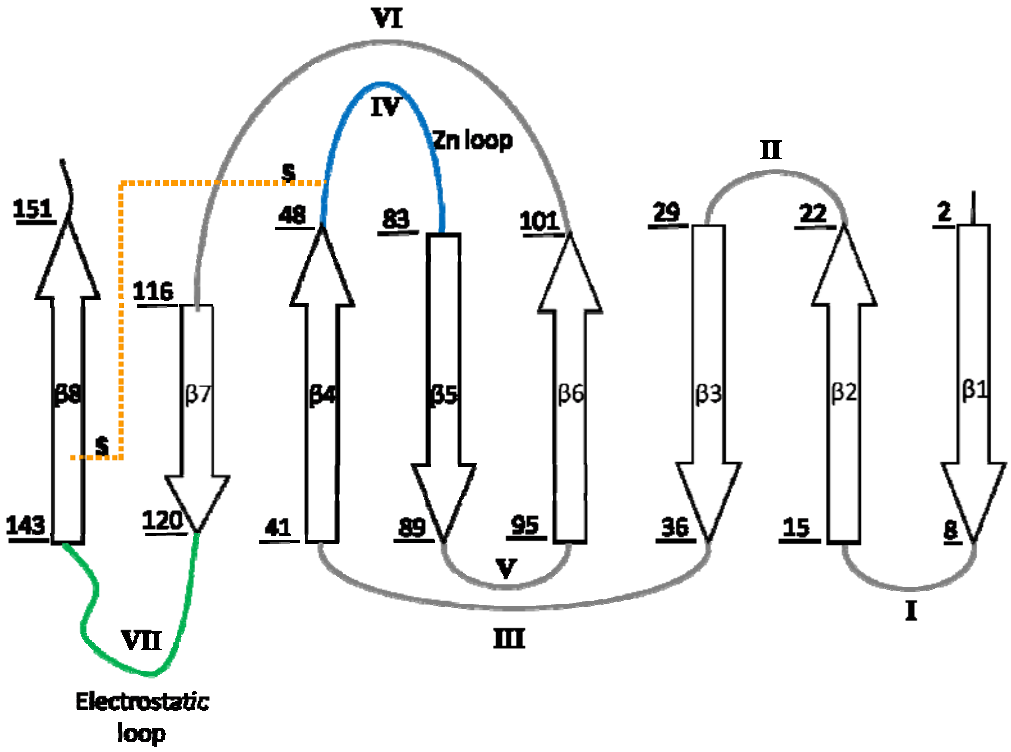

SOD1 Maturation

While the nascent SOD1 chain is able to fold into a stable structure without any post-translational modifications, a series of maturation steps are required for the protein to attain its most stable conformation. Folding of the nascent chain occurs without any metal binding and precedes disulfide-bond oxidation. This step is ATP independent, suggesting that chaperones do not playing a significant role in the folding of the WT protein.[37] The resulting metal-free, disulfide-reduced monomer is unable to dimerize prior to either Zn binding or disulfide oxidation.[38] The unfolded form of this immature species is biologically important as it is the only species that can be transported into the intermembrane space of mitochondria.[39] Further oxidation of the disulfide bond, dimerization, and Cu and Zn insertion leads to the formation of the catalytically active SOD1.

The Disulfide Bond

Each monomer of SOD1 contains an intramolecular disulfide bond between C57 and C146, which is highly conserved between species. The oxidation of the disulfide bond is critical in maintaining the quaternary structure of the protein,[40] and may also play a role in Cu insertion.[41; 42] Reduction of the disulfide bond in the absence of metals leads to the dissociation of the dimer[38] and consequently a significant reduction in the

thermodynamic stability.[43; 44] Thus, keeping the disulfide bond oxidized in the reducing environment of the cytosol is likely critical in preventing the aggregation of the protein.

In the cell, the order of the maturation steps is not well understood but it is likely that disulfide-bond oxidation precedes Zn binding, as the presence of Zn does not accelerate the formation of the disulfide bond of human SOD1 expressed in rabbit reticulocyte lysates.[37] This is surprising because studies of yeast SOD1, which is dependent on the copper chaperone of SOD1 (CCS) to oxidize the disulfide bond, have suggested that Zn binding was required to mediate the CCS-SOD1 interaction.[42] These seemingly contradictory results may reflect differences in the maturation pathway of yeast and human SOD1, as human SOD1 is not entirely dependent on CCS for disulfide-bond oxidation.[45]

The redox potential of the disulfide bond of budding yeast SOD1 is -0.23 eV,[42] and human SOD1 expressed in budding yeast can be reduced by cytosolic glutaredoxin.[46] Therefore, the oxidized status of the disulfide bond must be kinetically controlled. This is supported by the resistance of mature WT SOD1 against disulfide reduction by TCEP over 24 hour incubation[47] while unfolded SOD1 can be reduced in a matter of minutes (CK, CRM unpublished). Structural evidence provides an explanation for the resistance of the SOD1 disulfide bond against reduction. Once formed, the disulfide bond is significantly protected from solvent by packing against V118, the aliphatic portion of

R143, and the gamma methyl group of T116, as well as by contributions from the C-terminus of β1. The stability of the disulfide bond is also coupled with metal binding, as evidenced by the significantly lower Zn affinity of the disulfide-reduced protein reported in this thesis. The stabilization of the disulfide bond by folding, dimerization and metal binding likely explains its persistence in the reducing environment of the cytosol.

Zinc Binding

While the binding of Cu is related to catalytic activity, Zn serves a strictly structural role in stabilizing the native fold of the protein. Studies reported in this thesis have demonstrated that Zn binds progressively more tightly along the folding reaction coordinate of SOD1. Zn binding enhances the stability of SOD1 monomers by 7 kcal mol^{-1} under standard state conditions and further stabilizing the dimer by at least an additional 1.7 kcal mol^{-1}.[48] These results are consistent with measurements of the increased stability of Zn-bound SOD1 reported by differential scanning calorimetry experiments[33]. While apo-SOD1 has a T_m of 52 °C, the binding of Zn increases the melting point by ~24 °C, to 76 °C.

This observed stabilization is likely due to a number of structural changes upon Zn binding. First and foremost, upon Zn ligation by H63, H71, H80, and D83 (Figure 1.4), the Zn-binding and electrostatic loops become well ordered.[35; 36; 49] This facilitates the formation of a tight channel near the active site, restricting the access of non-native

Figure 1.4. The Cu and Zn binding sites of SOD1.

The Cu^{2+} and Zn^{2+} binding sites of SOD1 (PDB: 2C9V) are depicted in orange and blue respectively. The shared ligand, H63 has been highlighted with both colors. Parts of the protein have been hidden for clarity.

Figure 1.4. The Cu and Zn binding sites of SOD1.

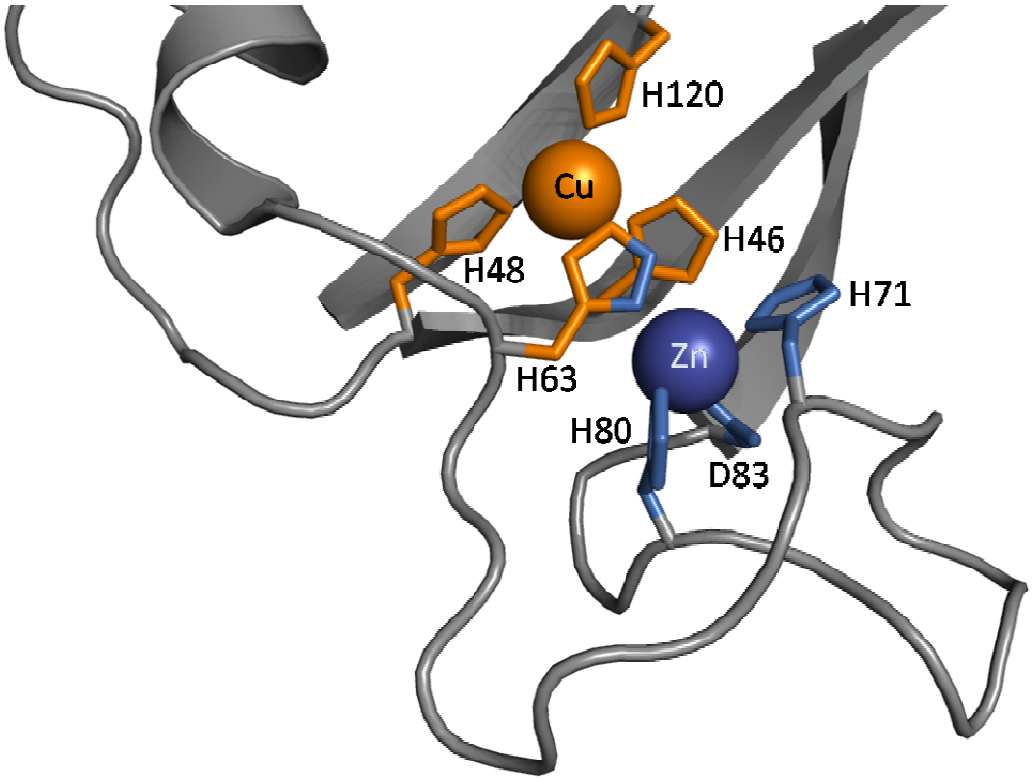

substrates to the highly reactive copper cation.[50] It also appropriately positions the dimer interface contacts of the Zn-binding loop, making Zn-bound monomers dimerization competent even in the absence of the disulfide bond. Despite these inter-subunit contacts, the metal binding regions in one subunit of SOD1 share very limited contacts with the alternate subunit, consistent with a small loss in catalytic activity for monomeric versions of the protein.[51] The β-strands connected by loop IV and loop VII, β4, β5, and β7 also become lengthened upon Zn binding to the extent observed in the holo-SOD1. Most significantly, β4 becomes elongated to include two Cu binding residues His46 and His48. The packing of H48, V117 and H120 against the disulfide bond may serve to explain the coupling between disulfide bond status and Zn affinity (Figure 1.5).

Copper binding

The final step in SOD1 maturation is thought to be Cu binding. For human SOD1, copper binding is largely mediated by the copper chaperone of SOD1 (CCS). However, it can also be activated by chaperone independent pathways that may involve copper bound by glutathione.[52] The pathway for activation can also vary by species. For instance, the yeast SOD1 is entirely dependent on the CCS pathway,[45] while the *C. elegans* SOD1 is entirely independent of the CCS pathway.[53] The requirement for CCS is highly dependent on sequence, particularly around the conserved disulfide bond. The yeast and human SOD1 share 54% sequence identity, yet display significant differences in CCS requirement, and

Figure 1.5. The structural connection between Zn and the disulfide bond.

The coupling between the Zn affinity and the disulfide bond can be explained structurally. The Zn binding site is located proximal to the disulfide bond and structurally orients the Cu binding histidines to the appropriate final geometry, in the absence of Cu. These histidines pack against V118, which directly packs against the disulfide bond. Furthermore, Zn binding induces order in loop IV, which contains C57, likely favoring disulfide bonding.

Figure 1.5. The structural connection between Zn and the disulfide bond.

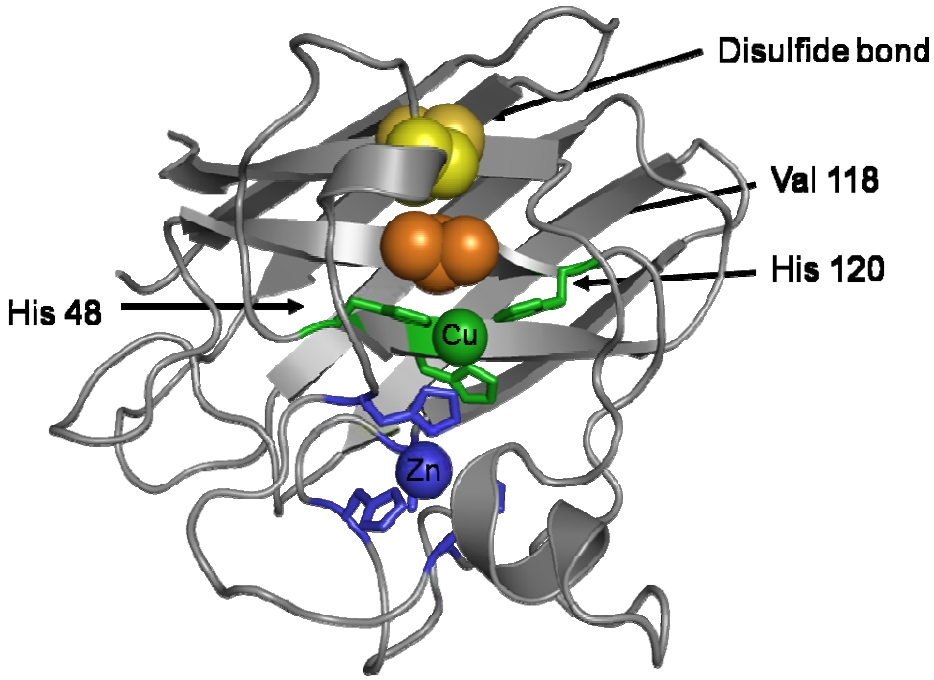

strikingly a single point mutation at P144 can confer CCS independence to the yeast protein.[45]

It is thought that the CCS transfers the copper ion to the copper-free SOD1 through direct insertion via heterodimerization with a SOD1 monomer and is dependent on the presence of oxygen.[45; 54; 55] The structural consequences of Cu binding are far less dramatic due to the fact that the amino acids that ligate this cation – H46, H48, H63, H120 – are predominantly found in the β-strands which are already well structured in the apo-state (Figure 1.4).[35] The only exception is H63, the shared ligand between the Cu and Zn ions, which is found in the Zn-binding loop.

Cu binding, while structurally less significant than Zn, does lead to a further increase in thermodynamic[32; 56] and kinetic[57] stability, and it is likely that Cu and Zn binding to SOD1 act synergistically in stabilizing SOD1. This is partially due to the presence of a shared ligand, H63, and the secondary hydrogen bonding network formed upon Zn binding. This secondary bridge is critically dependent on D124, which forms hydrogen bonds between H46, a copper ligand, and H71, a Zn ligand. In the electrostatic loop, another important hydrogen bond is formed between the side chains of D125 and S134. The combination of these interactions effectively communicates the structural organization of the Zn binding loop by Zn binding to the electrostatic loop. Any substitutions in these residues will likely result in disorder in the electrostatic loop even

in the presence of Zn, as observed for the S134N variant by NMR. While D124V and D125H, also ALS variants, have not been characterized structurally, they may be expected to exhibit similar structural characteristics.

Mechanisms of Toxicity

While the exact mechanism of how mutant SOD1 leads to motor neuron loss is unclear, it is well accepted that this toxicity is due to a gain-of-function that is independent of a loss in dismutase activity of SOD1. First, over-expression of the mutant human transgene in mice[58; 59] and rats[60; 61] leads to a disease with symptoms comparable to ALS symptoms in humans. Neither the presence of endogenous mouse or rat SOD1, nor co-expression of WT human SOD1 prevents disease symptoms.[23] In fact, co-expression with WT has been shown to increase toxicity in an A4V mouse model with low protein expression.[62] Mice lacking SOD1 do not develop ALS,[63] while loss-of-function mutations in Cu ligands, such as H46R or H48Q, have been identified in humans patients. Comparable variants lacking two[64] or four Cu ligands,[65] when expressed in mice, also leads to the disease. Loss of catalytic activity can also be induced by knocking out CCS, which is partially required for loading copper for mouse and human SOD1. This also has no affect on disease[66] and co-expression of human CCS actually leads to an exacerbation of the disease.[67] In mice, the age of onset as well as the time from diagnosis to death is

generally coupled with the expression levels of the protein.[68] Yet, high expression levels are not a strict requirement for recapitulating ALS in mice.[69; 70]

Though mutant SOD1 expression leads to the death of motor neurons, recent work has revealed that mutant SOD1 toxicity is not cell autonomous (reviewed in Glabe, JBC 2008[71]). The susceptibility of motor neurons to mutant SOD1 expression over dorsal root ganglia or hippocampal neurons can be demonstrated in cell culture models of ALS.[72] However, attempts at recapitulating the disease phenotype induced by mutant SOD1 expression in motor neurons in vivo has either failed,[73; 74] or resulted in a mild disease phenotype when the protein is expressed in very high levels.[75] The involvement of specific cell types in ALS was tested by the use Cre-Lox system in mice which allows for the tissue specific excision of genes flanked by lox sites upon the expression of Cre recombinase. Deletion of mutant SOD1 expression in motor neurons, but not astrocytes, delayed the onset of symptoms but did not provide any slowing of disease progression after onset.[76; 77] Conversely, in the same studies it was found that the excision of SOD1 from microglia had little effect on disease onset but the duration of the disease after onset was significantly increased. These results suggest that disease initiation may be triggered by the toxic action of SOD1 in motor neurons, while disease progression may be influenced by the response from microglial cells and the inflammatory response.

Aberrant Catalytic Activity

But what is the molecular mechanism for the toxicity of mutant SOD1? Several hypotheses have been proposed for the gain-of-function toxicity imparted by SOD1 mutations and can be divided into two categories: aberrant catalytic functions and misfolding/aggregation. The aberrant catalytic function theory suggests that structural changes in SOD1 due to mutations may lead to the increased access of non-native substrates. In addition to dismutase activity, WT and mutant SOD1 have been shown to exhibit some level of superoxide reductase or oxidase activities.[78] One potential aberrant catalytic activity proposed is the formation of peroxynitrite by the combination of superoxide and nitric oxide in the active site of SOD1, which is strongly exacerbated with the depletion of zinc from SOD1.[79] Alternatively, hydrogen peroxide, the normal end-product of oxidized SOD1 (Cu^{2+}), could react with the reduced form of SOD1 (Cu^{+}) to produce the reactive hydroxyl radical.[80]

While these mechanisms may play some role in ALS, it is likely that they cannot be the definitive underlying cause of the disease. Elevated levels of free nitrotyrosine, a byproduct of damage by peroxynitrite, have been reported in patients[81] and mouse models,[82] but no evidence of protein-bound nitrotyrosine was reported.[82] Furthermore, these mechanisms require some retention of catalytic activity of SOD1, yet SOD1 with all four copper binding histidines removed is still capable of causing ALS in mouse models.[65] As stated earlier, mutations have been found in humans which result in the loss

of some or all metal content from the enzyme, and consequently the loss of all catalytic activity.[83] One alternative Cu binding site was suggested involving C111 but the affinity of this site for Cu was determined to be in the micromolar range and is likely too weak to bind Cu *in vivo*.[84] Additionally, the G86R mutation in mouse SOD1, which has a serine instead of a cysteine at position 111, have also been found to cause an ALS phenotype,[18] effectively ruling out a causative role in Cu binding to C111 as a cause of aberrant catalytic activity.

Misfolding and Aggregation

An alternative possibility lies in the potential for SOD1 to misfold and aggregate, and that these aggregates themselves exert some toxic effect. While aggregates are observed in many misfolding diseases, the morphology of the aggregates can vary. Unlike the amyloid fibrils that are characteristic of Alzheimer's and Parkinson's disease, aggregates of SOD1 appear more amorphous and dynamic.[85] Though the toxic nature of these aggregates is not well understood, it is thought that smaller, soluble aggregates are a likely source of the toxicity. In the G93A SOD1 mouse model, studies have observed the presence of hydrophobic species of SOD1 enriched in spinal cord extract from birth.[70] Additionally, in the G127insTGGG mouse model, nearly 20% of all SOD1 in spinal cord extracts was found as a detergent soluble proto-aggregate at all stages of the mouse's life.[70] These results, in combination with evidence that larger insoluble aggregates appear concomitantly with the onset of disease symptoms[86; 87] support the hypothesis that the

toxicity of mutant SOD1 is due to the proto-oligomeric species, rather than end-stage aggregates.

It is likely that this enhanced toxicity of proto-aggregate material is a common theme underlying many protein misfolding and aggregation diseases. Similar results have been observed for both familial amyloid neuropathy,[88] which involves the aggregation of transthyretin, as well as Parkinson's disease, which involves the aggregation of α-synuclein[89]. Toxicity to motor neurons has also been observed in prefibrillar forms of non-disease related HypF-N from *E. coli*, the SH3 domain from bovine phosphotidylinositol 3' kinase, horse lysozyme and sperm whale apomyoglobin.[90; 91; 92] Furthermore, the existence of conformationally-specific antibodies which can target fibrillar and prefibrillar aggregates,[93] independent of the sequence of the aggregating protein, suggests that the aggregation/toxicity phenotype may be a general phenomenon of protein misfolding.

The Molecular Mechanism of SOD1 Aggregation

Aggregation Due to Structural Changes of the Native State

To date, several hypotheses have emerged as to what the aggregation prone species of SOD1 may be. One potential aggregation pathway of SOD1 involves local unfolding of

the protein. This sort of behavior has been observed for the ALS variant S134N, where the unfolding of the electrostatic loop leads to non-native intermolecular interactions in solution[94] and novel contacts to form a nanotube like structure in crystals.[95] This variant partially mimics the metal-free state of SOD1 where both the electrostatic and Zn binding loops are disordered. Similar destabilization or de-protection of the electrostatic loop has been observed by native state hydrogen exchange experiments for the G85R, D124V and D125H variants as well.[96] This pathway for aggregation may represent a differentiation point between classes of ALS variants as many other variants for which crystal or NMR structures have been determined, such as A4V, G37R, G93A, and I113T, show only small differences compared to the WT protein.[97; 98; 99; 100]

Aggregation by Intermolecular Crosslinking

Alternatively, the aggregation of SOD1 could be facilitated by the intermolecular crosslinking of the two free cysteines, C6 and C111. C6 is part of the hydrophobic cluster that makes up the interior of the β-sandwich, while C111 is largely solvent exposed near the dimer interface (Figure 1.2). While intermolecular crosslinking via these residues is an attractive possibility for initiating or propagating aggregation,[43; 101; 102] the causative role of the free cysteines in aggregation has been highly controversial. Some *in vitro* experiments have demonstrated that the aggregation of SOD1 is highly dependent upon the presence of both free cysteines.[101; 102] On the other hand, *in vitro* studies from the

Valentine lab, investigating the aggregation of SOD1 into fibril-like aggregates, have suggested that neither C6 nor C111 are required to aggregate SOD1.[8]

A causative role for non-native disulfide formation is cast further into doubt by the existance of fALS mutations at each of the four cysteine residues of SOD1. This is supported by work from the Borchelt lab investigating mutant SOD1 aggregation in cell culture, which has demonstrated that SOD1 mutants lacking all cysteine residues (C6F/C57S/C111Y/C146R) or mutants which contain just C6 or C111 but not the other cysteines can readily aggregate.[103] In this study the choice of the amino acid replacing C6, glycine or phenylalanine, greatly altered the aggregation propensity of the mutant SOD1. The C6G variant remained soluble while the C6F variant caused significant aggregation. Interestingly, the presence of C6 and C111 were observed to enhance the aggregation propensity of the G85R variant of SOD1. Collectively, these studies suggest that C6 and C111 may play a role in modulating the aggregation propensity of SOD1 and may be required for some studies investigating aggregation *in vitro*. Nevertheless, these results suggest that the free cysteines are not necessary to initiate or stabilize mutant SOD1 aggregation.

Aggregation from Immature, Partially-Folded Species

While aggregation may be caused by an altered native structure, another pathway exists from immature species of SOD1. Monomeric intermediates have been observed in *in*

vitro aggregation studies[104] and are supported by the observation that antibodies targeting the dimer interface of SOD1 can stain tissues extracted from the brain and spinal cord of ALS mice.[105] The species may be populated by the destabilization of the native state (Figure 1.6), as well as transiently after synthesis but prior to any post-translational modifications. Immature species are efficiently degraded by the proteosome[106] and the aggregation of mutant SOD1 has been shown to be highly sensitive to proteosome activity,[107] suggesting that cells have evolved to remove these species of SOD1 from the cytoplasm. This effect may be due to the increased hydrophobicity observed for metal-free and/or disulfide-reduced SOD1.[47; 108] It is also known that unstructured regions are required for efficient degradation by the proteosome,[109] and the dynamic nature of the SOD1 loops in the apo-state may provide just such a structural feature.

Not surprisingly, premature species of SOD1 have been consistently linked with aggregation. Disulfide-reduced proteins have been found to be enriched in spinal cord extracts of mutant SOD1 expressing mice[69] and the presence of small amounts of disulfide-reduced SOD1 has been shown to greatly enhance aggregation kinetics in *in vitro* studies[8]. Additional evidence supporting the toxic potential of immature species of SOD1 comes from the protective effect of Zn binding, which is known to greatly stabilize the native fold of SOD1. The loss of Zn is thought to be a necessary step in the pathway to aggregation,[110] and it may be an early step in the unfolding pathway of the protein under denaturational stress.[111; 112] The presence of Zn has consistently slowed aggregation

of SOD1 *in vitro* and Zn-free SOD1 has been shown to be cytotoxic in motor neuron cultures.[79]

Applying Protein Folding to ALS

The Folding Pathway of SOD1

It is likely that aggregation-prone species are present on the folding free energy surface of nearly any protein.[2] Mutations in exons can lead to changes in amino acid sequence that may destabilize the native structure and predispose these variants to develop increased populations of aggregation-prone partially folded or misfolded species. Detailed analyses of the folding mechanism of both metal-free[113; 114; 115] and metal-bound[48; 116] SOD1 have revealed a three-state folding mechanism where monomers fold autonomously and then rapidly dimerize to form the native structure, $2U \leftrightarrows 2M \leftrightarrows N_2$.

The thermodynamic consequence of a very slow monomer folding rate, followed by a very rapid dimer association step, is a two-state-like equilibrium unfolding reaction, $2U \leftrightarrows N_2$.[48; 114; 115] The visualization of monomer stability in equilibrium titrations of the dimeric protein requires high concentrations of stabilizing salts such as ammonium sulfate. The presence of these osmolytes makes comparisons with cellular phenomena ambiguous.[115] Furthermore, the folding free energy landscape is such that monomer

folding is always rate-limiting in refolding experiments. In unfolding, dimer dissociation is rate limiting at high denaturant concentrations; however, near the transition region the kinetics become protein-concentration dependent, suggesting that the dimer association rate is contributing to the observed rate. A detailed global analysis of the kinetic unfolding and refolding measurements is required to validate the folding model for SOD1, determine the rates of folding and unfolding, and accurately predict the populations of species on the folding pathway.[114; 117]

Because monomer unfolding is never rate-limiting, monomeric constructs of SOD1 were created to monitor monomer folding/unfolding reactions that are not perturbed or concealed by the dimerization reaction. This monomeric SOD1 was created by the replacement of Phe50 and Gly51, near the dimer interface (Figure 1.2), with glutamic acid. Variants of this protein with the free cysteines at positions 6 and 111 replaced with alanine, mAA-SOD1, or alanine and serine, respectively, mAS-SOD1, have been studied extensively. A comparison of the crystallographic and NMR structures of SOD1 reveals that mAS-SOD1 is very similar to a monomer subunit in a SOD1 dimer.[49; 118] The catalytic activity of mAS-SOD1 is reduced ~10-fold relative to WT.[51] Considering SOD1 is a diffusion-limited enzyme, the mAS-SOD1 still retains significant catalytic activity. From experiments performed in the Matthews lab, the stability and folding kinetics of mAS-SOD1 recapitulate those of the SOD1 monomer without the F50E/G51E mutations.[117] These results are also supported by the near identical folding kinetics of

reduced mAA-SOD1, and reduced AA-SOD1, which is also monomeric.[113] Together these observations justify a study of the characteristics of the SOD1 monomer to facilitate the understanding of the dimer folding reaction.

Thermodynamic destabilization and the effect on populations

To take the simple perspective of the disulfide-oxidized, dimeric apo-protein, mutations could result in the destabilization of the dimer, the monomer or both.[119] A destabilization of the dimer would result in increased populations of folded monomeric species. Conversely, destabilization of the dimer results in an increase in both folded and unfolded monomers, while a destabilization of the monomer leads to an increase in unfolded monomeric species (Figure 1.6). By characterizing the folding free energy landscape of WT SOD1 and the ALS variants, it is possible to determine changes in the populations of the species. A consistent increase in one species may reveal the aggregation prone species.

The apo-protein is a reasonable model for protein folding studies, but is it a relevant system? The issue of whether all mutations in SOD1 result in a destabilized protein has been of some debate,[43; 120; 121] and the consensus is that not all mutations result in a significantly destabilized apo-protein. Nevertheless, the majority of variants with stabilities equal or greater than WT are the result of amino acid replacements in metal-binding ligands. These results suggest that metal-binding affinity must be taken into

Figure 1.6. Changes in populations in response to mutations.

Destabilization of the protein can lead to increased populations of immature species. The destabilization of the native dimer (red arrow) can lead to increased folded monomer populations (red population plot) compared to the WT protein (blue populations). Destabilization of the monomer (green+red arrows) and the dimer can lead to the increase of both folded and unfolded monomer populations (green population plot).

Figure 1.6. Changes in populations in response to mutations.

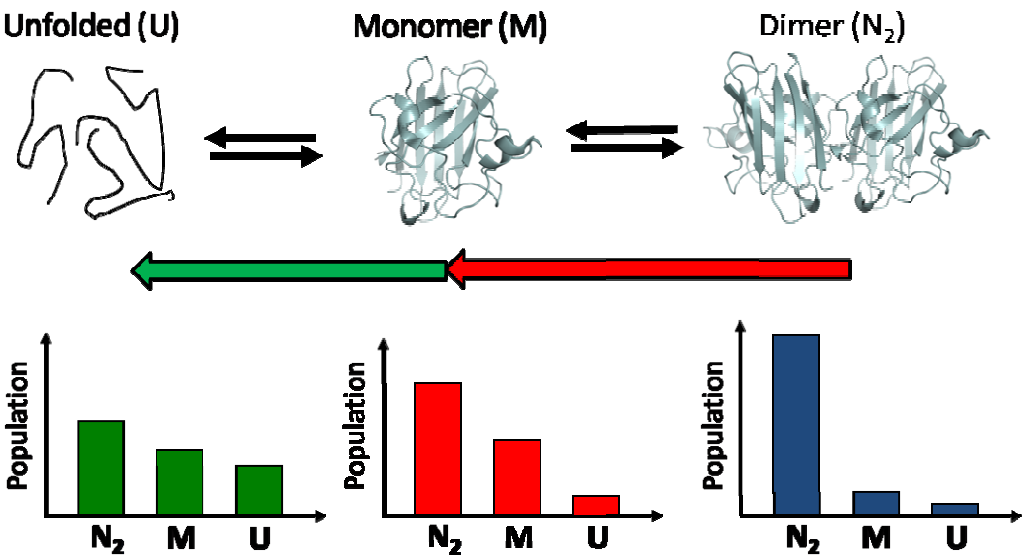

consideration when studying the effects of amino acid replacements on the folding free energy surface of SOD1.

Furthermore, variants such as E100K or D101N, which reduce the net charge of SOD1, have been reported to leave stability and the metal affinity unaffected. It is possible that these mutations in fact do not cause ALS, as a recent report has cast doubt on the pathogenic nature of E100K.[122] Nevertheless, these mutations can be regarded as lowering the activation energy barrier for aggregation by reducing the net charge of a protein and decreasing the electrostatic repulsion between identical proteins. This phenomenon may be especially relevant to E100K and D101N which are found in the edge β-strands of the β-sandwich structure, part of the "negative design" observed in β-rich proteins to prevent aggregation.[123] These strands often exhibit a large number of solvent-exposed charged residues and are thought to serve as gatekeepers for preventing aggregation in SOD1.[124]

Variants Studied

The work in this thesis concentrates on five specific ALS variants representing a range of structural perturbations to SOD1. All five mutations result in amino acid replacements of highly conserved residues: A4V, L38V, G93A, L106V and S134N.[22] All of these mutations are dominant and patients expressing the mutant SOD1 exhibit typical age of onset and mean life expectancy for fALS.[7]

Variants have generally been partitioned in two groups based on their catalytic activity: wild-type-like (WTL), and metal-binding region (MBR) mutants with reduced dismutase activity.[125] WTL variants are generally those with amino acid substitutions in the β-barrel, while MBR mutants are found in the Zn-binding and electrostatic loops. Nevertheless, there are notable exceptions such as H46R and H48Q, which are replacements of Cu binding residues, but are located in β4. Mutations can exhibit several different but not mutually exclusive phenotypes. Some mutations decrease the stability of the structure of apo-SOD1, other mutations decrease the metal affinity, and another group of mutations increase the intrinsic aggregation propensity of SOD1. These complex responses highlight one of the major difficulties in applying protein folding methodologies to the problem of SOD1 mediated ALS. The variety of post-translational modifications involved in SOD1 maturation result in a complicated folding free energy surface with as many as 44 microstates.[126] We chose to study the states that would likely be the most significantly populated given the current knowledge on SOD1folding and maturation. These include all combinations of disulfide-bond status and Zn binding to the SOD1 monomer, and the apo and Zn-bound SOD1 dimer.

Mutations that decrease the stability of apo-SOD1 have been extensively studied in the literature. Many of these involve hydrophobic residues in the tightly-packed core of the β-sandwich of SOD1 and fall into the WTL category. Four such variants were studied in

Figure 1.7. Crystal structure showing ALS variants studied.

The ALS variants studied in this thesis are highlighted in orange on a monomer subunit of the crystal structure of holo-SOD1 (PDB 2C9V). The Zn ion and the disulfide bond are depicted in blue and yellow respectively. The two residues mutated to glutamic acid to make the obligate monomer F50/G51 are shown in red. The image on the right is a 90° clockwise rotation, into the page, of the image on the left.

Figure 1.7. Crystal structure showing ALS variants studied.

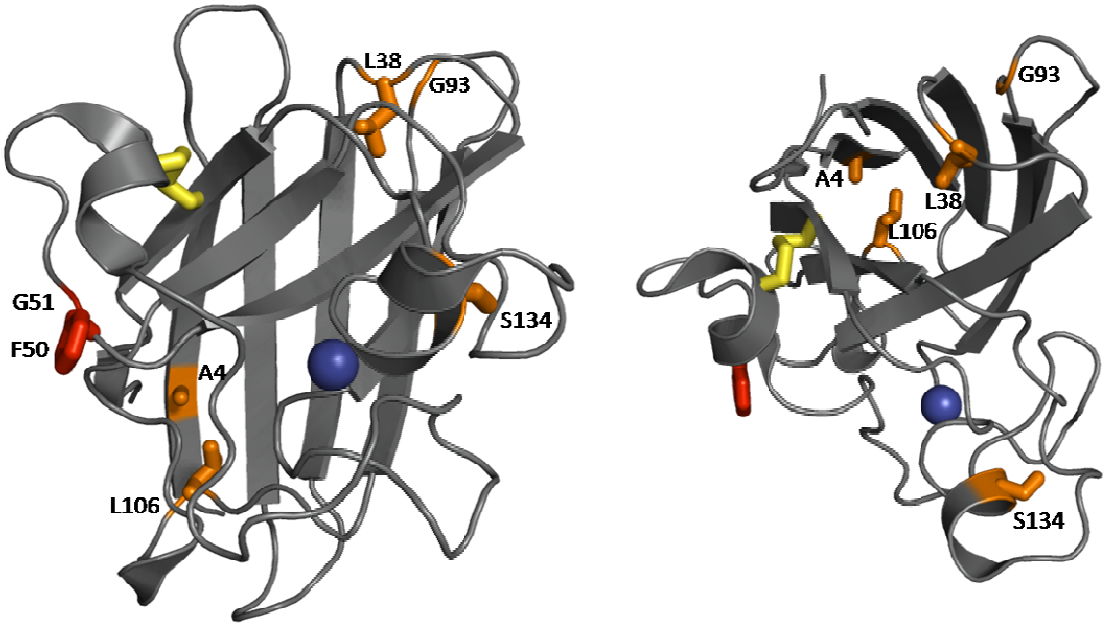

this thesis: A4V, L38V, G93A and L106V. Of these variants, A4V, and G93A (Figure 1.7) have been characterized structurally by x-ray crystallography. The crystal structure of both A4V and G93A holo-SOD1 are nearly superimposable on the WT protein,[97; 98; 100] implying that the thermodynamic consequences of destabilization, rather than changes to the native structure, may be playing a primary role in the pathogenicity of these variants.

The L38 and L106 residues lie on the "top" and "bottom" of the β-sandwich (Figure 1.7) and play key roles in capping the hydrophobic interior of the protein. The loss of a methyl group when replacing Leu with Val would be expected to cause minimal structural perturbations but a significant loss of thermodynamic stability may be expected. While the metal affinity for the L106V variant has not been measured, due to the structural similarities between these variants, it could be similar to the L38V variant, which was found to be reduced 30 fold compared to the WT protein.[127]

The S134N variant has significant disruption and disorder in the electrostatic loop when compared to the WT holo-enzyme. This variant is thought to possess much lower Zn and Cu affinity and was found to bind little or no metals when isolated from insect cells.[83] Because this loop is disordered in the absence of metals, the stability of the apo-protein should be unaffected.

Summary of Thesis

We propose that the majority of ALS mutations lead to the destabilization of the metal-bound and/or metal-free species of SOD1, leading to increased populations of partially folded or unfolded species. Non-native interactions between these molecules and with other proteins found in the cell can lead to the formation of soluble and insoluble aggregates, which may explain the gain-of-function toxicity of mutant SOD1. To test this hypothesis, we have employed biophysical techniques to characterize the thermodynamic and structural properties of the major species in the folding pathway of SOD1, and the effect of ALS mutations on these species.

Chapter II. Zinc Binding Modulates the Entire Folding Free Energy Surface of Human Cu,Zn Superoxide Dismutase

To investigate the role of Zn in SOD1 folding, we performed a detailed equilibrium and kinetic analysis of SOD1 monomer and dimer in the presence of stoichiometric Zn. The results show that Zn binds progressively tighter along the folding free energy surface, imparting the greatest stabilization to the native dimer, the net result of which is a reduction in monomeric species. Since Zn-binding has been shown to decrease the propensity for aggregation, these results suggest that the aggregation prone species may be a folded or unfolded monomeric species of SOD1.

Chapter III. Disulfide-Reduced ALS Variants of Cu, Zn Superoxide Dismutase Exhibit Increased Populations of Unfolded Species

In order to investigate the thermodynamic and kinetic folding differences between WT and ALS variants of SOD1 on the immature species, we probed the coupling between folding, disulfide-bond status and amino acid replacements on the stability of monomeric SOD1. Surprisingly, only minimal differences were observed in the Zn-binding affinity, even for the S134N variant. While the destabilization due to ALS-causing amino acid replacements was comparable in the disulfide-oxidized and disulfide-reduced metal-free forms, the changes in the unfolded state populations were significantly different. Under physiological conditions, the four β-sandwich variants were >50% unfolded when the disulfide-bond was reduced. It was also determined that the Zn affinity of the disulfide-reduced protein was reduced ~750 fold compared to the oxidized SOD1, suggesting that disulfide-oxidation may precede Zn binding. The persistence of partially unfolded, disulfide-reduced protein after synthesis may explain the increased aggregation propensity observed for some ALS variants.

Chapter IV. Enthalpic barriers associated with desolvation dominate the folding reaction of SOD1 monomers.

The slow folding relaxation time of disulfide-oxidized and reduced, apo-SOD1 monomers motivated a detailed investigation of the nature of the barriers involved in the formation of the folding and unfolding transition state ensemble. These studies were

performed both to gain insights into the folding pathway of immunoglobulin-like proteins and to determine if SOD1 had unique folding properties which may explain the link with ALS. Both the folding and unfolding barriers were found to be dominated by enthalpic barriers. In combination with the observation that little or no compaction is observed for SOD1 prior to the rate-limiting folding step, these results suggest that dehydration of the chain is the main source of this energetic barrier. The change in heat capacity upon folding, the relative contribution between entropy and enthalpy to the folding free energy, and the viscosity dependence of SOD1 folding are all in the expected range of proteins with two-state folding mechanisms, suggesting that these characterisitcs are unlikely to explain why mutant SOD1 causes ALS. On the other hand, the insights obtained from SOD1 folding can be applied to answering the more general question of how amino acid sequence defines the folding pathway and final structure of a protein.

Chapter V. Structural characterization of the native and higher energy states of SOD1.

A combination of in solution small angle x-ray scattering (SAXS) and native state hydrogen exchange (NS-HX) techniques were utilized to characterize potential structural differces between WT and ALS variants of SOD1. The NS-HX studies revealed that exchange from the dimeric state may occur in two steps, potentially reflecting differential protection in the dimer and monomer. The core of the monomer was highly protected in these measurements, suggesting that fraying of the interface and edge strands may be

occuring upon dimer dissociation. Puzzlingly, exchange from the monomeric state proceeded too slowly to be explained by the global unfolding rate, potentially due to some residual protection in the unfolded state. Structural characterization by SAXS revealed significant differences in the size and shape of the variants studied in the apo disulfide-reduced and disulfide-oxidized forms. Both the addition of Zn and the oxidation of the disulfide bond was found to lessen the differences between the ALS variants and the WT SOD1.

Chapter II. Zinc Binding Modulates the Entire Folding Free Energy Surface of Human Cu, Zn Superoxide Dismutase

Abstract

Over 100 amino acid replacements in human Cu, Zn superoxide dismutase (SOD1) are known to cause amyotrophic lateral sclerosis, a gain-of-function neurodegenerative disease that destroys motor neurons. Supposing that aggregates of partially-folded states are primarily responsible for toxicity, the role of the structurally-important zinc ion in defining the folding free energy surface of dimeric SOD1 was determined by comparing the thermodynamic and kinetic folding properties of the zinc-free and zinc-bound forms of the protein. The presence of zinc was found to decrease the free energies of a peptide model of the unfolded monomer, a stable variant of the folded monomeric intermediate and the folded dimeric species. The unfolded state binds zinc weakly with a micromolar dissociation constant, and the folded monomeric intermediate and the native dimeric form both bind zinc tightly, with sub-nanomolar dissociation constants. Coupled with the strong driving force for the subunit association reaction, the shift in the populations towards more well-folded states in the presence of zinc decreases the steady-state populations of higher-energy states in SOD1 under expected *in vivo* zinc concentrations (~nanomolar). The significant decrease in the population of partially-folded states is expected to diminish their potential for aggregation and account for the known protective effect of zinc. The ~100-fold increase in the rate of folding of SOD1 in the presence of micromolar concentrations of zinc demonstrates a significant role for a pre-organized

zinc-binding loop in the transition state ensemble for the rate-limiting monomer folding reaction in this β-barrel protein.

Introduction

Amyotrophic lateral sclerosis (ALS) is a neurodegenerative disease, characterized by systematic loss of the motor neurons in the brain and spinal cord.[128] Though no definitive biochemical mechanism has been discovered, a subset of familial ALS (fALS) cases has been linked to mutations at the Cu, Zn superoxide dismutase (SOD1) locus.[14; 129] Despite constituting only 2-5% of all known cases, SOD1 mediated fALS is the most prominent, identified, heritable cause of the disease. Moreover, sporadic cases of ALS are clinically and pathologically similar to fALS cases,[128] suggesting both forms may share a common underlying mechanism.

In its native form, SOD is a 153 amino acid, cytosolic protein that catalyzes the dismutation of superoxide into hydrogen peroxide and oxygen.[21] SOD is catalytically active as a homodimer with both a copper and a zinc ion bound to each monomer. The fold of an SOD1 monomer is a β-sandwich composed of eight antiparallel β-strands supporting a pair of large loops that follow β4 and β7, loops IV and VII, respectively (Figure 2.1). Loop IV is covalently linked to β8 by a disulfide bond between Cys57 and Cys146.[118] Loops IV and VII coordinate the metals and provide the catalytic and electrostatic components of the active site.[50] The copper redox cycle drives the disproportionation reaction, and the zinc ion is thought to play a role in defining the structure and stability of SOD1.[35; 36; 49] The binding of zinc to dimeric SOD1 is very tight,

Figure 2.1. Crystal structure of SOD1.

(A) The crystal structure of SOD1 (PDB: 2C9V).[130] The zinc ion is depicted in yellow, with the metal-binding region of the zinc-binding loop (loop IV), as well as the residues that bind zinc, shown in dark blue. Proximal to this region, the electrostatic loop is colored in teal. The region of loop IV involved in or near the intramolecular disulfide bond (in dark orange) between C57-C146 is shown in light yellow, and the dimer interface portion of loop IV is highlighted in orange. Shown in blue is the copper ion with the histidines to which it binds depicted in green. In red are F50 and G51 that were replaced with glutamic acid to create mAS-SOD1. (B) The sequence of the zinc-binding loop with the zinc-binding residues indicated in red. The non-native residues are shown in teal for the C-terminal tryptophan and yellow for the N-terminal cysteine, which was further modified with an EDANS molecule.

Figure 2.1. Crystal structure of SOD1.

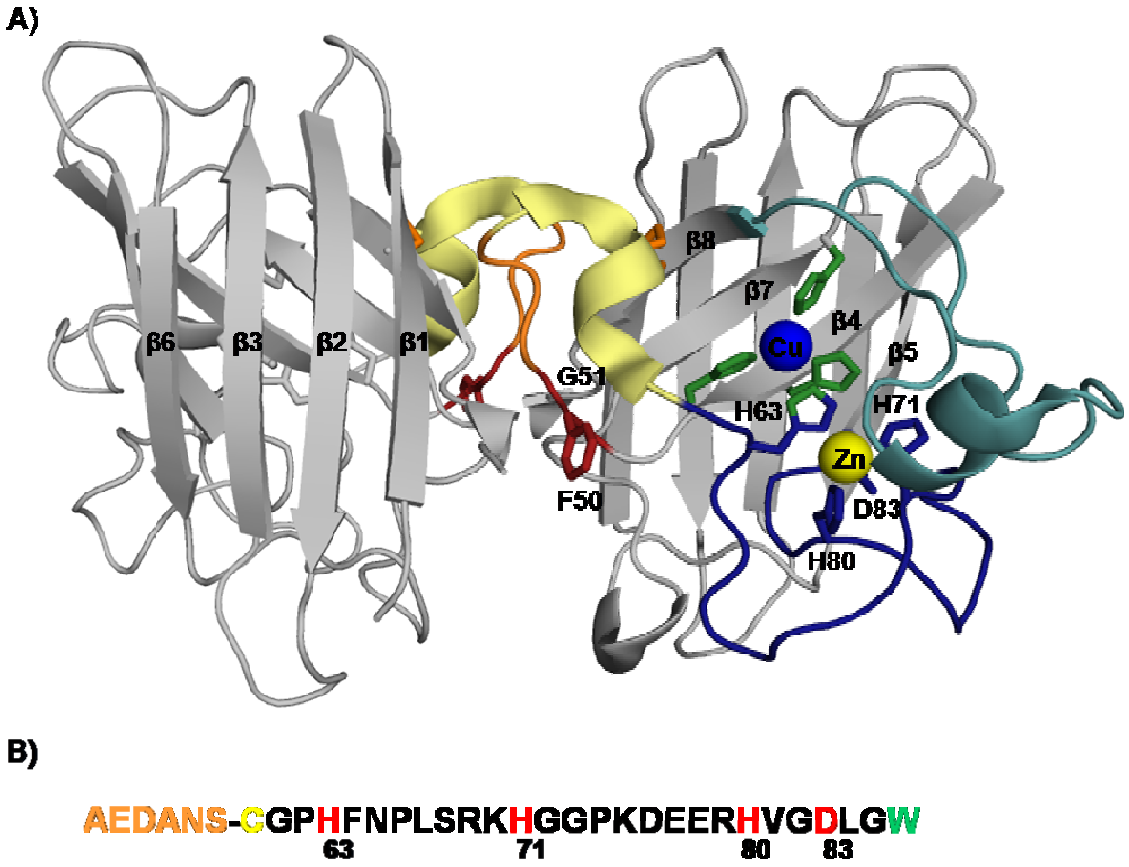

with a K_d of $<10^{-8}$ M by isothermal titration calorimetry[131] and a K_d of $\sim10^{-14}$ M by competition experiments.[127] While the order of the metal-binding and disulfide-bonding events *in vivo* is not definitively known, it is thought that zinc binds first to the disulfide-reduced protein. This complex then interacts with the copper chaperone of SOD1, which loads the copper and oxidizes the intramolecular disulfide bond.[126]

Although several hypotheses have been proposed to explain the toxic gain of function of SOD1 variants,[5; 132; 133; 134] a prevailing view holds that amino acid replacements increase populations of partially-folded states and induce subsequent aggregation.[132; 135; 136] The rationale for the unfolding/aggregation hypothesis is based on the fact that well over 100 replacements and C-terminal truncations (see http://alsod.iop.kcl.ac.uk/Als/ for a complete list), covering nearly 50% of the sequence, can cause ALS.[137] Many of these variants lead to the deposition of amorphous aggregates in and around the motor neurons of patients afflicted with ALS, and a debate has ensued about whether small oligomers or macroscopic aggregates are the toxic agents.[138] It has been demonstrated that loss of zinc may result in aggregation, reinforcing the structural importance of zinc.[110] Candidates for aggregation have focused on zinc-free partially-folded monomeric states of SOD1, including those with the disulfide bond intact and those in which the disulfide bond has been reduced.[139] More recently, the unfolded state, extruded from the ribosome and prior to disulfide bond formation or folding, has also been proposed as a candidate for aggregation and toxicity.[140]

The unfolding/aggregation hypothesis has been tested by comparative biophysical analysis of the thermodynamic folding properties of wild-type and ALS-inducing SOD1 variants in both their disulfide-oxidized[119] and disulfide-reduced[113; 141] forms. Detailed analyses of the folding mechanisms of disulfide-intact SOD1 have shown that both apo-SOD1[113; 114; 115] and Cu, Zn-SOD1[116] fold by a three-state mechanism involving a folded monomeric intermediate. Left unanswered in these studies were several questions on the specific role of zinc on the folding and stability of SOD1 that pertain to its influence on nonnative states that might be responsible for aggregation. Pertinent to the argument that newly-synthesized chains might be the source of toxicity, at what stage of folding does zinc become bound to SOD1? Once the native state is reached, what are the quantitative ramifications of zinc binding to diminish the propensity of the disulfide-bonded native dimer and the folded monomer to populate less structured, aggregation-prone states? In the event that the folded monomer is a source of aggregation, does zinc binding alter the relative populations of monomeric and dimeric forms of SOD1 at equilibrium to favor the fully-folded form? A comparative analysis of the thermodynamic and kinetic folding properties of disulfide-bonded AS-SOD1 in the presence and absence of zinc demonstrated that zinc binding modulates its entire folding free energy surface. The results provide a benchmark for future studies on metal-binding ALS-inducing variants containing disulfide bonds and on disulfide-reduced SOD1.

Results

Quantitative information on the effect of zinc binding on high energy states in SOD1 was obtained by chemical denaturation analysis of both the thermodynamic and kinetic properties of the reversible folding reaction. The C6A/C111S variant, AS-SOD1, was used in place of the wild-type SOD1 because it has been shown to fold reversibly with wild-type like stability.[142] The elimination of the free cysteines precludes intermolecular disulfide bond formation and intramolecular disulfide bond interchange. The results obtained can be compared with those from a previous study of metal-free apo-AS-SOD1[114] to determine the decrease in the free energy, i.e. the increase in stabilization relative to the unfolded state, of the zinc-bound states in the absence of denaturant.

Thermodynamic analysis

Chemical denaturation of dimeric AS-SOD1.

The effects of zinc binding on the thermodynamic properties of disulfide-intact AS-SOD1 were determined by chemical denaturation experiments in the presence and absence of zinc and monitored by circular dichroism spectroscopy. It has been previously shown that the ellipticity at 230 nm is a sensitive probe of global structure in AS-SOD1[114] and provides optimal signal to noise compared to measurements at the typical

minimum for β-rich structures, 218 nm. Although urea is a sufficiently potent denaturant to unfold apo-SOD1,[114; 120] guanidine hydrochloride (Gdn-HCl) was required to unfold zinc-bound AS-SOD1. The Gdn-HCl unfolding titration curves at 230 nm, pH 7.2 and 20 ºC, for apo- and stoichiometric zinc-bound Zn-AS-SOD1 (2 zinc ions per dimer) are shown in Figure 2.2. The native dimeric form of apo-AS-SOD1 is stable up to ~1 M Gdn-HCl, where it experiences a cooperative unfolding transition that is complete by ~2 M Gdn-HCl. In the presence of stoichiometric zinc, Zn-AS-SOD1 is stable up to ~2 M Gdn-HCl, where it also undergoes a cooperative unfolding transition that is complete by ~3 M Gdn-HCl. The reversibility of the Zn-AS-SOD1 unfolding reaction was demonstrated by the coincidence of a refolding transition curve beginning with denatured AS-SOD1 (data not shown). As has been observed previously with Cu, Zn SOD1,[116] the full equilibration of the Zn-AS-SOD1 samples at pH 7.2 for both unfolding and refolding curves was exceedingly slow, requiring 7 days at room temperature.

Chemical denaturation of monomeric AS-SOD1.

Previous analyses of the chemical denaturation of apo-SOD1[114] and Cu, Zn SOD1[116] have implicated an essential role for a folded monomeric species that subsequently undergoes a diffusion-limited association reaction to produce the native dimer. Insight into the effect of zinc binding on the stability of the monomeric folding intermediate was obtained by examining the enhancement of stability for a stable monomeric version of AS-SOD1, mAS-SOD1, upon zinc binding. The mAS-SOD1 variant was created by

Figure 2.2. Equilibrium titrations of Zn-bound and apo-SOD1.

Equilibrium Gdn-HCl titrations measured by the ellipticity in 20 mM HEPES, pH 7.2, at 20 ^{o}C. Representative data at 230 nm are shown with fits to a two-state model for the metal-free apo-AS-SOD1 (open squares) and apo-mAS-SOD1 (open circles) and with fits to a three-state model for stoichiometric Zn-AS-SOD1 (filled squares) and Zn-mAS-SOD1 (filled circles). Protein and zinc concentrations were 10 μM for AS-SOD1 and 5 μM for mAS-SOD1.

Figure 2.2. Equilibrium titrations of Zn-bound and apo-SOD1.

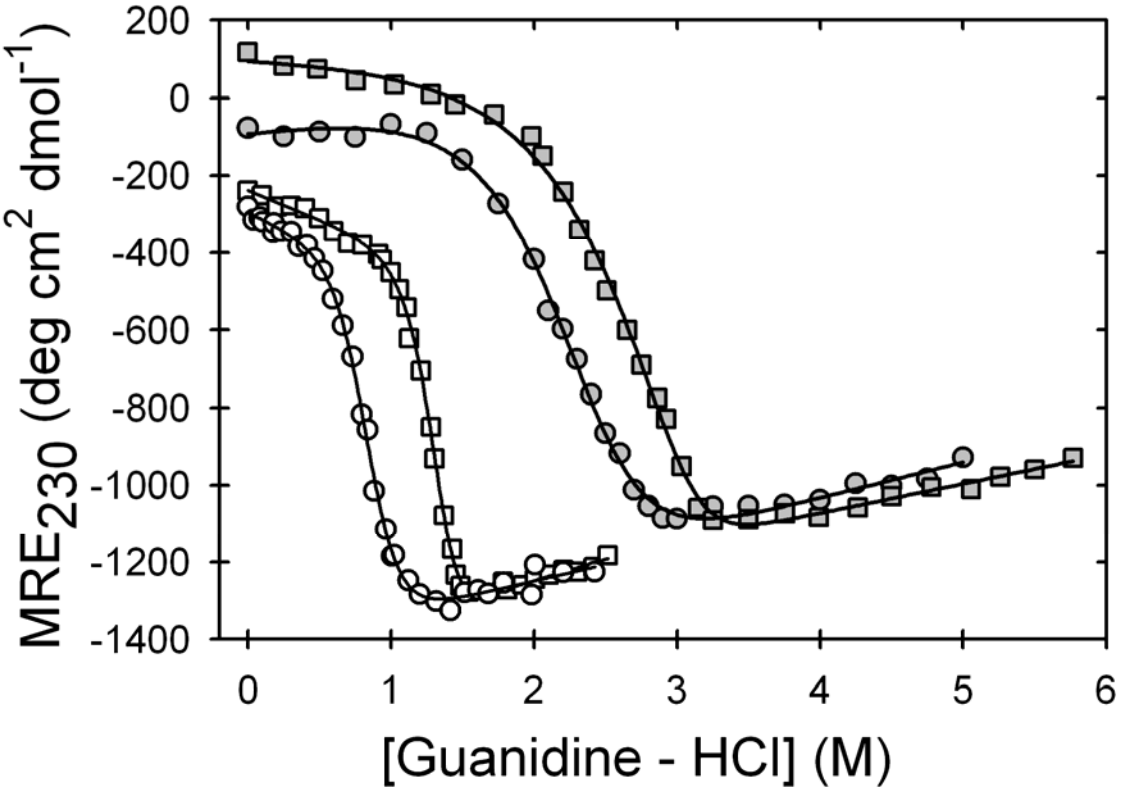

replacing two subunit interface residues, F50 and G51, with glutamic acid.[143] In the absence of zinc, the native mAS-SOD1 is stable up to ~0.7 M Gdn-HCl where it undergoes a cooperative unfolding transition that is complete by ~1 M Gdn-HCl. Similar to AS-SOD1, the addition of stoichiometric zinc to mAS-SOD1 (1 zinc per chain) significantly stabilizes the protein. The Zn-mAS-SOD1 is stable up to ~1.5 M Gdn-HCl, where it undergoes a cooperative unfolding transition that is complete by ~2.8 M Gdn-HCl.

Stoichiometry and location of zinc binding to AS-SOD1.

Inspection of the titration curves in Figure 2.2 reveal a distinctly more positive ellipticity at 230 nm under native conditions for the stoichiometric Zn-AS-SOD1, and possibly Zn-mAS-SOD1, compared to their metal-free counterparts. Realizing that this signal could be used to monitor zinc binding to the folded dimeric form of AS-SOD1, the ellipticity at 230 nm was monitored as a function of zinc concentration. The ellipticity increased linearly with increasing concentration of zinc up to the level at which the stoichiometric zinc concentration was reached (Figure 2.3). Further addition of zinc led to a decrease in the ellipticity that is complete when an equivalent of 6 zinc ions per dimer has been added. The data imply that zinc binds to at least two different sites on apo-AS-SOD1, possibly the zinc and copper sites nested in loops IV and VII (Figure 2.1).

Figure 2.3. Zn titration of AS-SOD1.

Titration of AS-SOD1 in buffer monitoring the change in ellipticity at 230 nm as a function of the zinc concentration. The titration was performed in 20 mM HEPES, pH 7.2, at 20 ^{o}C. Protein concentration was 10 µM.

Figure 2.3. Zn titration of AS-SOD1.

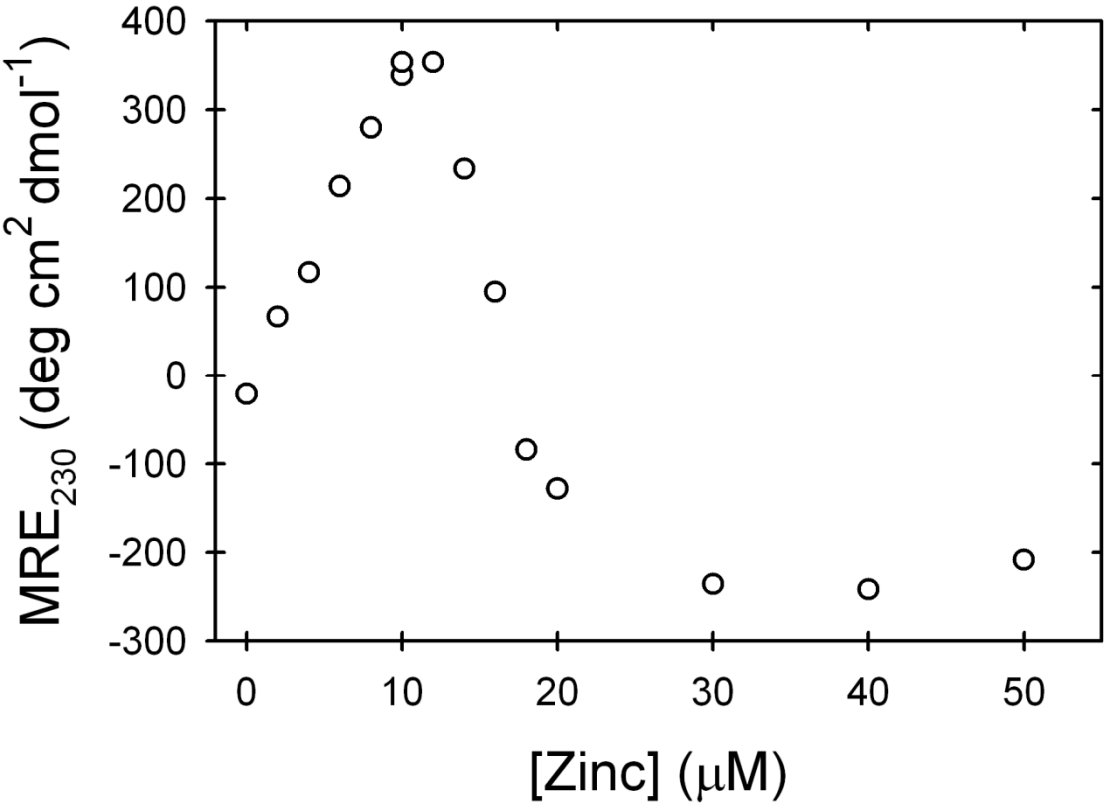

The assumption that the initial increase in ellipticity upon addition of zinc corresponds to zinc binding at the zinc site was tested using the cobalt ion as an optical probe. Cobalt is an excellent mimic for zinc because its divalent form has an ionic radius and geometric preferences that are similar to zinc. Although zinc is spectroscopically silent, cobalt gives a strong absorbance in the visible region when bound to the zinc site in SOD1. Addition of stoichiometric cobalt to apo-AS-SOD1 yielded strong absorption bands between 500 and 650 nm, very similar to the previously determined spectra of cobalt ion bound to the zinc site (Figure 2.4).[144] By contrast, the addition of stoichiometric cobalt after apo-AS-SOD1 was pre-incubated with stoichiometric zinc results in dramatically reduced absorption bands (Figure 2.4); further addition of zinc eliminates the small residual absorption band. These data show that zinc binds preferentially to the zinc site on AS-SOD1. Excess zinc binds to one or more additional sites, possibly the copper site, on each subunit. Crystallographic studies of SOD1 in the presence of excess zinc show zinc binding in the copper site,[130] and cobalt binding to the copper site produces absorption band in this same region.[144] This conclusion is also consistent with the findings of an extensive dialysis against buffer of a sample of AS-SOD1 pre-incubated with 10-fold excess zinc. Atomic absorption analysis revealed an average of 2.5 zinc ions per dimer, implying a second weaker binding site for zinc in AS-SOD1.

Zinc binding to unfolded AS-SOD1.

Figure 2.4. Cobalt binding to AS-SOD1.

Visible absorbance spectra of AS-SOD1 in 20mM HEPES, pH 7.2, at room temperature. Traces shown are protein with (A) no metal added, (B) after addition of 1 cobalt ion per monomer, (C) after pre-incubation of protein with 1 zinc ion per monomer followed by the addition of 1 cobalt ion per monomer, and (D) after pre-incubation with 6 zinc ions per monomer followed by the addition of 1 cobalt ion per monomer. The protein concentration for all four traces was 123 μM.

Figure 2.4. Cobalt binding to AS-SOD1.

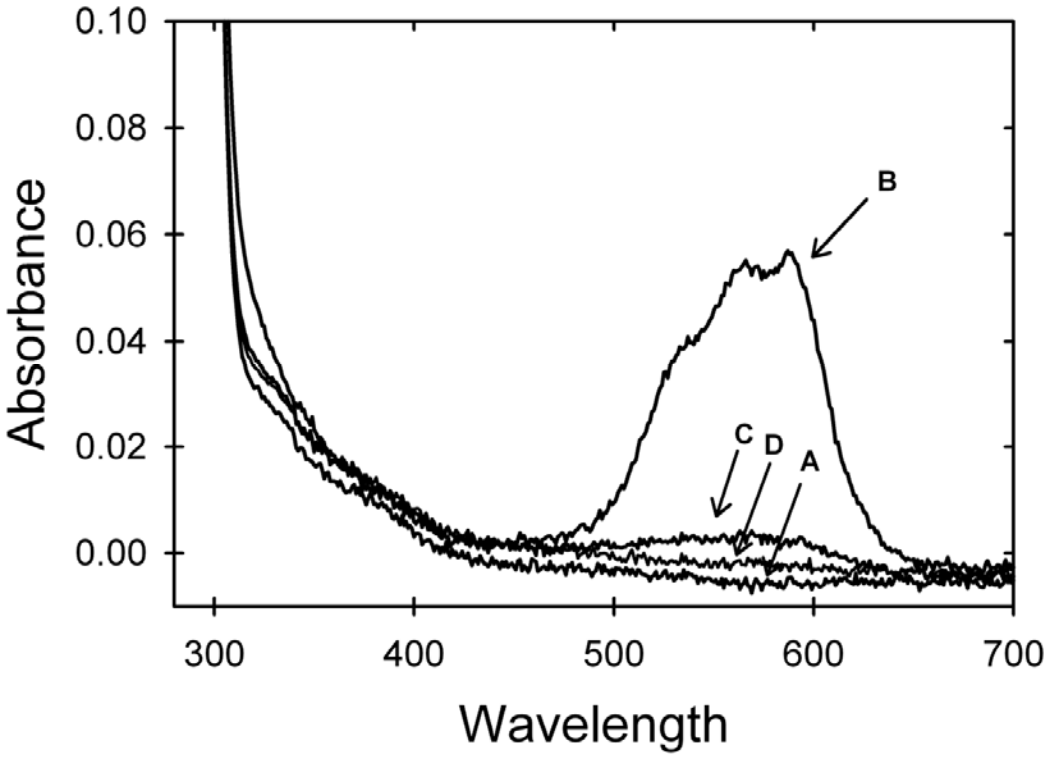

Although it is not surprising that the folded state of AS-SOD1 binds zinc in the zinc site with high affinity, it is possible that the unfolded state may also bind zinc. Previous studies on azurin[145; 146] have found that zinc can bind to the chemically-denatured protein, complicating estimates of stability by denaturation experiments. Binding to the unfolded state of AS-SOD1 was tested by synthesizing a 27-residue peptide that corresponds to the sequence containing all four zinc-binding side chains, H63, H71, H80 and D83 (Figure 2.1B). The potential acquisition of structure upon zinc binding to the peptide was monitored by Förster resonance energy transfer (FRET) from a tryptophan added at the C-terminus to an EDANS acceptor covalently attached to an additional cysteine at the N-terminus.

As shown in Figure 2.5A, the fluorescence intensity of the tryptophan emission at 360 nm decreased and the EDANS emission at 500 nm increased with increasing zinc concentration. The quenching of the tryptophan donor by the EDANS acceptor implies that zinc induces structure in the peptide in the micromolar concentration range. The affinity of this peptide for zinc was calculated by fitting the data in buffer to a simple binding isotherm (Figure 2.5B). The dissociation constant of the zinc/peptide complex is 1.1±0.1 μM, and the free energy of binding is -8.0±0.3 kcal (mol monomer)$^{-1}$ at the standard state (1 M in each component). Relevant to the denaturation analysis of AS-SOD1, the binding becomes progressively weaker in the presence of increasing Gdn-HCl concentrations to over 60 μM at 4 M Gdn-HCl. Significant zinc binding to the peptide is

Figure 2.5. Zn affinity of the peptide model of the unfolded state.

Zinc binding affinity of a peptide model of the unfolded state of SOD1. The change in fluorescence intensity of a FRET pair at the termini of a peptide encompassing the four zinc binding residues of SOD1 was monitored at various zinc concentrations and in the presence of varying amounts of Gdn-HCl. (A) The addition of zinc causes a decrease in the tryptophan fluorescence (λ_{max}= 360 nm) and a proportional increase in EDANS fluorescence (λ_{max}= 500 nm). Traces shown are at 1 M Gdn-HCl and represent zinc concentrations of 1 μM (solid line), 7 μM (dotted line), 20 μM (dashed line) and 60 μM (dashed and dotted line). (B) Quenching of the tryptophan emission at 360 nm by EDANS as zinc induces structure in the peptide of the zinc-binding loop. The isotherms shown are for 0 M Gdn-HCl (filled circles), 0.5 M Gdn-HCl (open circles), 1 M Gdn-HCl (filled upside-down triangles), 2 M Gdn-HCl (open triangles), 4 M Gdn-HCl (filled squares) and 5 M Gdn-HCl (open squares). These data represent two different preparations of the peptide with different labeling efficiencies so the intensities were normalized to the zinc-free value to show relative differences. The peptide concentration for all experiments was 4 μM in 20 mM HEPES, pH 7.2, and 20 ^{o}C.

Figure 2.5. Zn affinity of the peptide model of the unfolded state.

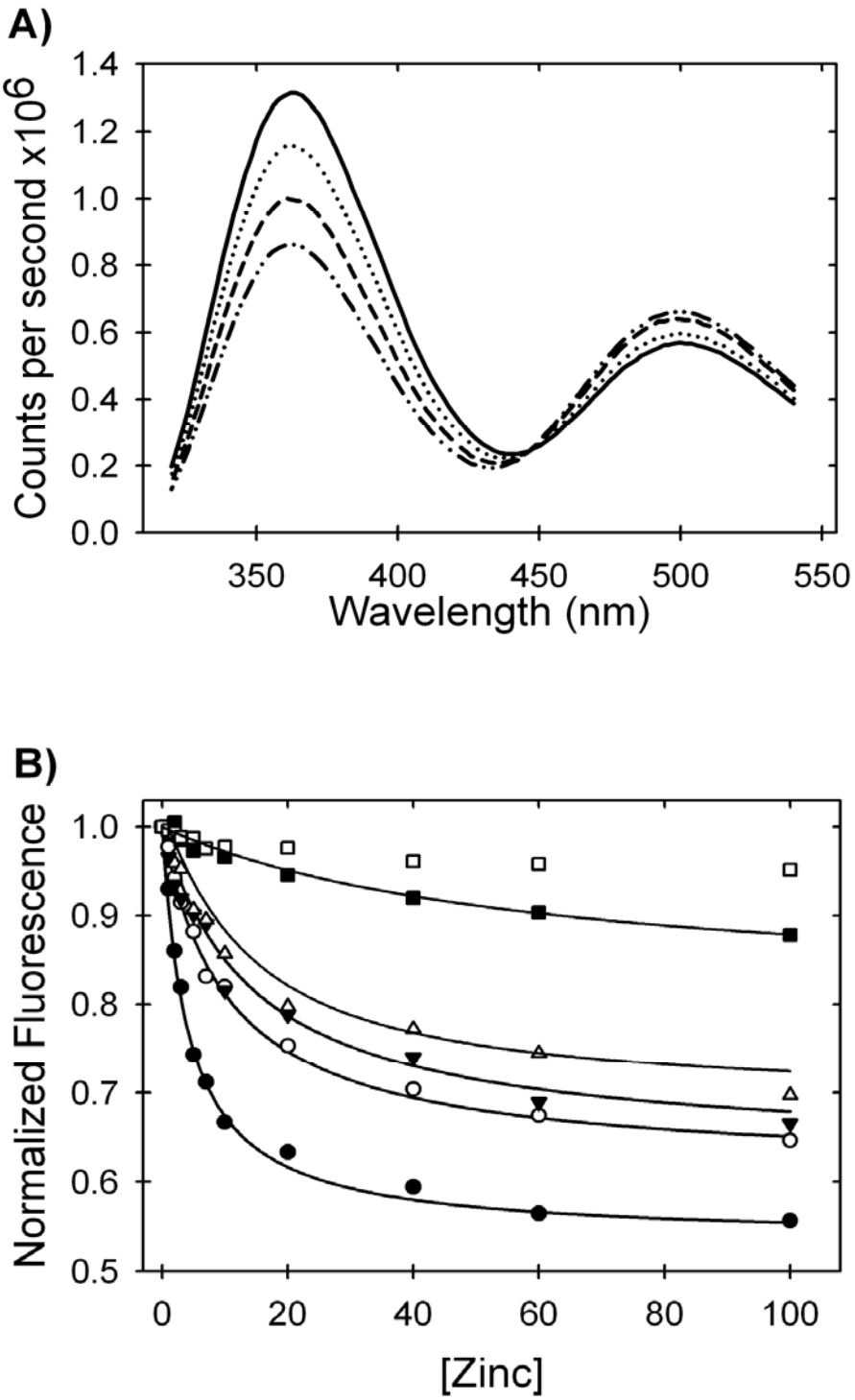

not detected above 5 M Gdn-HCl (Figure 2.5B). A plot of –RT ln(K_d), i.e., the free energy of the dissociation reaction at the standard state, ΔG_d^o, vs. the concentration of Gdn-HCl is linear (Figure 2.6). This behavior is typical of protein folding reactions when the free energy of folding is plotted vs. the concentration of denaturant. The free energy of the dissociation reaction in the absence of denaturant, ΔG_d^o, obtained by extrapolation, -7.6 kcal (mol monomer)$^{-1}$ agrees well with the value obtained by direct measurement, -8.0 kcal (mol monomer)$^{-1}$, and the denaturant dependence of ΔG_d^o, the m-value, is 0.42 kcal (mol monomer)$^{-1}$ M^{-1} (Table 2.1). Thus, under equilibrium conditions, there is a significant perturbation of the free energy of the unfolded state of SOD1 from zinc binding to the zinc-binding loop peptide. This behavior influences the Gdn-HCl unfolding reaction of SOD1 and must be accounted for in the extraction of accurate thermodynamic parameters (see below).

Thermodynamic parameters for AS-SOD1 and Zn-AS-SOD1.

The evident cooperativity of the Gdn-HCl unfolding reaction and the results of previous studies on apo-AS-SOD1 denatured in urea[114] motivated the test of a simple two-state equilibrium model for the unfolding of apo-AS-SOD1, 2U ⇆ N_2, and a three-state equilibrium model for Zn-AS-SOD1 with Gdn-HCl, 2U + 2Zn ⇆ 2(U•Zn) ⇆ $(N•Zn)_2$. The latter fits were done by fixing the change in free energy in the absence of denaturant and the m-value for the 2(U•Zn) ⇆ 2U + 2Zn step to twice the values obtained from the Zn/peptide complex described above. The accuracy of the parameters was enhanced by

Table 2.1. Equilibrium thermodynamic parameters.

Thermodynamic parameters measured at 20 ^{o}C and pH 7.2 for the Gdn-HCl induced equilibrium unfolding reactions of dimeric and monomeric apo and zinc-bound AS-SOD1 and the zinc titration of the peptide of the zinc-binding region of SOD1.

	ΔG° Kinetic	ΔG° Equilibrium	m-value Kinetic	m-value Equilibrium	K_d
Apo-mAS-SOD1[a]	-3.6±0.1	-4.3±0.1	4.9±0.3	5.1±0.5	NA[d]
Apo-AS-SOD1[b]	-20.6±0.3	-18.6±0.3	ND[c]	9.3±0.2	NA[d]
Zn-mAS-SOD1[a]	-17.0±0.7	13.4±0.6	4.6±0.3	2.6±0.2	100±122 pM[e]
Zn-AS-SOD1[b]	-49.4±1.5	-33.0±1.4	ND[c]	4.2±0.3	22±35 pM[e]
Peptide[a]	NA	-8.0±0.3	NA	0.42±0.08	1.1±0.1 μM

[a]Units for ΔG^{o} are kcal (mol monomer)$^{-1}$; units for m are kcal (mol monomer)$^{-1}$ M^{-1}.
[b]Units for ΔG° are in kcal (mol dimer)$^{-1}$; units for m are kcal (mol dimer)$^{-1}$ M^{-1}.
[c]The m-value could not be calculated because the protein concentration-dependent kinetic data in the transition region were inaccessible in Gdn-HCl.
[d]Not applicable.
[e]Calculated from kinetic parameters.

Figure 2.6. Gdn-HCl dependence of Zn binding to the unfolded state.

The Gdn-HCl dependence of the zinc-binding free energy of the peptide of the zinc binding loop. The values were obtained by simultaneously fitting the zinc titration at each wavelength of the tryptophan and EDANS emission spectra to a single binding site isotherm model. The error of reproducibility between two data sets taken on two different preparations of the peptide is ±0.65 kcal (mol monomer)$^{-1}$.

Figure 2.6. Gdn-HCl dependence of Zn binding to the unfolded state.

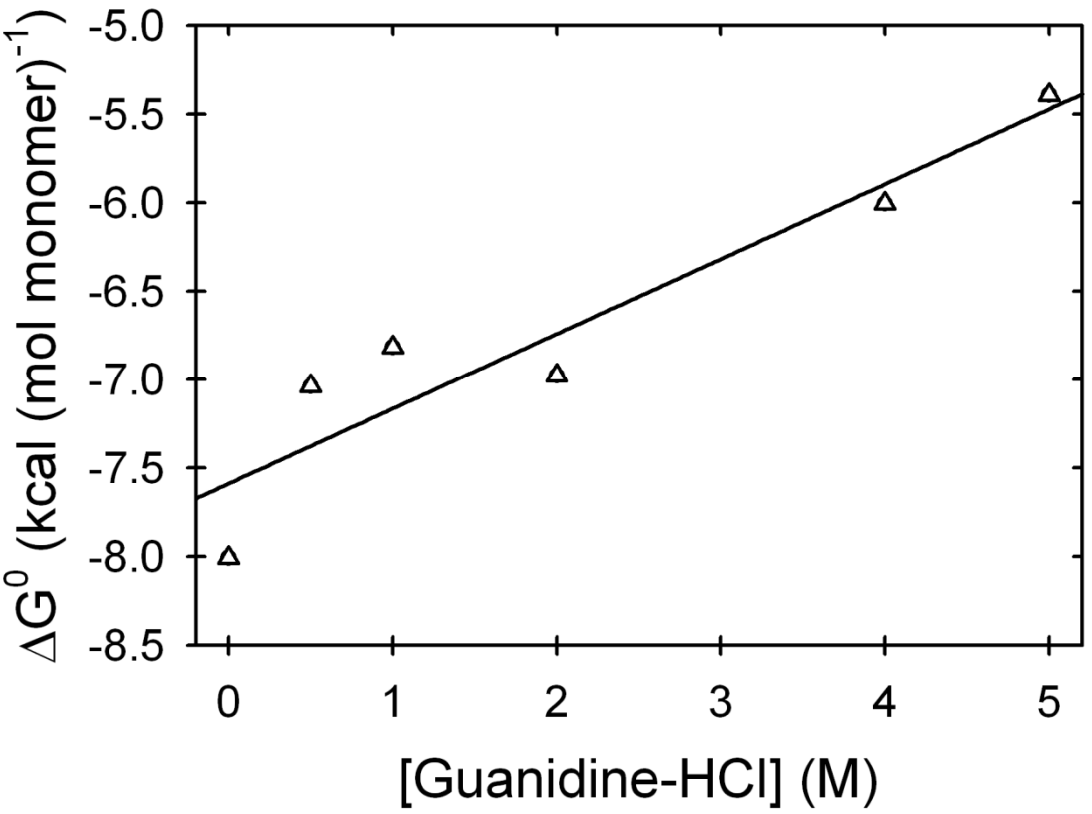

simultaneously fitting all of the CD data between 220 and 240 nm to the models for both forms (see Materials and Methods for a more detailed description of the analysis).

The stability of the apo-AS-SOD1 at standard state concentrations (1 M in each of the components), at 20 ºC and pH 7.2 is -18.6±0.3 kcal (mol dimer)$^{-1}$ (Figure 2.2 and Table 2.1), in good agreement with the previously determined value by Gdn-HCl denaturation monitored by CD, -17±2 kcal (mol dimer)$^{-1}$,[115] as well as with the value determined by urea denaturation monitored by CD, -20.4±1.0 kcal (mol dimer)$^{-1}$.[114] The denaturant-dependence of the free energy difference between the folded dimer and the unfolded monomer, the m-value, is 9.3±0.2 kcal (mol dimer)$^{-1}$ M^{-1}.

The binding of zinc increases the stability of AS-SOD1, as evidenced by the increase in the apparent midpoint of the unfolding transition from ~1.3 to ~2.6 M Gdn-HCl (Figure 2.2). Fitting the titration data to the 3-state model, $2U + 2Zn \leftrightarrows 2(U{\bullet}Zn) \leftrightarrows (N{\bullet}Zn)_2$, the free energy change and the m-value for the $2(U{\bullet}Zn) \leftrightarrows (N{\bullet}Zn)_2$ reaction were found to be -17.0±0.2 kcal (mol dimer)$^{-1}$ and 3.4±0.1 kcal (mol dimer)$^{-1}$ M^{-1}. When the free energy change for this reaction is added to that for the $2U + 2Zn \leftrightarrows 2(U{\bullet}Zn)$ reaction, -16.0±1.2 kcal (mol dimer)$^{-1}$ and 0.84 kcal (mol dimer)$^{-1}$ M^{-1}, the total free energy difference between the $(N{\bullet}Zn)_2$ and the 2U + 2Zn states is -33.0±1.4 kcal (mol dimer)$^{-1}$ at the standard state.

Surprisingly, the sum of the m-values for the folding/subunit dissociation step, 3.4±0.1 kcal (mol dimer)$^{-1}$ M^{-1}, and twice the m-value for the zinc dissociation step, 0.84 kcal (mol dimer)$^{-1}$ M^{-1}, 4.2±0.2 kcal (mol dimer)$^{-1}$ M^{-1}, is significantly lower than the m-value for apo-SOD1, 9.3±0.2 kcal (mol dimer)$^{-1}$. The magnitude of the m-value has been shown to correlate with the exposure of buried surface area during unfolding[147]. Therefore, if zinc binding induces structure in native SOD1, one might expect that the total m-value for the dimer unfolding and zinc dissociation steps would be at least equal to if not exceed the m-value for the unfolding of apo-SOD1. As will be shown below, the aberrant m-value for the unfolding of AS-SOD1 in the presence of stoichiometric zinc has another explanation.

Thermodynamic parameters for mAS-SOD1 and Zn-mAS-SOD1.

The stability enhancement for zinc binding to mAS-SOD1 was obtained by similar two-state and three-state fits of the unfolding titration data (Figure 2.2) for the apo and zinc-bound stable monomeric form (see Materials and Methods). The stability of apo-mAS-SOD1, -4.3±0.1 kcal (mol monomer)$^{-1}$ (Table 1) is in good agreement with the value previously determined by urea denaturation, -4.27±0.48 kcal (mol monomer)$^{-1}$. The m-value for the monomer unfolding reaction is 5.1±0.5 kcal (mol monomer)$^{-1}$ M^{-1}. The free energy change for the (U•Zn) ⇆ (M•Zn) reaction is -5.8±0.3 kcal (mol monomer)$^{-1}$, and the m-value is 2.3±0.1 kcal (mol monomer)$^{-1}$. When zinc binding to the unfolded

state is considered, the total free energy change for the (M•Zn) ⇆ U + Zn reaction is -13.8±0.9 kcal (mol monomer)$^{-1}$ and the total m-value is 2.6±0.2 kcal (mol monomer)$^{-1}$ M^{-1}. Similar to Zn-AS-SOD1, the m-value for the unfolding of the zinc-bound stable monomeric form is significantly less than its apo-mAS-SOD1 counterpart.

There are two possibilities for the discrepancies in the m-values for the apo- and zinc-bound forms of AS-SOD1 and mAS-SOD1. First, the reduced m-values in the presence of zinc could reflect the population of additional species in the transition region. Obvious candidates are the metal-free N state and zinc bound to non-zinc sites – possibly the copper site - evident at super-stoichiometric zinc concentrations (Figure 2.3). The possibility that zinc-bound monomers are populated is unlikely since both AS-SOD1 and mAS-SOD1 exhibit the same behavior. Kinetic analysis of the AS-SOD1 folding reaction resolves the discrepancies between the m-values and provides reliable estimates of the thermodynamic parameters sought in this study.

Kinetic analysis

The thermodynamic analysis of the equilibrium unfolding reactions of AS-SOD1, mAS-SOD1 and a peptide model for the zinc-binding loop has shown that zinc can bind to all three species in the kinetic folding mechanism. Kinetic folding studies are required to determine the effects of zinc binding on the intervening transition states. Importantly,

kinetic analysis also provides an alternative approach towards determining the magnitude of the stabilizing effect of zinc on the monomeric and dimeric forms of AS-SOD1.

Folding kinetics of AS-SOD1 and Zn-AS-SOD1.

Semi-log plots of the relaxation times as a function of the final denaturant concentration, chevron plots,[148] for apo-AS-SOD1 and Zn-AS-SOD1 are shown in Figure 2.7A. The single unfolding relaxation time for dimeric apo-AS-SOD1 decreases exponentially above 3 M Gdn-HCl, and the single refolding relaxation time decreases exponentially below 1 M Gdn-HCl. Neither phase depends upon the protein concentration under strongly unfolding or refolding conditions (data not shown). Previous studies of the urea denaturation reaction for apo-AS-SOD1,[114] have shown that the unfolding phase at high denaturant concentration corresponds to the unimolecular dissociation of the dimer. The single refolding phase observed by CD at 230 nm corresponds to the rate-limiting folding of the monomer. The non-exponential dependence in the unfolding leg of the chevron between 1.5 and 3 M Gdn-HCl reflects the coupling of the monomer refolding/unfolding and the dimer association/dissociation reactions in the transition zone.[114]

The presence of zinc has a significant effect on both the unfolding and refolding reactions of AS-SOD1 (Figure 2.7A, Table 2.2). Unfolding is slowed by 5-fold at 6 M Gdn-HCl, and refolding is accelerated by a factor of ~100-fold at 0.6 M Gdn-HCl. The denaturant

Figure 2.7. Zn-bound AS-SOD1 and mAS-SOD1 kinetics.

Observed refolding (open symbols) and unfolding (filled symbols) relaxation times for (A) AS-SOD1 and (B) mAS-SOD1 as a function of final Gdn-HCl concentration in the presence (squares) and absence (circles) of zinc as monitored by CD at 230 nm. In panel A, the dashed and dotted lines represent the linear extrapolations used to determine the relaxation times for the rate-limiting folding reactions, and the dashed lines represent the extrapolations used to determine the dimer dissociation reaction in the absence of denaturant. In panel B, the lines represent the fits of the data to simple two-state chevrons. The results yield the unfolding and refolding relaxation times and their reciprocal rate constants in the absence of denaturant. The two observed relaxation times of the unfolding of 1 zinc per dimer AS-SOD1 is shown by the open star symbols in panel A. The filled upside-down triangle in panel B is the observed relaxation time for the unfolding double-jump experiment at stoichiometric zinc concentration. Protein concentrations were 10 μM for both AS-SOD1 and mAS-SOD1, and the buffer contained 20 mM HEPES, pH 7.2, 20 ^{o}C.

Figure 2.7. Zn-bound AS-SOD1 and mAS-SOD1 kinetics.

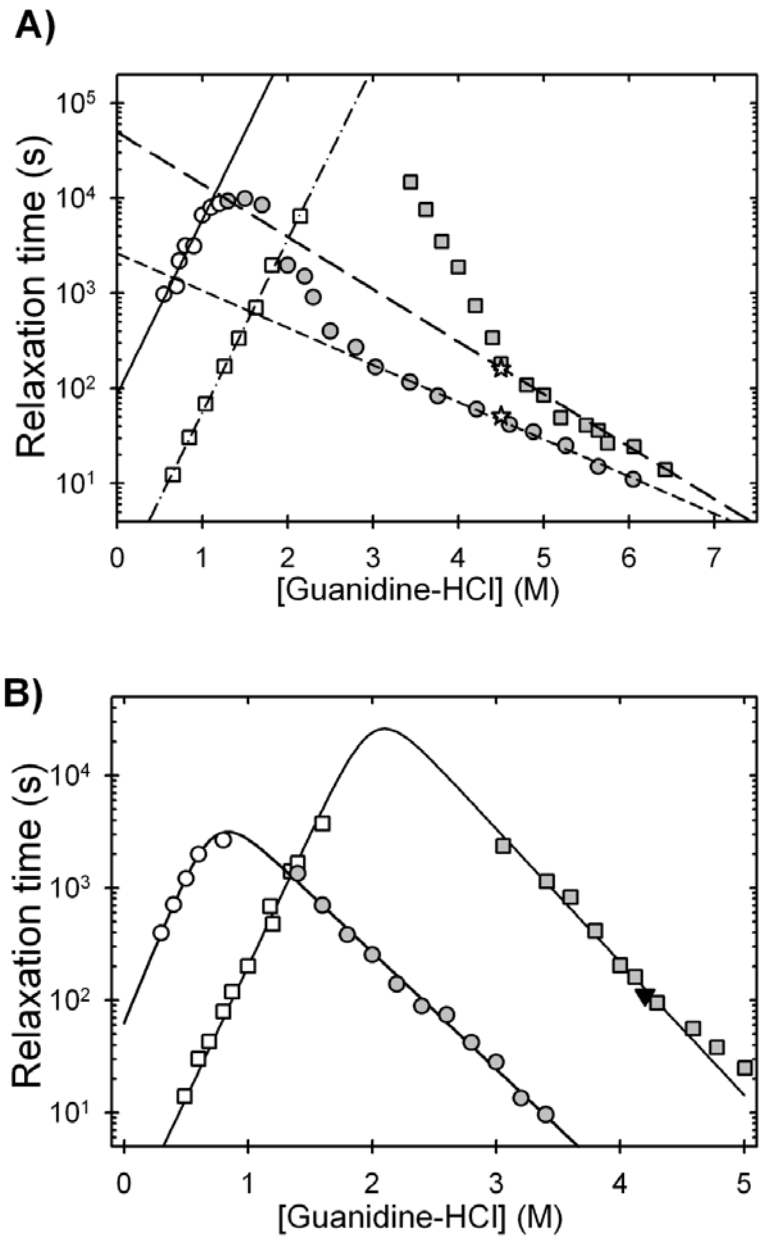

Table 2.2. Microscopic rate constants, kinetic m‡ values and the effect of zinc binding on the activation free energy of the transition state ensembles of AS-SOD1 measured at 20 oC and pH 7.2.

	Apo-AS-SOD1[a]	Zn-AS-SOD1[a]	$\Delta G^{\ddagger}$ [b] Apo-AS-SOD1	$\Delta G^{\ddagger}$ [b] Zn-AS-SOD1	$\Delta\Delta G^{\ddagger}$ [b]
k_f [c]	0.012±0.002	1.19±0.05	5.2±0.2	0.2±0.08	-5.0±0.1
$m_f^{\ddagger}$ [c]	3.17±0.53	3.13±0.01	NA[h]	NA	NA
k_u [d]	$(3.1\pm1.5)\times10^{-5}$	$(2.0\pm1)\times10^{-7}$	-12.0±0.6	-18.0±0.6	6.0±0.7
$m_u^{\ddagger}$ [d]	-1.39±0.07	-1.45±0.11	NA	NA	NA
k_a [e]	$(6.9\pm8.3)\times10^{6}$	$(6.9\pm8.3)\times10^{6}$	18.2±1.2	18.2±1.2	0
$m_a^{\ddagger}$	ND[g]	ND	NA	NA	NA
k_d [f]	$(38.1\pm0.9)\times10^{-5}$	$(2.1\pm0.4)\times10^{-5}$	-4.6±0.1	-6.3±0.1	1.7±0.1
$m_d^{\ddagger}$ [f]	-0.67±0.03	-0.95±0.06	NA	NA	NA

[a]Units for the monomer folding rate constants (k_f), unfolding rate constants (k_u), dimer association rate constants (k_a) and dimer dissociation rate constants (k_d) are s^{-1}; units of the denaturant dependence of monomer folding ($m_f^{\ddagger}$) and unfolding ($m_u^{\ddagger}$) rate constants are kcal (mol monomer)$^{-1}$ M^{-1}, and units for the denaturant dependence of the dimer dissociation rate constant ($m_d^{\ddagger}$) are kcal (mol dimer)$^{-1}$ M^{-1}.

[b]Units for the activation free energy barrier ($\Delta G^{\ddagger}$) and the change in the free energy barrier upon zinc binding to the transition state ensemble ($\Delta\Delta G^{\ddagger}$) are kcal (mol dimer)$^{-1}$.

[c]Calculated from the linear extrapolation of the refolding leg of the AS-SOD1 chevron (Figure 6A).

[d]Calculated from the 2-state fit of the mAS-SOD1 chevron (Figure 6B).

[e]The dimer association rate constant was taken from Svensson et al. (Manuscript in preparation)

[f]Calculated from the linear extrapolation of the >5.5 M Gdn-HCl region of the unfolding leg of the zinc-bound AS-SOD1 chevron and the >3.8 M Gdn-HCl region of the unfolding leg of the apo-AS-SOD1 chevron (Figure 2.7A).

[g]Not determined.

[h]Not applicable.

dependence of the dimer dissociation relaxation time in the presence of zinc between 5.5 and 6.8 M Gdn-HCl, -0.95±0.06 kcal (mol dimer)$^{-1}$ M^{-1}, is larger than that for apo-AS-SOD1 between 3.8 M and 6.0 M Gdn-HCl, -0.67±0.03 kcal (mol dimer)$^{-1}$ M^{-1}. As a result, the dimer dissociation relaxation time in the absence of denaturant, estimated by linear extrapolation, is ~20-fold longer in the presence of zinc. The small increase in the denaturant dependence of the relaxation time implies an enhancement of structure as the zinc-binding and electrostatic loops are organized by zinc binding. Given the quite similar denaturant dependence of the refolding relaxation times for apo- and Zn-AS-SOD1, the kinetic refolding data yield a 100-fold acceleration of the refolding rate by zinc in the absence of Gdn-HCl. Although the linear extrapolations in Gdn-HCl may be questioned,[149] the differences between the extrapolated relaxation times in the presence and absence of zinc should be minimal.

Valentine and her colleagues,[131] on the basis of isothermal titration calorimetry experiments, have proposed that the binding of the first zinc ion to the SOD1 dimer may contribute the majority of the stability induced by zinc binding. By implication, the 1 zinc per dimer species should comprise the entire population at half saturation. This conclusion was investigated by incubating AS-SOD1 with 1 zinc ion per dimer and monitoring the unfolding reaction. The observed unfolding reaction could not be fit to a single exponential expected for a homogeneous population. When fit to two exponentials, the observed relaxation times corresponded well with the unfolding relaxation times of

the apo-protein and the zinc-bound protein (Figure 2.7). This result is better explained by a binomial distribution of zinc in the two zinc sites per dimer, reflecting the metal-free protein, the half-saturated protein and the fully-saturated protein. The absence of a third phase suggests that the unfolding relaxation time of the 1 zinc per dimer species is similar to that for the 2 zinc per dimer species. As noted above, the unfolding of AS-SOD1 incubated with 2 zinc per dimer is well described by a single exponential at the same concentration of Gdn-HCl (Figure 2.7). The discrepancies between these results and those from the Valentine laboratory may reflect the different pH values at which the two studies were performed. It is likely that the histidines that ligate zinc are protonated at pH 5.5, where the isothermal titration calorimetry studies were done. The zinc binding properties would undoubtedly be altered from those at pH 7.2, perhaps to include a preferential binding of the first zinc ion to the dimeric protein.

Attempts to visualize the protein concentration dependence in the transition region, 1.5 to 3.0 M Gdn-HCl, as previously observed for the urea denaturation reaction[113; 114] and required for the determination of the association rate constant, were not successful. The relaxation times in this Gdn-HCl concentration range exceed experimental limitations, $>10^5$ s, precluding accurate measurements.

Folding kinetics for mAS-SOD1.

In the absence of direct information on the association reaction, the effect of zinc binding on refolding/unfolding reactions of the stable monomer, mAS-SOD1, was examined. Oliveberg and his colleagues[119] have previously used this approach towards partitioning the global free energy change for the unfolding of AA-SOD1 into its monomer folding reaction and monomer/dimer association reaction components. In the absence of zinc, apo-mAS-SOD1 unfolds via a simple exponential reaction whose relaxation time decreases linearly with increasing denaturant concentration from ~1 to ~ 3.5 M Gdn-HCl (Figure 2.4B). The single refolding relaxation time decreases linearly with decreasing Gdn-HCl below ~1 M denaturant, and the two legs of the chevron intersect at ~ 1 M Gdn-HCl. The maximum in the relaxation time corresponds closely with the mid-point in the equilibrium titration for apo-mAS-SOD1 (Figure 2.2), as expected for a simple two-state folding reaction[148]. Extrapolation of both relaxation times, τ, to the absence of denaturant yields rate constants, k ($k = 1/\tau$) of $k_u = 3.05\times10^{-5}$ s^{-1} for unfolding and $k_f = 0.015$ s^{-1} for refolding. The denaturant dependence of the rate constants, the $m^{\ddagger}$ values, are -1.4 and 3.5 kcal (mol monomer)$^{-1}$ M^{-1}, respectively. The free energy of folding of apo-mAS-SOD1, estimated from $\Delta G^0 = -RT \ln(k_u/k_f)$, is -3.6±0.1 kcal (mol monomer)$^{-1}$, in reasonable agreement with the stability estimated from the equilibrium titration, 4.3±0.1 kcal (mol monomer)$^{-1}$ (Table 2.1).

The kinetic consequences of unfolding and refolding mAS-SOD1 in the presence of stoichiometric zinc are to increase the unfolding relaxation time by ~110-fold at 3 M

Gdn-HCl and to decrease the refolding relaxation time by ~100-fold at 0.6 M Gdn-HCl (Figure 2.4B). As in the case of the dimeric AS-SOD1, the refolding relaxation time is independent of the zinc concentration at and above stoichiometric zinc concentrations (data not shown). Below stoichiometric zinc concentrations, a small faster phase with a relaxation time equal to that for apo-mAS-SOD1 appears (data not shown). The two phases reflect the independent folding of the zinc-bound unfolded and zinc-free unfolded AS-SOD1. The $m^{\ddagger}_{u}$ and $m^{\ddagger}_{f}$ values in the presence of zinc are similar to those in the absence of zinc, insuring that the differences in the relaxation times observed in Gdn-HCl are maintained in the absence of denaturant.

Preferential binding of zinc to the zinc site in refolding was tested by a double-jump experiment. Metal-free mAS-SOD1 was unfolded in 3.9 M Gdn-HCl, and then refolded by a 10-fold dilution to 0.4 M Gdn-HCl containing stoichiometric zinc. After 30 s of refolding, approximately three times the refolding relaxation time under these conditions (Figure 2.4A), the protein was unfolded in 4.2 M Gdn-HCl and the unfolding reaction was monitored by CD. The observed unfolding relaxation time is within error to the observed relaxation time for a single-jump unfolding reaction to the same final conditions when the protein is incubated with stoichiometric zinc in the native state (Figure 2.7B). Given the preferential binding of zinc to the zinc site in native AS-SOD1 (Figure 2.4), zinc must also bind preferentially to the zinc site during the refolding reaction.

The obvious perturbations of the unfolding and refolding relaxation times for mAS-SOD1 at stoichiometric concentrations of monomer and zinc (Figure 2.7B) and the knowledge that zinc binds to both folded and unfolded protein in low concentrations of denaturant allows a simple two-state analysis of the U•Zn ⇆ M•Zn reaction from the chevron. The free energy difference between these states, $\Delta G = -RT \ln(k_u/k_f)$, is -9.0±0.1 kcal (mol monomer)$^{-1}$ in the absence of denaturant. When this value is added to the free energy of binding of zinc to the peptide model of the unfolded state, -8.0±0.3 kcal (mol monomer)$^{-1}$, the free energy of the zinc-bound folded monomeric form relative to the zinc-free unfolded state is found to be -17.0±0.4 kcal (mol monomer)$^{-1}$.

The kinetic chevrons for apo-mAS-SOD1 and Zn-mAS-SOD1 also provide a resolution to the anomalously low m-value for the equilibrium titration of Zn-mAS-SOD1. For two-state reactions, the sum of the absolute values of the kinetic $m^{\ddagger}$-values is equal to the m-value for the equilibrium titration. The equilibrium m-value for apo-mAS-SOD1, 5.1±0.5 kcal (mol monomer)$^{-1}$ M^{-1}, is in good agreement with the value determined from the rate constants for folding and unfolding, 4.9±0.1 kcal (mol monomer)$^{-1}$ M^{-1}. By contrast, the equilibrium m-value for Zn-mAS-SOD1, 2.6±0.2 kcal (mol monomer)$^{-1}$ M^{-1} is about half that of the value determined from the chevron for this system, 4.6±0.1 kcal (mol monomer)$^{-1}$ M^{-1}. These contradictory estimates for the equilibrium m-value reflect the complexity of the equilibrium Zn-mAS-SOD1 folding reaction. At equilibrium in the transition zone, the m-value is sensitive to the presence of all of the states that bind zinc

and are significantly populated under these conditions. The kinetic experiment, by contrast, reveals the rate constants for specific steps in the mechanism, U•Zn → M•Zn, and M•Zn → U•Zn, that pass through a common transition state ensemble. The sum of the absolute values of the denaturant dependences of these rate constants provides an accurate measure of the equilibrium m-value and, with the extrapolated intercepts of the rate constants, an accurate estimate of the stability of the Zn-mAS-SOD1 not available from the equilibrium titration experiment.

The good agreement between the m-values for apo-mAS-SOD1 and Zn-mAS-SOD1 obtained from the kinetic analysis (Table 2.2) implies that the buried surface induced by zinc binding is similar for the M•Zn, the U•Zn and the intervening TSE compared to their respective apo-states. If zinc were binding to non-zinc sites in unfolded AS-SOD1 so as to reduce the equilibrium m-value by a factor of two, one might expect to observe a significant decrease in the $m^{\ddagger}_{f}$-value for the folding reaction. The very similar $m^{\ddagger}_{f}$-values for apo- and Zn-mAS-SOD1 (Figure 2.7 and Table 2.2) argue against this possibility.

Reaction coordinate diagram for Zn-AS-SOD1.

The folding data for the apo- and zinc-bound forms of AS-SOD1 and mAS-SOD1 and the thermodynamic data for the binding of zinc to the peptide model of the zinc binding loop can be combined to determine the effect of zinc on the folding reaction coordinate diagram of AS-SOD1 under standard state conditions. The free energies are those for the

dimeric systems: $2U \leftrightarrows 2M \leftrightarrows N_2$ for apo-AS-SOD1 and $2(U\bullet Zn) \leftrightarrows 2(M\bullet Zn) \leftrightarrows (N\bullet Zn)_2$ for Zn-AS-SOD1. Although the conversion of the kinetic data to transition state energies depends upon the formalism adopted,[150] the perturbations in the free energies of the transition states induced by zinc binding should, to a first-approximation, be independent of the formalism because the same kinetic mechanisms are operative.

The procedure by which the thermodynamic and kinetic data on the folding of Zn-AS-SOD1 were converted into a reaction coordinate diagram was as follows:

The unfolded apo-monomer, 2U, was chosen as the reference state for both the apo-AS-SOD1 and Zn-AS-SOD1 diagrams (Figure 2.8).

The energy of the unfolded zinc-bound monomer, U•Zn, relative to the U state was determined by converting the dissociation constant for the zinc-peptide complex using $\Delta G = -RT \ln(K_d) = -8.0$ kcal (mol monomer)$^{-1}$ (Table 2.1). For the dimeric system, the free energy of the 2(U•Zn) state is -16.0 kcal (mol dimer)$^{-1}$ lower than that of the 2U state.

Figure 2.8. The folding free energy surface of Zn-AS-SOD1

Reaction coordinate diagrams of apo-AS-SOD1 and Zn-AS-SOD1 in the dimer reference frame and at the standard state, 1 M in each of the components. Apo-states are depicted in gray, while zinc-bound states are shown in black. Solid lines are thermodynamic states, where 2U is the unfolded state, 2M is the folded monomer and N_2 is the native dimer. Dotted lines represent the energies of the transition states, where $2TSE_M$ is the transition state ensemble of monomer folding and TSE_D is the transition state ensemble of dimer formation. The absolute values of the TSE energies depend upon the formalism chosen to determine these energies. All changes in free energy induced by zinc binding, reported under the bar representing the zinc-bound states, are given in units of kcal $(\text{mol dimer})^{-1}$.

Figure 2.8. The folding free energy surface of Zn-AS-SOD1.

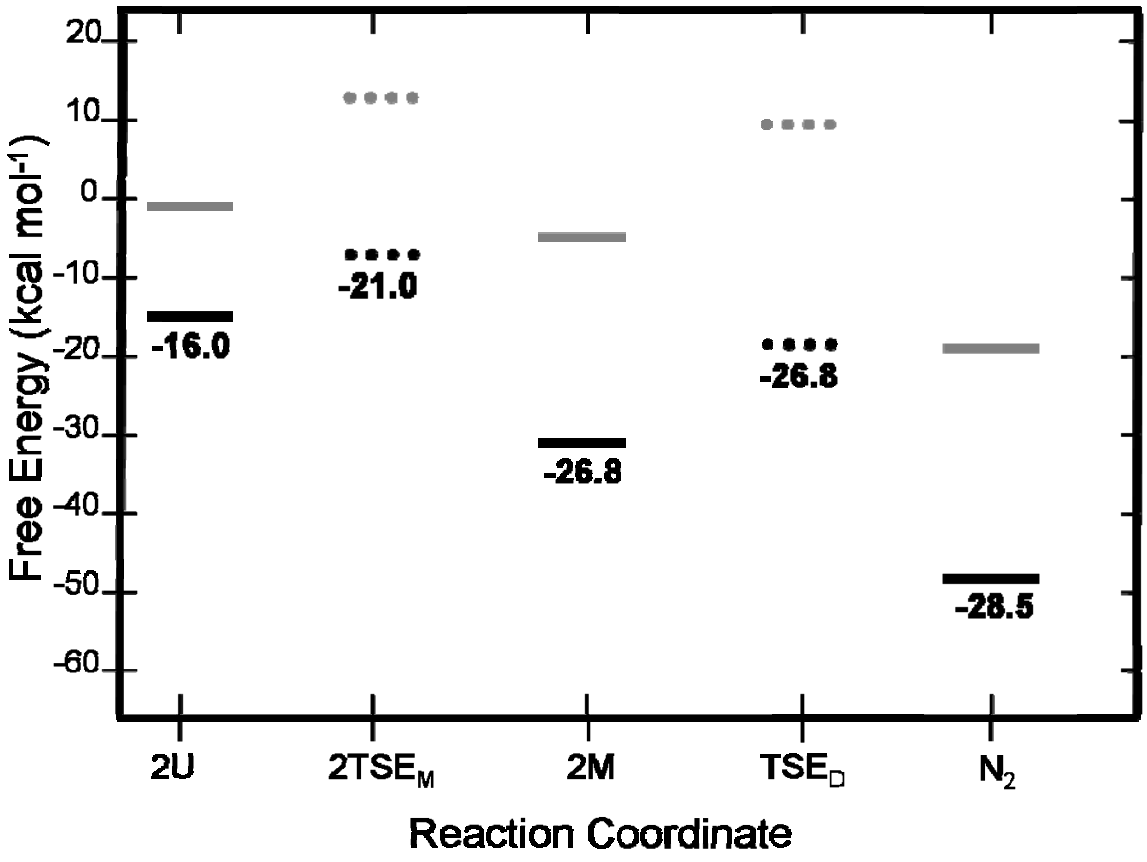

The chevron analysis of apo-mAS-SOD1 (Figure 2.7B) revealed that the folded monomeric state, 2M, is -7.2 kcal (mol dimer)$^{-1}$ lower than the 2U state.[114] The thermodynamic stability of Zn-mAS-SOD1 was calculated by fitting its kinetic chevron to a two-state model, and the free energy difference between the U•Zn ⇆ N•Zn states was determined from $\Delta G^o = -RT\ln(k_u/k_f)$ to be -9.0 kcal (mol monomer)$^{-1}$. The binding free energy of zinc to the unfolded state, U+Zn ⇆ U•Zn, -8.0 kcal (mol monomer)$^{-1}$, was added to yield a total free energy for the U+Zn ⇆ U•Zn ⇆ N•Zn reaction of -17.0 kcal (mol monomer)$^{-1}$. The energy of the 2(M•Zn) state is -34.0 kcal (mol dimer)$^{-1}$ lower than the 2U state and -26.8 kcal (mol dimer)$^{-1}$ less than that of the 2M state. Therefore Zn-mAS-SOD1 is 13.4 kcal (mol monomer)$^{-1}$ more stable than apo-mAS-SOD1 (Table 2.1).

The free energy of the $(N•Zn)_2$ state was calculated by the sum of twice the free energy of the Zn-mAS-SOD1 and the free energy change for the dimerization reaction. The latter free energy change was calculated from the dissociation rate constant, $k_d = 2.1\times10^{-5}$ s^{-1}, obtained by linear extrapolation of the unfolding relaxation time at high denaturant concentration (Figure 2.7A) and the association rate constant, $k_a = 6.9\times10^{6}$ M^{-1} s^{-1}, determined by global kinetic analysis of the urea-denaturation reaction.[117] These rate constants yield a $\Delta G^o_{2U/N2} = 2(\Delta G^o_{U/M}) - RT\ln(k_a/k_d)$ = -49.4 kcal (mol dimer)$^{-1}$ for the $(N•Zn)_2$ state relative to the 2U + 2Zn state. The same calculation performed for the metal-free AS-SOD1 yields a free energy difference of -20.9 kcal (mol dimer)$^{-1}$ for the

N_2 state relative to the 2U state. Therefore, the free energy of the $(N•Zn)_2$ state is 28.5 kcal (mol dimer)$^{-1}$ less than the N_2 state.

The activation free energy of the transition state ensemble for the 2M ⇆ N_2 reaction, TSE_D, was placed relative to the M state using the Eyring formalism, $\Delta G^{‡} = -RT \ln[(k_a h)/k_B T)]$, where k_a is the association rate constant in the absence of denaturant, 6.9×10^6 M^{-1} s^{-1}, h is the Planck constant, k_B is the Boltzmann constant and T is the absolute temperature; $\Delta G^{‡}$ =18.2 kcal (mol dimer)$^{-1}$. The TSE_D for the 2(M•Zn) ⇆ $(N•Zn)_2$ reaction, relative to the (M•Zn) state, is identical to that for the metal-free M state because the association reaction is near diffusion-limited and, therefore, will not be affected by zinc binding.

The activation free energy for the transition state ensemble for the 2U ⇆ 2M reaction, $2TSE_M$, can be placed with the rate constant for folding in the absence of denaturant, 0.008 s^{-1}, and the Erying formalism as described above. Similarly, the $2TSE_M$ for the 2(U•Zn) ⇆ 2(M•Zn) reaction can be placed relative to the 2(U•Zn) state, recognizing that the 100-fold acceleration in folding due to zinc binding corresponds to a decrease in the barrier of 5.0 kcal (mol dimer)$^{-1}$ (Table 2.2).

It is evident that zinc binding perturbs the entire folding reaction coordinate for AS-SOD1. The implications of this observation for the unfolding/aggregation hypothesis for ALS are discussed below.

Discussion

Modulation of the folding free energy surface

The thermodynamic and kinetic data for the effects of zinc binding on the folding and stability of AS-SOD1 (Tables 2.1 and 2.2) provide quantitative answers to the following questions about the role of zinc in protecting cells against the aggregation of partially-folded states of SOD1.

At what stage of the folding reaction does zinc become bound to SOD1 and potentially offer protection against aggregation? Zinc binds rapidly to the zinc site in the unfolded state with micromolar affinity *in vitro* and remains bound throughout the reaction. The binding of zinc to the peptide model for unfolded SOD1 provides a ready explanation for its dramatic acceleration of the monomer folding reaction *in vitro* and offers insights into the source of the very slow folding reaction for apo-AS-SOD1 (see below). The nanomolar concentration of free zinc in cells,[151] however, is not sufficient to saturate the zinc-binding loop segment, and the lifetime of unfolded SOD1 would be that of the metal-free protein following synthesis on the ribosome.

What are the quantitative ramifications of zinc binding on the propensity of the native dimer and the folded monomer to populate, at equilibrium, less well structured states that

may be prone to aggregate? Zinc binding significantly stabilizes the native dimer and folded monomer relative to the unfolded state by comparable amounts, -28.5±1.8 and -26.8±0.8 kcal (mol dimer)$^{-1}$ respectively, at the standard state of 1 M in each component. The calculated zinc dissociation constants (Table 2.2) are within the range, 10^{-8} and 10^{-14} M^{-1}, which have been reported previously.[127; 131] The wide range of affinities are likely the result of different buffer conditions used. Correcting to a 10 μM standard state, subtracting –RT ln[protein] = +6.7 kcal (mol monomer)$^{-1}$ for mAS-SOD1 and –3RT ln[protein] = +20.1 kcal (mol dimer)$^{-1}$ for AS-SOD1, the zinc-bound monomer is stabilized 6.7 kcal (mol monomer)$^{-1}$ relative to the metal-free monomer state and the relative population of the metal-free monomer would decrease by 10^5-fold. Zinc stabilizes dimeric AS-SOD1 by 14.8 kcal (mol dimer)$^{-1}$, corresponding to a decrease in the relative population of the metal-free dimer of 10^{11}. Thus, the effects of zinc binding on all of the species in the reaction coordinate diagram are dramatic.

Chakrabartty and coworkers have recently demonstrated that the major unfolding pathway of SOD1 at high concentrations of Gdn-HCl involves the initial dissociation of the dimer coupled with zinc release. Subsequently, the monomer unfolds and copper is released.[111] The results of this study may appear surprising given the very high affinity of SOD1 for zinc at neutral pH. However, as acknowledged by the authors, zinc dissociation could occur either during dimer dissociation or subsequently via a rapid reaction. The results of the present study support the latter possibility in that zinc dissociation from the

unfolded state, U, follows the rate-limiting dimer dissociation reaction and the faster monomer unfolding reaction.

Does zinc binding alter the relative populations of monomeric and dimeric forms of SOD1 at equilibrium? Although the propagation of error analysis finds the stabilities of monomeric and dimeric AS-SOD1 to be comparable (Table 2.1), the 20-fold slower dissociation of Zn-AS-SOD1 vs. AS-SOD1 shows that zinc actually stabilizes dimeric AS-SOD1, relative to monomeric AS-SOD1, by 1.7 kcal (mol dimer)$^{-1}$. The lower free energy for the $(N•Zn)_2$ state relative to the 2(M•Zn) state means that the equilibrium between the monomeric and dimeric zinc-bound states will shift to favor the native dimer of AS-SOD1 in the presence of zinc. Although the major protective effect of zinc binding on SOD1 would be to decrease the relative populations of metal-free forms, the decrease in the population of the zinc-bound folded monomeric form might also be a factor.

Implications for aggregation

The capacity of all of the components in the folding mechanism of wild-type SOD1, including the TSEs, to bind zinc has significant implications for the aggregation propensity of ALS-inducing variants. It has been shown that zinc-bound SOD1 is very resistant to aggregation, reinforcing the structural and protective role of zinc.[101] Two distinct scenarios for aggregation can be envisioned, an equilibrium scenario and a

kinetic scenario. The equilibrium scenario involves fully-folded disulfide-bonded protein occasionally sampling partially-folded or unfolded aggregation-prone states, whereas the kinetic scenario involves the aggregation of transient folding intermediates that are highly populated during the folding reaction following synthesis on the ribosome.

Equilibrium scenario.

The sub-nanomolar binding of zinc to native dimeric SOD1, coupled with the intrinsic affinity of the metal-free subunits for each other,[114] means that the coupled equilibria will flow towards the dimeric state for the wild-type protein. As a result, the populations of all zinc-free states will decrease. Conversely, ALS variants containing mutations that lead to the loss of metal binding[83] will shift their populations toward zinc-free monomeric states. For example, the population of the monomeric metal-free form of AS-SOD1 would increase by 20-fold relative to its metal-bound wild-type counterpart for a 10 μM concentration of the metal-binding variants. Due to the higher order nature of aggregation reactions, even small changes in the concentration of these aggregation prone species can be amplified into a large change in the rate of aggregation.

One possible scenario is partial unfolding of the monomeric intermediate state, leaving the protein susceptible to aggregation. Oliveberg and his colleagues have argued that β5 and β6, edge strands in the β-sandwich (Figure 2.1), serve as gate keepers for the β-

sandwich by preventing the aggregation of the monomeric species.[123; 124] The boundary position of these two β-strands would make them logical candidates for spontaneous dissociation in a rapidly-interconverting ensemble of conformers in a manifold of states representing the folded monomer of SOD1. Supporting this model are molecular dynamics simulations which have predicted that mutations and dimer destabilization have the effect of partially unfolding β5 and β6.[152] The disorder induced in the zinc-binding and electrostatic loops in the absence of zinc could propagate to the adjacent β5 strand (Figure 2.1) and, thereby, enhance the propensity for aggregation of monomeric SOD1 in the absence of zinc. The increased tendency for metal-free ALS variants to bind hydrophobic dyes may be a manifestation of this phenomenon.[47]

Alternatively, the unfolded state could provide a platform for aggregation. The micromolar affinity of the unfolded state for zinc and the sub-nanomolar affinities (Table 2.1) of the folded monomeric and dimeric states of AS-SOD1 means that the unfolded state will not bind zinc, but the folded monomeric intermediate and the dimeric native state will be saturated at nanomolar concentrations of zinc *in vivo*[151] for the wild-type protein. The folded states of metal-binding variants, which would not be stabilized by metal binding, will not benefit from this shift in equilibrium for the wild-type protein towards more folded states in the presence of zinc. Once again, this effect will be amplified in the rate of aggregation by the higher order kinetics that characterize multi-component reactions.

Kinetic scenario.

Arguments have also been made for a kinetic pathway for aggregation, where polypeptide chains misfold and aggregate after synthesis.[153] The micromolar dissociation constant for zinc binding to a peptide model for unfolded SOD1 means that the folding reaction cannot be accelerated and the lifetime of the unfolded state decreased by nanomolar zinc concentrations *in vivo*. The increased temperature in motor neurons, 37 ºC vs. 20 ºC *in vitro*, would only serve to decrease the affinity of zinc for the unfolded state because zinc binding is exothermic.[131] As a result, immediately following synthesis on the ribosome, zinc would not be expected to offer protection against aggregation of unfolded, disulfide-reduced ALS-inducing variants of SOD1.

Implications for the folding mechanism of SOD1.

The significant acceleration of the monomer folding rate by the binding of zinc to unfolded AS-SOD1 provides insights into the structure of the TSE_M. A previous mutational analysis of monomeric SOD1 revealed that β1-β4 and β7, representing contributions from both sides of the β-sandwich (β1/β2/β3 and β4/β7; Figure 2.1), are integral components of the TSE_M.[124] A surprising property of the zinc-free monomer folding reaction is its very small rate constant, 0.012 s^{-1} (Table 2.2). This value is ~10^4 less than the rate constant predicted by the relative contact order, a measure of the sequence separation between contacting residues in the native structure, of the fully-

folded SOD1 monomer.[154] This significant discrepancy shows an important aspect of the rate-limiting folding reaction is not captured by this topological metric. The 100-fold acceleration of this reaction by zinc suggests that disorder in the zinc-binding loop might be partially responsible. Application of an algorithm to assess the propensity for disorder, PONDR,[155] to the SOD1 sequence reveals that the zinc-binding loop and, to a lesser extent, the electrostatic loop as well as β5 and β6 are expected to be natively disordered. The prediction for disorder in the loops and in β5 is in accord with experimental observations on monomeric SOD1.[35; 36] Both of these loops follow β-strands that are adjacent and integral to the β-sheet on one side of the β-sandwich, β4 and β7, and these loops pack on each other in the fully-folded structure (Figure 2.1). Thus, the pre-organization of the zinc-binding loop in the presence of zinc and its potential recruitment of the electrostatic loop might be expected to enhance the probability of accessing the crucial β4/β7 pair of strands in the TSE_M. The significance of C-terminal organization is also consistent with slower refolding kinetics observed for disulfide-reduced SOD1,[113] in which the crosslink between C57 and C146 near the C-terminus is absent. It would be interesting to test the proposed involvement of the zinc and electrostatic loops in the TSE_M by performing a mutational analysis on side chains in these loops in the presence and absence of zinc.

Overview on ALS-inducing variants of SOD1.

The biophysical analyses presented previously[104; 115; 124; 156] support a general mechanism for the gain-of-function via aggregation of partially-folded states whose populations are enhanced in ALS-inducing variants of SOD1. As would be expected for a highly cooperative system, the contributions of the inherent protein stability, the disulfide bond and the affinity for metal binding are strongly coupled.[37; 141] This coupling is evident in the present study by the enhanced binding of zinc along the reaction coordinate. It is also evident in previous studies by the loss of affinity for zinc of aggregation-prone ALS variants.[83] and by the increased susceptibility of ALS variants for disulfide bond reduction.[157] Although chaperones and proteosomes may mitigate the potential for aggregation, the diminished potency of these house-keeping systems in aging cells[4; 158; 159] may eventually lead to the formation of toxic aggregates by either the thermodynamic or kinetic scenario. Detailed analyses on the stability and folding of ALS-inducing variants of SOD1 would provide quantitative metrics on the properties of the unfolded and monomeric intermediate states for comparisons with biological measures of aggregation and toxicity. These experiments are currently in progress.

Materials and Methods

Protein purification.

Human C6A/C111S SOD1 and the monomeric variant C6A/C111S/G50E/F51E SOD1 recombinant proteins were expressed in pET3d/BL21-Gold(DE3) *Escherichia coli* cells (Stratagene®, Inc., Cedar Creek, TX) induced with 1 mM IPTG. All centrifugation steps were done using a Beckman JA 25.50 rotor and performed for 45 min at 4 °C unless otherwise specified. The cells were pelleted by centrifugation at 9000 RPM for 15 min and resuspended in lysis buffer (100 mM HEPES, pH 7.2, 150 mM NaCl, 1 mM $ZnSO_4$, 1 mM DTE, 1 mg mL^{-1} lysozyme and one protease inhibitor tablet (F. Hoffmann-La Roche Ltd, Switzerland) per 50 mL lysate. After stirring for 30 min at room temperature, the cells were sonicated (30 s on, 90 s off) and centrifuged at 20,000 RPM. The resulting pellet was then resuspended in lysis buffer lacking lysozyme, 0.6 mL per gram of pellet, and the sonication and centrifugation steps were repeated. The combined supernatants were placed in a 47 °C water bath and incubated for 45 min and then centrifuged at 20,000 RPM (this step was not performed for mAS-SOD1). The supernatant from the heat incubation was allowed to cool to room temperature, mixed with an equal volume of 4 M $(NH_4)_2SO_4$, stirred at room temperature for 30 min, and centrifuged at 20,000 RPM.

The resulting supernatant was dialyzed extensively against standard buffer (20 mM HEPES, pH 7.2) and loaded onto a Q Sepharose column and eluted with a linear gradient to 40% high salt buffer (300 mM KCl, 20 mM HEPES, pH 7.2) over 10 column volumes. The presence of AS-SOD1 in the fractions was determined by SDS-PAGE. The pooled fractions were concentrated to <10 mL using a YM-10 membrane on an Amicon® concentrator and dialyzed against standard buffer. The protein was demetalated and tested for purity as previously described.[114] The concentration of protein was calculated using a molar extinction coefficient at 280 nm of 5400 M^{-1} cm^{-1} for the monomer of AS-SOD1, and, unless otherwise specified, all protein concentrations are given in terms of moles of monomer of AS-SOD1 per liter of solution.

Peptide labeling and purification.

The peptide fragment representing the metal binding region of loop IV, amino acids 61-86, was purchased from Sigma-Aldrich and modified by adding an N-terminal tryptophan and a C-terminal cysteine. Purity was assessed by a single high pressure liquid chromatography peak and by mass spectroscopy provided by the manufacturer. The covalent modification of the cysteine with the FRET acceptor N-(iodoacetaminoethyl)-1-naphthylamine-5-sulfonic acid (IAEDANS) was performed at peptide concentrations of 1 mg mL^{-1} in 20 mM HEPES buffer pH 7.2, with the addition of 1 mM TCEP. Initially, 10-fold excess free IAEDANS was incubated with the peptide at room temperature for 2 hours. Another 10-fold excess of label was then added and the reaction mixture was

incubated for another 2 hours at 4 ^{o}C. The labeled peptide was separated from free dye by running the reaction mixture on two sequential 5 mL HiTrap^{TM} desalting column (GE Healthcare Life Sciences). Labeling efficiency was determined by comparing the ratios of the absorbance peaks for EDANS and Trp, 340 nm and 280 nm respectively. The extinction coefficients of 5700 M^{-1} cm^{-1} at 340 nm and 6400 M^{-1} cm^{-1} at 280 nm were used to calculate the concentration of peptide and dye.

Fluorescence data were collected on a Spex fluorolog fluorometer with an excitation frequency of 280 nm. The concentration of peptide, a mixture of labeled and unlabeled, was 4 μM. Emission from the donor and acceptor were collected over 320 nm to 570 nm with a collection time of 1 s/nm. The excitation and both emission slits were set to 3 nm. It should be noted that this lead to significant photobleaching of the peptide and a smaller excitation slit width is recommended for future experiments.

Equilibrium folding experiments.

All circular dichroism (CD) spectroscopy was performed on a Jasco-810 spectropolarimeter (Jasco Inc., Easton, MD) equipped with a water-cooled Peltier temperature control system. The Gdn-HCl induced unfolding curves were monitored from 220-240 nm in a 0.5 cm path length quartz cuvette using a scan rate of 20 nm min^{-1} and a response time of 8 s. Gdn-HCl concentrations were determined by refractive index [160] on a Leica Mark II refractometer. Unless otherwise stated, titration samples were

made from concentration matched stocks of folded protein in buffer and unfolded protein at 7 M Gdn-HCl and incubated at room temperature for 1 day for apo-protein and 7 days for zinc-bound protein. Coincident unfolding and refolding curves from companion experiments in which denaturant was added to native protein and buffer was added to unfolded protein insured that the samples were fully equilibrated in this time frame. The stocks were mixed precisely using a Hamilton Microlab 500 titrator interfaced with in-house software to calculate the mixing ratios, and the index of refraction of each sample was measured after the experiment was completed. The protein concentrations, given in monomer units, were 10 μM for AS-SOD1 and 5 μM for mAS-SOD1 for the equilibrium unfolding experiments.

Kinetic experiments.

The unfolding and refolding kinetics of AS-SOD1, initiated by manual mixing, were monitored by CD. Data were collected at 230 nm in a 1 cm^2 cuvette under continuous mixing with a solution volume of 1.8-2.0 mL. Unfolding jumps were initiated from protein in 0 M Gdn-HCl and refolding jumps were initiated from protein denatured overnight in 5-6 M Gdn-HCl to various final concentrations. For zinc-loaded samples, the protein was incubated in stoichiometric zinc prior to dilution in the buffer. The final concentration of Gdn-HCl was measured by index of refraction. Protein concentrations were 10 μM for both AS-SOD1 and mAS-SOD1 for the kinetic folding experiments.

Analysis of equilibrium folding data.

To determine the folding free energy of metal-free AS-SOD1 and mAS-SOD1 from the equilibrium unfolding titrations, the data were fit to a simple two-state mechanism. While it is known that SOD1 folds via a monomeric intermediate,[113; 114; 116] it is not populated significantly at these protein concentrations,[115] making a 2-state folding model an adequate approximation. For all thermodynamic analyses, the free energy of folding in the absence of denaturant was calculated assuming a linear dependence of the apparent free energy on the denaturant concentration. Equilibrium data were analyzed by globally fitting the CD signal at 20 different wavelengths (220-240 nm) to the same thermodynamic parameters. All data were fit using Savuka 6.2, an in-house non-linear least squares program using the Marquardt-Levenberg algorithm.[161] In the absence of zinc, equilibrium folding data were fit to a two-state model, $U \leftrightarrows N$ for mAS-SOD1 and $2U \leftrightarrows N_2$ for AS-SOD1 as previously described.[114]

For equilibrium titrations in the presence of zinc, the data were modeled as a three state reaction.

$$U+Zn \leftrightarrows U\bullet Zn \leftrightarrows N\bullet Zn$$

$$2U+2Zn \leftrightarrows 2(U\bullet Zn) \leftrightarrows (N\bullet Zn)_2$$

The Gdn-HCl induced unfolding transition for these titrations involves the native zinc-bound monomer (N•Zn),or dimer $(N\bullet Zn)_2$, state, the zinc-bound unfolded state U•Zn or 2(U•Zn) and the zinc-free unfolded chains, U+Zn and 2U+2Zn, respectively. The equilibrium constants can be defined for the stable monomeric form, Zn-mAS-SOD1, as:

$$K_D = \frac{[U][Zn]}{[U \cdot Zn]}, \quad K_U = \frac{[U \cdot Zn]}{[N \cdot Zn]}$$

and for the dimeric form, Zn-AS-SOD1:

$$K_D = \frac{[U]^2[Zn]^2}{[U \cdot Zn]^2}, \; K_U = \frac{[U \cdot Zn]^2}{[N \cdot Zn]}$$

An equation for total protein concentration may be written as a function of K_U, the equilibrium constant of unfolding, K_D, the dissociation constant for zinc, total protein concentration (P_t), total zinc concentration (Z_t), and the concentration of unfolded protein ([U]) (See supplemental for a more detailed derivation).

Zn-mAS-SOD1:

$$P_t = \frac{[U] \cdot Z_t}{[U] + [U] \cdot K_U + K_U \cdot K_D} + \frac{[U] \cdot Z_t}{[U] + K_D + \frac{[U]}{K_U}} + [U]$$

Zn-AS-SOD1:

$$P_t = \frac{2 \cdot [U]^2 \cdot x^2}{K_U \cdot {K_D}^2} + \frac{[U]}{K_D} \cdot x + [U], \quad x = \frac{\frac{-[U]}{K_D} - 1 + \sqrt{\left(\frac{[U]}{K_D} + 1\right)^2 + \frac{8 \cdot [U]^2 \cdot Z_t}{K_U \cdot {K_D}^2}}}{\frac{4 \cdot [U]^2}{K_U \cdot {K_D}^2}}$$

The titration data were fit by numerically solving the equations for the concentration of unfolded protein at each Gdn-HCl concentration. The value for K_D and its denaturant dependence were held fixed to the values obtained from an independent assessment of the zinc-peptide complex, and the value for K_U was optimized across the denaturant concentration and the wavelength range, 220 to 240 nm. The free energy differences between thermodynamic states were assumed to depend linearly on the Gdn-HCl concentration.

Analysis of kinetic folding data.

The unfolding and refolding relaxation times were obtained by jumping from 0 or 6 M Gdn-HCl to various final concentrations of denaturant and fitting the traces to exponentials as described previously.[114] The monomer folding and unfolding rates, for both apo- and Zn-mAS-SOD1 in the absence of denaturant, were calculated by fitting the chevron to a two-state folding model

$$k = k_f e^{(-m_f[D]/RT)} + k_u e^{(-m_u[D]/RT)}$$

Where k is the observed rate constant, k_f and k_u are the folding and unfolding rate constants in the absence of denaturant respectively, m_f and m_u are the denaturant dependence of the folding and unfolding rates respectively, [D] is the denaturant concentration, R is the gas constant and T is the absolute temperature. Knowing the

folding and unfolding rate constants in the absence of denaturant, the folding free energy can be calculated:

$$\Delta G_u = -RT \ln(\frac{k_u}{k_f})$$

The dimer dissociation rate constants in the absence of denaturant were calculated from linear extrapolations to 0 M Gdn-HCl of the >5.5 M Gdn-HCl region of the unfolding leg of the Zn-AS-SOD1 chevron and the >3.8 M Gdn-HCl region of the unfolding leg of the apo-AS-SOD1 chevron.

Analysis of zinc binding to the zinc-binding loop peptide.

All fluorescence spectroscopy was done on a T-format Spex Fluorolog-3 (Instruments S. A. Inc, Edison, NJ) at room temperature. The donor tryptophan was excited at 280 nm and the emission spectra were monitored from 320 to 540 nm to encompass both the tryptophan and EDANS fluorescence. The peptide was incubated at various concentrations of Gdn-HCl ranging from 0-6 M in standard buffer. Zinc was added in a stepwise manner, from a high concentration stock solution to minimize changes to the volume, to samples at each denaturant concentration. The fluorescence spectra were obtained at various zinc and denaturant concentrations and corrected for background fluorescence and the small change in volume accompanying the addition of zinc. The

fluorescence was measured as a function of zinc concentration, and all wavelengths were simultaneously fit to a binding isotherm with one binding site per peptide:

$$y = \frac{B_{\max} \times [Zn]}{K_D + [Zn]}$$

where y is the fluorescence intensity, B_{max} is the signal at saturating concentrations of zinc, K_D is the dissociation equilibrium constant and [Zn] is the concentration of zinc.

Acknowledgements

The authors would like to thank Drs. Osman Bilsel, Anna-Karin E. Svensson, Lawrence Hayward and Ashutosh Tiwari for their stimulating discussions and input during this project. The authors are also grateful to Dr. James Evans and the personnel at the Proteomics and Mass Spectrometry Core Facility of Massachusetts Medical School for the molecular weight and protein purity determinations. This work was supported by NIH grant GM 54836 to C.R.M.

Chapter III. Disulfide-Reduced ALS Variants of Cu, Zn Superoxide Dismutase Exhibit Increased Populations of Unfolded Species

Abstract

Cu, Zn superoxide dismutase (SOD1) is a dimeric metal binding enzyme responsible for the dismutation of toxic superoxide to hydrogen peroxide and oxygen in cells. Mutations at dozens of sites in SOD1 induce amyotrophic lateral sclerosis (ALS), a fatal gain-of-function neurodegenerative disease whose molecular basis is unknown. To obtain insights into effects of the mutations on the folded and unfolded populations of immature monomeric forms whose aggregation or self-association may be responsible for ALS, the thermodynamic and kinetic folding properties of a set of disulfide-reduced and disulfide-oxidized Zn-free and Zn-bound stable monomeric SOD1 variants were compared to the wild-type (WT) protein. The most striking effect of the mutations on the monomer stability was observed for the disulfide-reduced metal-free variants. Whereas the WT and S134N monomers are >95% folded at neutral pH and 37 ºC, A4V, L38V, G93A, and L106V ranged from 50% to ~90% unfolded. The reduction of the disulfide-bond was also found to reduce the apparent Zn affinity of the WT monomer by 750-fold, into the nanomolar range where it may be unable to compete for free Zn in the cell. With the exception of the S134N metal-binding variant, the Zn affinity of disulfide-oxidized SOD1 monomers showed little sensitivity to amino acid replacements. These results suggest a model for SOD1 aggregation where the constant synthesis of ALS-variants of SOD1 on ribosomes provides a pool of species in which the increased population of the unfolded state may favor aggregation over productive folding to the stable native dimeric state.

Introduction

Amyotrophic lateral sclerosis (ALS) is a fatal neurodegenerative disease that results in the death of motor neurons.[128] An inherited form of ALS has been linked to mutations in the gene encoding for the Cu, Zn superoxide dismutase (SOD1).[14; 129] To date, over 150 amino acid replacements, insertions, deletions and truncations throughout the sequence have been discovered that give rise to this deleterious gain-of-function disease (http://alsod.iop.kcl.ac.uk/Als/Index.aspx).[23] Although a number of mechanisms have been proposed for toxicity,[137] ALS variants of SOD1 often lead to the formation of macroscopic aggregates in the motor neurons of afflicted individuals. Recognizing that these types of sequence alterations typically destabilize proteins, it is reasonable to hypothesize that marginally soluble forms of SOD1 self-associate to produce toxic small oligomers or larger aggregates.[138] Nevertheless, the conformations of SOD1 responsible for aggregation are unclear, and a common molecular explanation for the formation of these aggregates has not been discovered.

SOD1 is a cytosolic protein responsible for the dismutation of superoxide, a toxic byproduct of metabolism, into hydrogen peroxide and oxygen through the cyclical oxidation and reduction of its catalytic Cu ion.[21] In its mature form, SOD1 is a homodimer with one Zn and one Cu ion bound to each subunit. The fold of each monomer can be described as a β-sandwich composed of eight β-strands supporting two

large loops. The Zn-binding loop binds the structurally-important Zn ion, and the electrostatic loop plays a role in guiding the superoxide anion to the active site. In addition, each monomer contains an intramolecular disulfide bond between C57 in the Zn-binding loop and C146 in β8 (Figure 3.1).

There has been growing interest in the role of immature monomeric species, i.e. metal-free and/or disulfide-reduced, in aggregation.[162] Monomeric species of SOD1 may be more prone to aggregation[98; 104; 105] because they are likely to be partially folded and marginally soluble.[70; 135; 136; 163] This hypothesis is consistent with the three-state folding mechanism of SOD1, $2U \leftrightarrows 2M \leftrightarrows N_2$, in which the rate-limiting monomer folding reaction from the unfolded state, U, to the folded state, M, is followed by the rapid association of the monomers to form the dimeric native state, N_2.[113; 114] As a consequence, the folded monomer population is minimized during the folding reaction of the WT protein. Also supporting this view is the observation that several ALS variants destabilize the native state, leading to increased populations of folded and unfolded monomeric species at equilibrium.[115; 117; 120] These studies focused on forms of SOD1 and its variants that contain the intramolecular disulfide bond, in essence, the mature species closely connected with the native conformation.

It has previously been shown that the reduction of the disulfide bond leads to the dissociation of the dimer in the absence of metal ions; zinc binding reverses this

process.[40] The reduction of the disulfide bond in several ALS-inducing variants decreases the apparent melting point below physiological temperature.[43] However the irreversibility of the thermal unfolding reaction and the requirement for a stabilizing osmolyte render this conclusion ambiguous. To obtain unambiguous quantitative insight into the thermodynamic coupling between disulfide bond, Zn binding and amino acid replacements on immature SOD1, a combined thermodynamic and kinetic analysis of the reversible folding reactions of a monomeric version of SOD1 (mAS-SOD1), C6A/F50E/G51E/C111S, and five ALS variants introduced into this background (Figure 3.1) was performed. The A4V mutation increases the side chain volume in a tightly packed hydrophobic cluster inside the β-sandwich. Both L38 and L106 serve as hydrophobic capping residues for the β-sandwich, and replacement with valine at these positions decreases the side chain volume and replaces a γ-branched side chain with a β-branched side chain. The main chain of G93 is in a tight loop, and the dihedral angles are disfavored for all but glycine at this position. Finally, S134 is involved in the hydrogen bonding network that links the electrostatic loop to the Zn-binding loop, and its replacement with asparagine leads to decreased metalation (For a general review see Valentine *et al.*[137]).

With the exception of S134N, both oxidized and reduced monomeric forms of the remaining variants exhibited a significant loss of thermodynamic stability for their metal-free forms. By contrast, S134N was the only variant studied which exhibited a

Figure 3.1. Crystal structure highlighting ALS variants studied.

Crystal structure of holo-SOD1 (PDB: 2C9V). The Cu ion and the other monomer have been omitted. The disulfide bond is highlighted in yellow, and the Zn ion in blue. The sites of ALS mutations studied are highlighted by the green side chains for the native amino acids. The two residues replaced by glutamic acid to create the monomer model, F50 and G51, are shown in red. The ALS-inducing variants studied are A4V, L38V, G93A, L106V and S134N.

Figure 3.1. Crystal structure highlighting ALS variants studied.

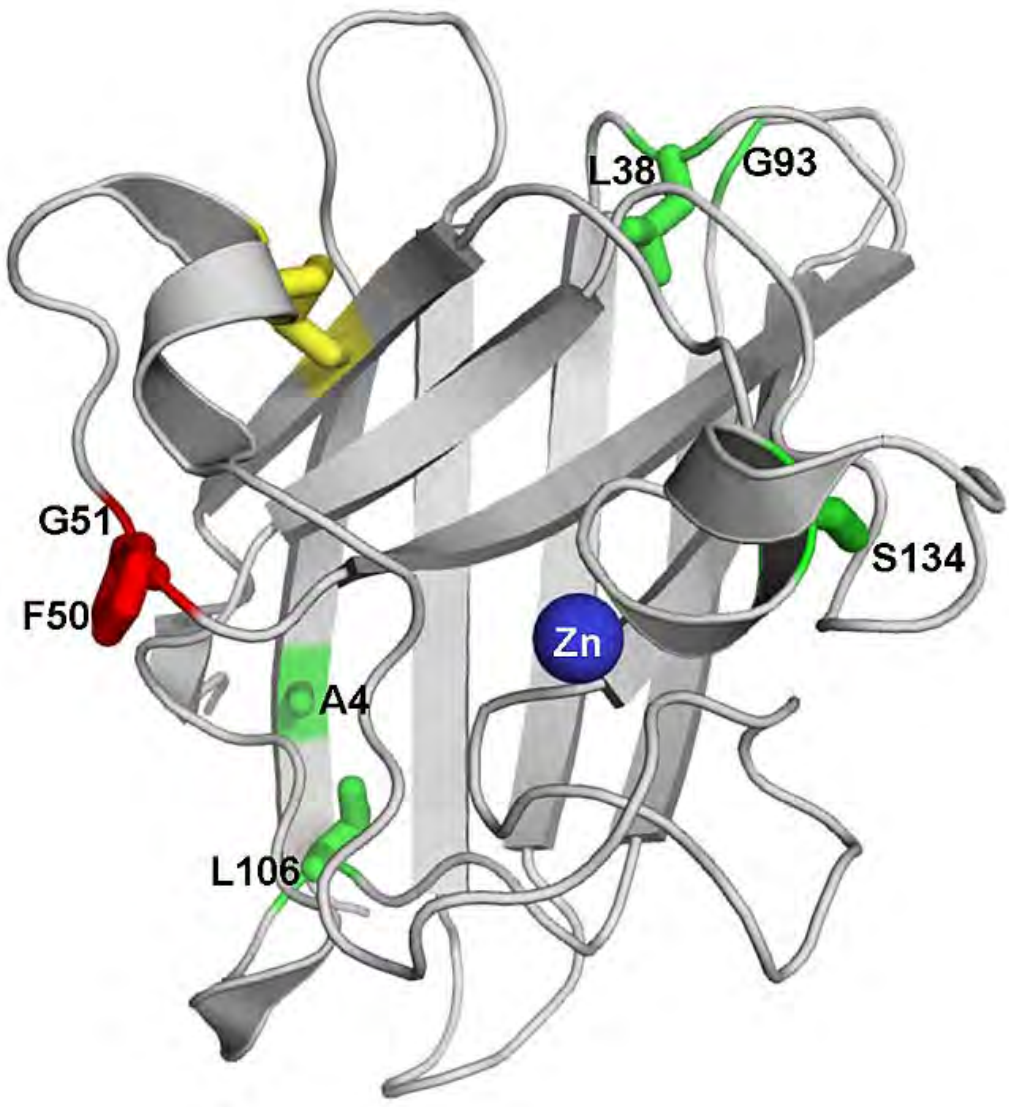

significantly weakened apparent Zn affinity. Surprisingly, the reduction of the disulfide bond decreased the affinity of mAS-SOD1 for Zn by ~750-fold. The substantially increased populations of the unfolded forms in four of the five disulfide-reduced ALS-variants of SOD1 at physiological temperature may provide the common link between mutations at many positions and protein aggregation. The reduction in the apparent Zn affinity of the S134N variant would allow this variant to more readily sample the metal-free folding free energy surface whose folded and/or unfolded monomeric populations might be sufficient to induce aggregation even for WT SOD1.

Results

The thermodynamic stability of the Zn-bound and/or disulfide-reduced states of monomeric WT, A4V, L38V, G93A, L106V and S134N SOD1 variants was determined by chemical denaturation experiments on the C6A/F50E/G51E/C111S model of SOD1 (Figure 3.1).[143] In this pseudo-WT model, the free cysteines, C6 and C111, have been replaced with non-oxidizable side chains to eliminate intramolecular disulfide-interchange in the unfolded state and intermolecular disulfide crosslinking in the native state. The F50 and G51 residues at the dimer interface have been replaced with glutamic acid to prevent dimerization.[49; 142] The structure of this stable monomer is very similar to that for the monomer in the context of the dimer,[36; 49] as is the thermodynamic stability.[113] This system enables measurements of highly reversible folding reactions solely for the monomeric forms of these ALS variants, in the absence of their self-association to dimeric species. Although the C6A/C111S and F50E/G51E mutations might themselves perturb the aggregation propensity of SOD1 (C6F, C6G and C111Y are ALS variants[162]), the introduction of ALS-inducing mutations into the same background allows for a direct comparison of their perturbations on the thermodynamic properties and populations of the SOD1 system.

Stabilities of disulfide-reduced apo-mAS-SOD1.

The role of the disulfide bond in stabilizing $mAS\text{-}SOD1_{Apo}$ was determined by reducing the disulfide bond and monitoring the ellipticity at pH 7.2 and 20 ºC as a function of the urea concentration. The choice of urea as the denaturant was necessitated by the expected low thermodynamic stability of these proteins. The far-UV circular dichroism (CD) spectra of the disulfide-reduced monomers can be seen in Figure 3.2A. WT and S134N $mAS\text{-}SOD1^{2SH}_{Apo}$ exhibit a minimum at ~208 nm and a slight shoulder at 230 nm, consistent with a significant degree of folding. In contrast, A4V, L38V, G93A and L106V $mAS\text{-}SOD1^{2SH}_{Apo}$ exhibit unfolded-like CD spectra with the minimum shifted to ~200 nm, and they lack the shoulder at 230 nm characteristic of the native fold.

The equilibrium urea denaturation curves for $mAS\text{-}SOD1^{2SH}_{Apo}$ variants are shown in Figure 3.2C. WT $mAS\text{-}SOD^{2SH}_{Apo}$ is stable to ~1.2 M urea, where it undergoes a cooperative unfolding reaction that is complete by ~2.6 M urea. The S134N variant is nearly coincident with WT with the exception of a slightly negatively sloped native baseline prior to the cooperative unfolding transition. The A4V, L38V, G93A and L106V variants are all completely denatured by 1 M urea and lack native baselines. These equilibrium data were fit to a two-state model, U⇆M, assuming a linear dependence of the apparent free energy of folding, ΔG^o, on the denaturant concentration: ΔG^o (urea) = ΔG^o (H_2O) –

Figure 3.2. Equilibrium studies.

CD spectra and urea titrations reveal that A4V, L38V, G93A and L106V $\mathrm{mAS\text{-}SOD1}^{2SH}_{Apo}$ are partially unfolded. The CD spectra of WT (solid gray), A4V (dash-dot black), L38V (dotted black), G93A (dashed black), L106V (solid black), S134N (dashed gray) (A) $\mathrm{mAS\text{-}SOD1}^{2SH}_{Apo}$ and (B) $\mathrm{mAS\text{-}SOD1}^{SS}_{Apo}$ at 20 ºC and pH 7.2. Equilibrium unfolding curves at 20 ºC and pH 7.2 for (C) $\mathrm{mAS\text{-}SOD1}^{2SH}_{Apo}$ and (D) $\mathrm{mAS\text{-}SOD1}^{SS}_{Apo}$ variants and the calculated fraction unfolded plots for (E) $\mathrm{mAS\text{-}SOD1}^{2SH}_{Apo}$ and (F) $\mathrm{mAS\text{-}SOD1}^{SS}_{Apo}$ variants measured by CD at 230 nm: WT (filled circle), A4V (triangle), L38V (hexagon), G93A (diamond), L106V (square), S134N (upside-down triangle). Best fit curves to a two-state U⇆M folding model are shown in solid lines. The thermodynamic data are presented in Table 3.1. The protein concentration for these experiments was 10 μM.

Figure 3.2. Equilibrium studies.

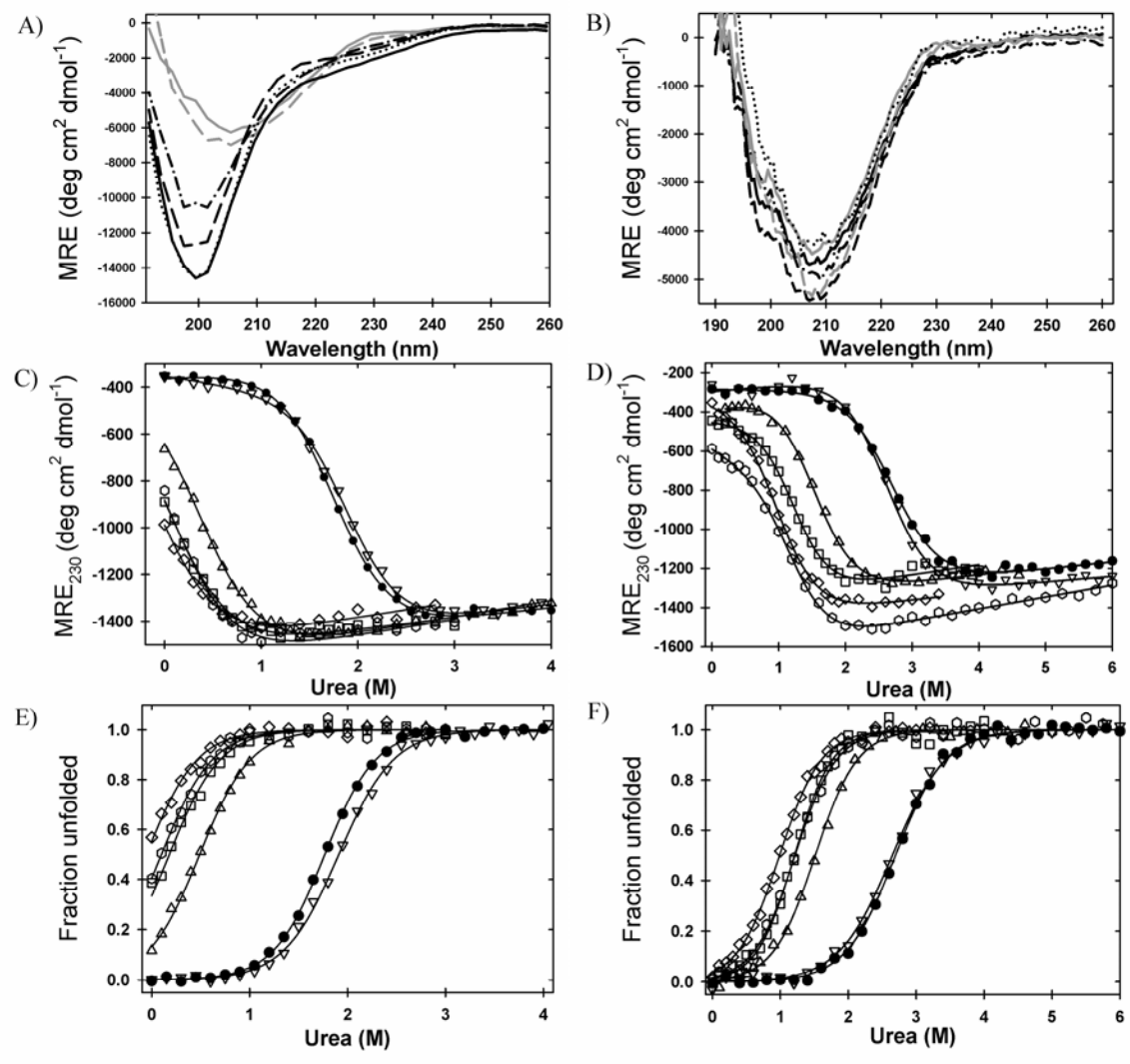

m[urea] (Table 3.1). All data were fit using Savuka 6.2, an in-house non-linear least squares program using the Marquardt-Levenberg algorithm. The fits were performed by globally analyzing the ellipticity at 20 different wavelengths between 220 and 240 nm.

Both WT and S134N $\mathrm{mAS\text{-}SOD1}^{\mathrm{2SH}}_{\mathrm{Apo}}$ exhibit well defined baselines and were fit without constraining the parameters. From the determined thermodynamic stability (Table 3.1), it is evident that both of these proteins are >99% folded under these conditions (Figure 3.2E). For the highly-destabilized ALS variants where no native baseline was observed, the *m*-value and the slope and intercept of the native baseline were fixed to the same values as WT. The constraint on several variables, required to fit these titrations, likely results in an underestimated error of the fit, suggesting caution in the accuracy of these estimates for stability. Nevertheless, the lack of native baselines and the reduced CD signal in the absence of denaturant (Figure 3.2B) make it clear that substantial fractions of A4V, L38V, G93A and L106V $\mathrm{mAS\text{-}SOD1}^{\mathrm{2SH}}_{\mathrm{Apo}}$ are unfolded at 20 ºC and pH 7.2 (Figure 3.2E).

The large fraction of unfolded protein for the A4V, L38V, G93A and L106V variants at 20 ºC and the known endothermic unfolding reaction for SOD1[56] prompted a comparison of the urea denaturation reactions for WT and A4V $\mathrm{mAS\text{-}SOD1}^{\mathrm{2SH}}_{\mathrm{Apo}}$ over the temperature range from 4 – 37 °C to determine the extent of unfolding at physiological temperature, 37 ºC. While the stability of WT protein can be measured reliably at 37 °C, A4V is too

Table 3.1. Thermodynamic parameters, microscopic rate constants and kinetic m‡-values for monomeric variants.*

	WT	A4V	L38V	G93A	L106V	S134N
Apo reduced[a]						
$\Delta G^{\circ}_{(U/M)}$ [b]	-3.95±0.10	-1.09[c]	-0.22[c]	+0.12[c]	-0.40[c]	-3.97±0.16
$m_{(U/M)}$	2.23±0.11	2.23[d]	2.23[d]	2.23[d]	2.23[d]	2.08±0.08
Apo oxidized[a, e]						
$\Delta G^{\circ}_{(U/M)}$ [b]	-4.48±0.07	-2.83±0.07	-2.32±0.15	-1.87±0.07	-2.52±0.08	-4.54±0.10
$m_{(U/M)}$	1.65±0.02	1.88±0.04	1.91±0.08	1.89±0.04	2.09±0.05	1.73±0.03
Apo oxidized[a, e]						
k_f	0.056±0.002	0.15±0.02	0.033±0.006	0.029±0.004	0.030±0.003	0.039±0.004
$m_f^{\ddagger}$	1.20±0.05	1.5±0.1	1.36±0.20	1.37±0.18	1.33±0.13	1.13±0.04
k_u	(2.0±0.40)×10^{-5}	(1.0±0.1)×10^{-3}	(3.5±1.5)×10^{-4}	(1.2±0.2)×10^{-3}	(5.0±1.0)×10^{-4}	(1.2±0.1)×10^{-5}
$m_u^{\ddagger}$	-0.58±0.01	-0.64±0.03	-0.78±0.09	-0.74±0.03	-0.74±0.05	-0.65±0.01
$\Delta G^{\circ}_{(U/M)}$	-4.61±0.12	-2.92±0.2	-2.65±0.28	-1.85±0.13	-2.37±0.13	-4.70±0.08
$m_{(U/M)}$ [f]	1.79±0.05	2.14±0.1	2.14±0.22	2.11±0.18	2.07±0.14	1.78±0.04
Zn oxidized[g]						
k_f	0.74±0.01	0.87±0.15	0.27±0.05	0.19±0.05	0.34±0.05	0.64±0.01
$m_f^{\ddagger}$	2.93±0.07	3.0±0.1	2.89±0.09	2.48±0.17	3.39±0.10	2.95±0.10
k_u	(0.23±0.08)×10^{-7}	(1.77±0.39)×10^{-7}	(2.8±0.8)×10^{-7}	(4.1±1.2)×10^{-7}	(13.3±3.9)×10^{-7}	(2.8±1.2)×10^{-7}
$m_u^{\ddagger}$	-1.76±0.05	-1.85±0.03	-2.01±0.06	-1.88±0.06	-1.68±0.06	-1.47±0.13
$\Delta G^{\circ}_{(U/M)}$ [h]	-18.0±0.2	-17.0±0.2	-15.3±0.5	-15.6±0.2	-15.2±0.2	-16.5±0.3
$m_{(U/M)}$ [f]	4.69±0.09	4.85±0.1	4.90±0.11	4.36±0.18	5.07±0.12	4.42±0.13
$\Delta\Delta G^{\circ}_{Zn}$	-13.4±0.2	-14.1±0.2	-12.7±0.5	-13.8±0.2	-12.8±0.2	-11.8±0.3
K_d [h]	100±39 pM	31±15 pM	360±350 pM	55±23 pM	270±110 pM	1600±840 pM

[*]Units for the U ⇆ M reaction: k_f and k_u, s^{-1}; $m_f^{\ddagger}$, $m_u^{\ddagger}$, and $m_{(U/M)}$, kcal mol^{-1} M^{-1}; $\Delta G^{\circ}_{(U/M)}$, $\Delta\Delta G^{\circ}_{Zn}$, kcal mol^{-1}.

[a] Denaturation was performed with urea.

[b] Equilibrium data were fit to a two-state model, U⇆M, by globally analyzing the CD signal at 20 different wavelengths between 220 and 240 nm.

[c] Due to the constraints required to fit these titrations, the error in the free energy of folding is approximated to be ±0.3 kcal mol^{-1}.

[d] Parameter was fixed to the WT value.

[e] WT values adapted from Svensson *et al.*[114]

[f] Calculated according to $m_{tot} = |m^{\ddagger}_{u}| + |m^{\ddagger}_{f.}|$

[g] Denaturation was performed with Gdn-HCl.

[h] The free energy difference between U+Zn ⇆ N•Zn and the Zn affinity was calculated as described in Kayatekin *et al.* [48]

destabilized at these temperatures to allow accurate fitting of the data. For both A4V and WT, the thermodynamic stability was determined by an singular value decomposition (SVD) analysis of CD spectra from 220-240 nm.[164] The SVD vectors were normalized to the unfolded baseline and fit by holding the slope and y-intercept of the native baseline fixed to the 4 ºC data set. A van't Hoff plot of the results is shown in Figure 3.3. The data are well-described by a simple linear dependence whose calculated enthalpy changes, 23.8±2.8 kcal mol^{-1} for WT and 20.3±2.2 kcal mol^{-1} for A4V, allow for the prediction of the stabilities at 37 °C.

The stability of WT $mAS\text{-}SOD1^{2SH}_{Apo}$ is 2.0 kcal mol^{-1} at pH 7.2 and 37 °C, meaning that ~97% of the protein is folded under these conditions. By contrast, the stability of A4V $mAS\text{-}SOD1^{2SH}_{Apo}$, which could be measured reliably up to 27 ºC, falls from 2.1 kcal mol^{-1} at 4 ^{o}C to 0.8 kcal mol^{-1} at 27 ºC. Linear extrapolation to 37 ºC reveals that the stability is reduced to ~0 kcal mol^{-1}, indicating that A4V is half unfolded under physiological conditions. These results are consistent with previous native-state hydrogen exchange experiments that showed WT $SOD1^{2SH}_{Apo}$ retained some protection against amide hydrogen exchange at 37 °C while A4V $SOD1^{2SH}_{Apo}$ did not.[165] Urea titrations at 37 ºC for all variants can be seen in Figure 3.4. For the highly destabilized variants, these titration curves entirely lack native baselines and display a very small portion of the unfolding transition, consistent with the conclusion that these proteins are largely unfolded at 37 ºC. On the

Figure 3.3. Temperature dependence of WT and A4V stability.

The van't Hoff plot of WT (circle) and A4V (triangle) $\mathrm{mAS-SOD1}_{\mathrm{Apo}}^{\mathrm{2SH}}$. The stability at each temperature was determined from a urea titration. Linear extrapolations to physiological temperature are shown by the solid black lines. The black, dashed, vertical line indicates 37 ^{o}C while the dashed line represents a folding free energy of zero, where the protein is half unfolded. The buffer used was 20 mM HEPES, 1 mM EDTA, 1 mM TCEP pH 7.2.

Figure 3.3. Temperature dependence of WT and A4V stability.

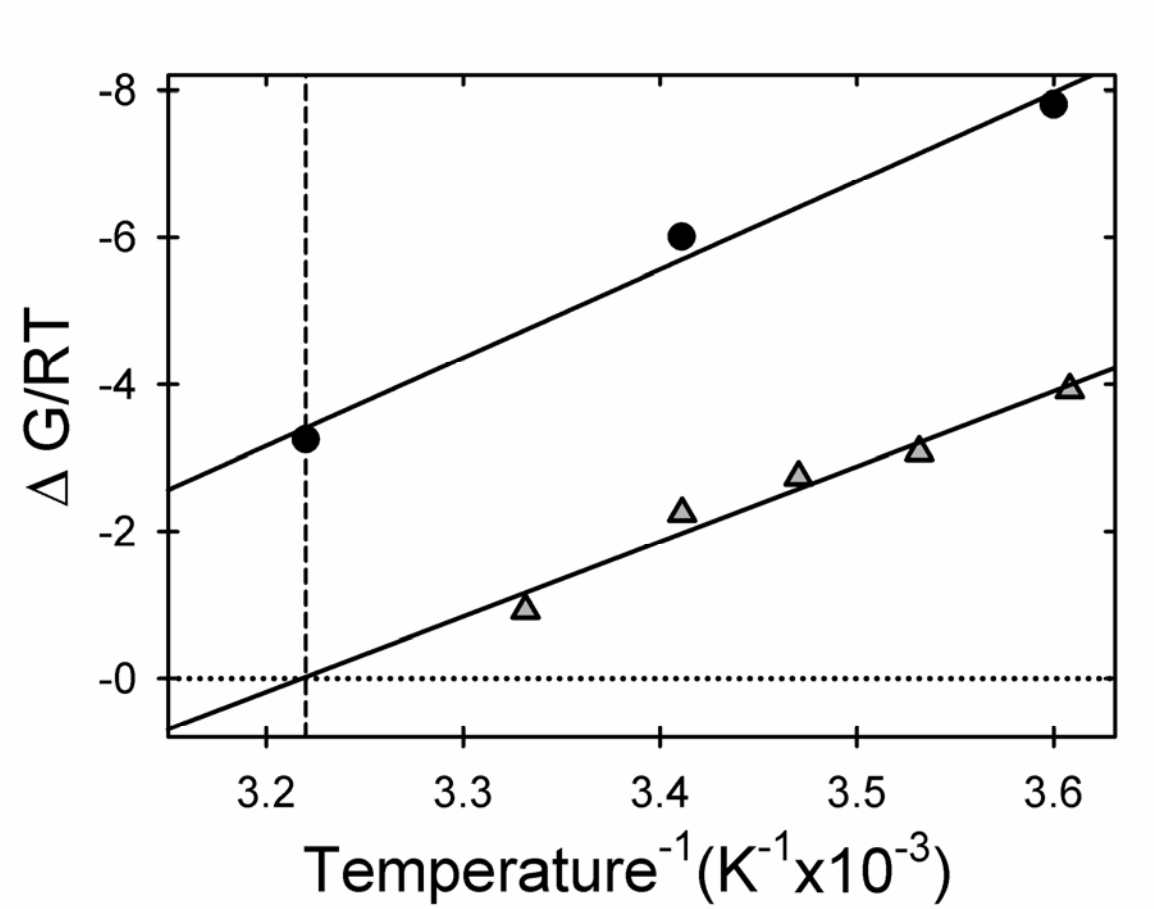

other hand, the S134N and WT variants are nearly indistinguishable and appear reasonably well folded under these conditions.

Stabilities of disulfide-oxidized apo-mAS-SOD1.

The far-UV CD spectra of the disulfide-oxidized monomers can be seen in Figure 3.2B. In contrast with disulfide-reduced proteins, all variants exhibit well folded CD spectra similar to WT $mAS\text{-}SOD1^{SS}_{Apo}$. Nevertheless, the characteristic shoulder at 230 nm is diminished for A4V, L38V, L106V and G93A, suggesting some structural differences may exist between these variants and WT $mAS\text{-}SOD1^{SS}_{Apo}$.

The stabilities of the disulfide-oxidized and metal-free variants were measured by both kinetic and equilibrium methods. These complementary approaches towards stability measurement are possible because both kinetic and equilibrium mechanisms are well-described by two-state processes. The equilibrium urea denaturation curves for $mAS\text{-}SOD1^{SS}_{Apo}$ variants at 20 ^{o}C and pH 7.2, and the fraction unfolded plots for these titrations are shown in Figure 3.2D and Figure 3.2F, respectively. WT and S134N $mAS\text{-}SOD1^{SS}_{Apo}$ are stable to ~1.8 M urea, where both proteins undergo a cooperative unfolding reaction that is complete by ~3.8 M urea. The next most stable variant, A4V undergoes a cooperative unfolding reaction beginning around 0.8 M urea and is complete by 2.8 M urea. L38V, G93A and L106V variants exhibit sloped native baselines and are

completely unfolded by 2 M urea. These equilibrium data were fit to a two-state model as described for the $mAS\text{-}SOD1^{SS}_{Apo}$ titrations, except no were constraints imposed on the thermodynamic parameters or baselines and CD spectra between 215 and 245 nm were fit. From the calculated stabilities (Table 3.1) and the fraction unfolded plots (Figure 3.2F), it is evident that all disulfide-oxidized variants are at least 95% folded at 20 ^{o}C and pH 7.2.

The stabilities of the $mAS\text{-}SOD1^{SS}_{Apo}$ variants were also measured kinetically in order to facilitate an appropriate comparison with the Zn-bound data (see below). The kinetic unfolding and refolding reactions of the $mAS\text{-}SOD1^{SS}_{Apo}$ ALS-variants at 20 ^{o}C and pH 7.2 were monitored by far-UV CD at 230 nm. Both reactions were well described by single exponentials. Semi-log plots of the relaxation times as a function of the final denaturant concentration, i.e., chevron plots, are shown in Figure 3.5. The rate constants for the global unfolding and refolding reactions in the absence of denaturant were obtained by linear extrapolation of the exponentially-dependent regions of the chevron plots and calculated by the reciprocal of the relaxation times, $k = 1/\tau$. The refolding rates only vary by a factor of 5 from the slowest, G93A, with a rate constant of 0.029 s^{-1}, to the fastest, A4V, with a rate constant of 0.15 s^{-1}. The largest perturbations are observed in the unfolding rates, ranging from 168-fold faster for G93A to 1.7-fold faster for S134N (Table 3.1), closely paralleling the perturbation in stability for each variant.

Figure 3.4. Equilibrium titrations at 37 °C.

Equilibrium unfolding curves at 37 ºC and pH 7.2 for WT $mAS\text{-}SOD1^{2SH}_{Apo}$ and ALS variants as measured by CD at 230 nm: WT (filled circle), A4V (triangle), L38V (hexagon), G93A (diamond), L106V (square), S134N (upside-down triangle). The buffer used was 20 mM HEPES, 1 mM EDTA, 1 mM TCEP pH 7.2.

Figure 3.4. Equilibrium titrations at 37 °C.

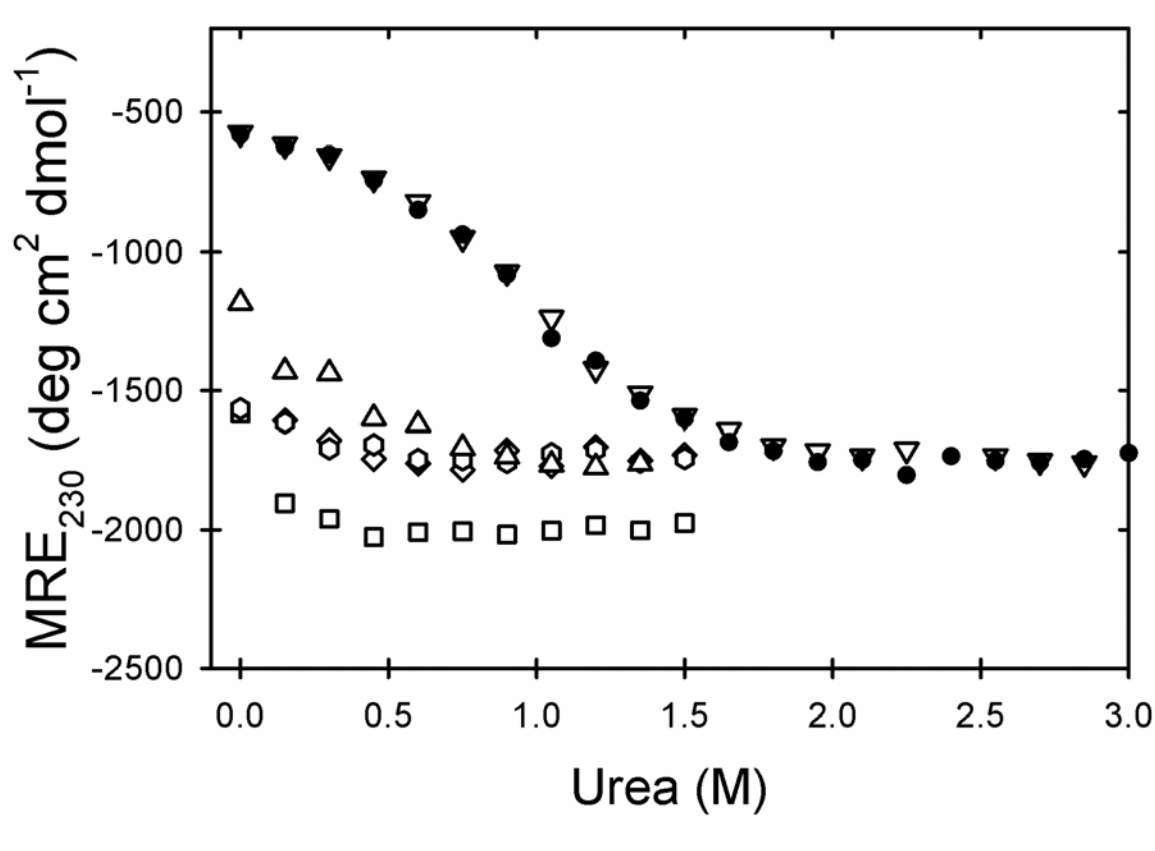

The free energy of folding for each variant, determined from the extrapolated rates, $\Delta G°=-RT\ln(k_f/k_u)$, is in very good agreement with the free energy of folding determined from the equilibrium titrations (Table 3.1). The observed change in stability range from no significant difference for S134N to as large as a 2.76 kcal mol^{-1} destabilization for G93A by the kinetic measurement (Table 3.1).

The effect of ALS mutations on the apparent Zn affinity of mAS-SOD1.

The apparent Zn affinity of $mAS\text{-}SOD1^{SS}$ variants was determined from the difference in the free energies of their Zn-bound and Zn-free forms relative to the Zn-free unfolded state. Accurate estimates of the stability of the $mAS\text{-}SOD1^{SS}_{Zn}$ species cannot be obtained from equilibrium titrations because Zn appears to scramble to the Cu site in the unfolding transition zone.[48] Alternatively, the equilibrium constant for the reversible unfolding reaction can be calculated from the ratio of the rate constants of unfolding and refolding reactions for zinc-bound unfolded state and the zinc-bound folded state. When combined with the affinity of Zn for the unfolded protein, estimated from a peptide model of the Zn-binding loop,[48] the free energy of Zn binding ($\Delta\Delta G°_{Zn}$), and the corresponding apparent Zn affinity, can be obtained from the difference in the metal-bound ($\Delta G°_{Zn}$) and the metal-free stability($\Delta G°_{Apo}$): $\Delta\Delta G°_{Zn} = \Delta G°_{Zn}(\text{Gdn-HCl}) - \Delta G°_{Apo}(\text{Urea})$, where $\Delta\Delta G°_{Zn}=-RT\ln(K_d)$ (see Kayatekin *et al.*[48] for a detailed explanation of the analysis).

Figure 3.5. Chevron plots of disulfide-oxidized variants.

Observed refolding (open symbols) and unfolding (filled symbols) relaxation times of $mAS\text{-}SOD1^{SS}_{Apo}$ variants monitored by CD at 230 nm, at pH 7.2 and 20 ºC, and plotted as a function of final denaturant concentration. The data for A4V (triangle), L38V (hexagon), G93A (diamond), L106V (square), S134N (upside-down triangle) are shown with the best fit line two a two-state folding reaction (solid lines). The fit to the disulfide-oxidized WT data (dashed-line) was adapted from Svensson et al.[114] The buffer used was 10 mM KPi, 1 mM EDTA pH 7.2.

Figure 3.5. Chevron plots of disulfide-oxidized variants.

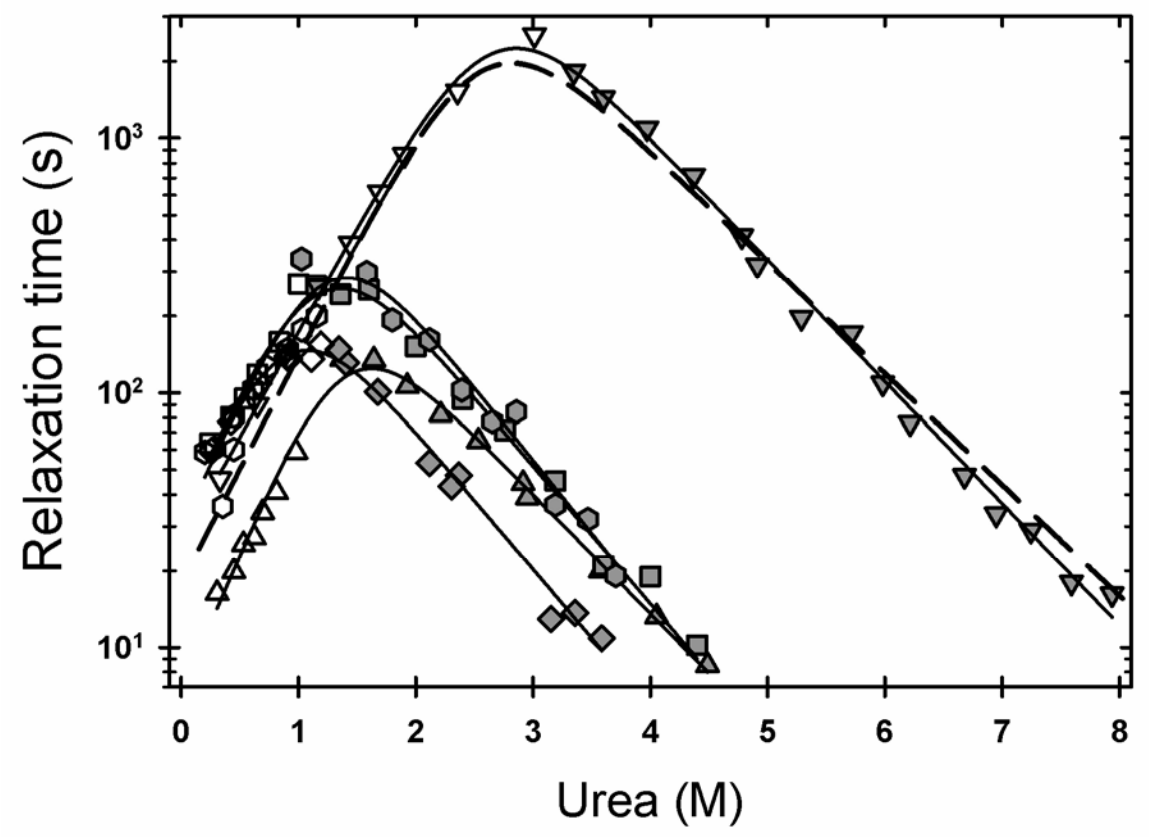

The unfolding and refolding reactions of 10 μM protein loaded with stoichiometric Zn at 20 ^{o}C and pH 7.2 were monitored by far-UV CD at 230 nm. Guanidine hydrochloride (Gdn-HCl) rather than urea was used as a denaturant to sample the entire folding reaction coordinate because Zn greatly enhances the stability of SOD1 and requires a more potent denaturant to access the unfolded state. The presence of Zn also required a HEPES buffer because $Zn_3(PO_4)_2$ precipitates at mM buffer concentrations. The requirement to change both the denaturant and the buffer to make this comparison means that the dissociation constants should be considered apparent and not absolute. However, because the WT and ALS-variants were subjected to the same procedures, the *differences* in the Zn binding free energies are expected to reflect the inherent differences in affinities induced by the mutations.

Above stoichiometric Zn:protein concentrations for all variants, the refolding reactions were well described by a single exponential phase, corresponding to the faster of the two observed relaxation times at stoichiometric or lower Zn concentrations. The slower reaction corresponds to the folding of $\mathrm{mAS\text{-}SOD1}^{SS}_{Apo}$.[48] The unfolding reactions displayed a second, faster exponential in the transition zone that has previously been attributed to the scrambling of the Zn ion to the Cu site.[48] The chevron plots for A4V, L38V and WT $\mathrm{mAS\text{-}SOD1}^{SS}_{Zn}$ are shown in Figure 3.6A, and the chevron plots for G93A and L106V and S134N are shown in Figure 3.6B.

Figure 3.6. Chevron plots of Zn-bound, disulfide-oxidized variants.

Observed refolding (open symbols) and unfolding (filled symbols) relaxation times monitored by CD at 230 nm, at pH 7.2 and 20 ºC, and plotted as a function of final denaturant concentration. (A) The data for mAS-$SOD1^{SS}_{Zn}$ WT (circle), A4V (triangle), L38V (hexagon) and (B) the data for mAS-$SOD1^{SS}_{Zn}$ G93A (diamond), L106V (square) and S134N (upside-down triangle) are shown with the best fit line two a two-state folding reaction. The WT mAS-$SOD1^{SS}_{Zn}$ data were adapted from Kayatekin et al.[48] The concentration of protein and Zn for all ALS variants was 10 μM and the buffer used was 20 mM HEPES pH 7.2.

Figure 3.6. Chevron plots of Zn-bound, disulfide-oxidized variants.

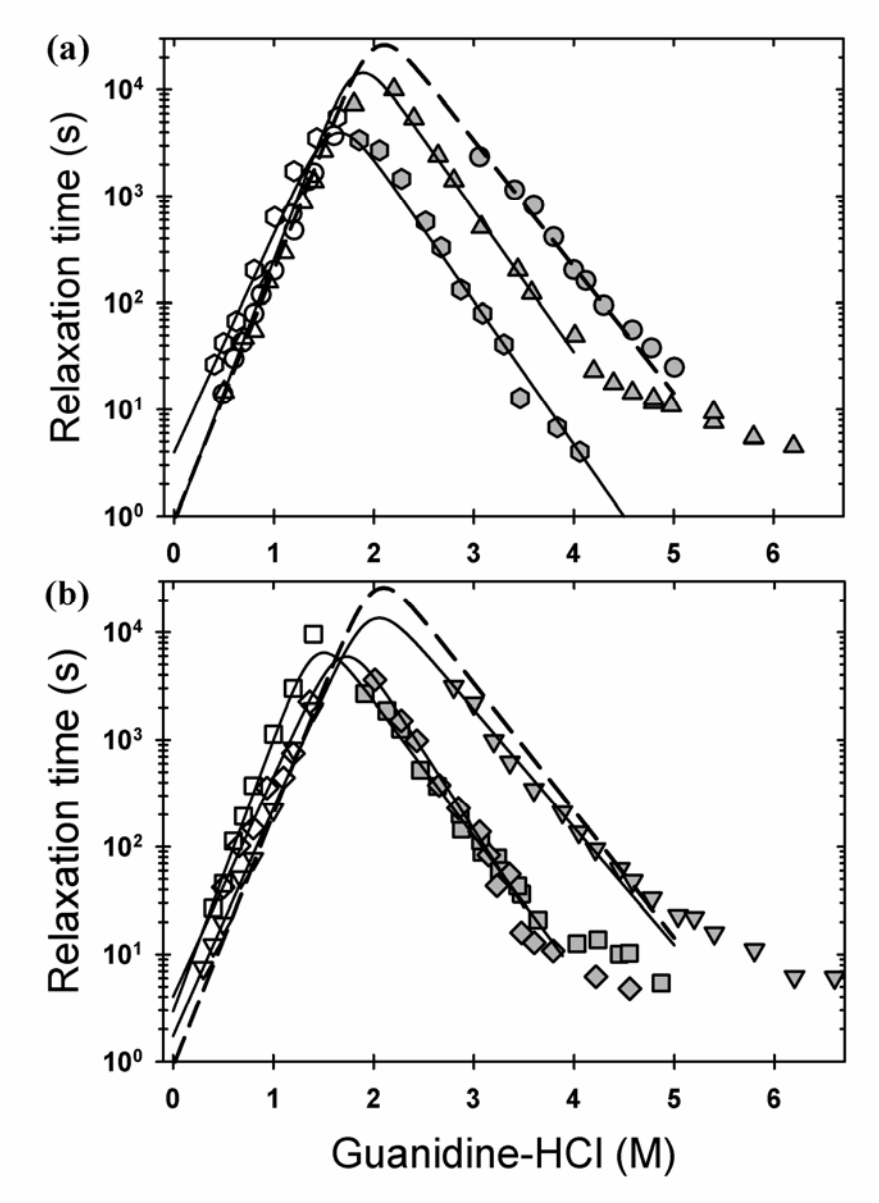

The refolding relaxation times increase exponentially with increasing denaturant concentration to a maximum around 1.8-2.2 M Gdn-HCl. At higher denaturant concentrations the unfolding reaction is favored and the observed unfolding relaxation times decrease exponentially with increasing denaturant concentration. Above 4-5 M Gdn-HCl, the unfolding relaxation times in the presence of Zn for WT mAS-SOD1$^{SS}_{Zn}$ and all of the variants except for L38V rollover to become nearly independent of the denaturant concentration. The L38V variant may roll over at fast unfolding rates which are within the dead time of a manual-mixing experiment. These data suggest either that Zn has introduced a rate-limiting rearrangement reaction in the native conformation or that Zn has slowed a rearrangement reaction that was previously undetectable for the apo-protein with manual-mixing techniques. Because this reaction is not kinetically coupled to the major unfolding reaction that controls unfolding above 4-5 M Gdn-HCl, its presence does not interfere with the kinetic measurement of stability

.

The refolding rate constants of all the proteins are within a factor of ~5 of each other, ranging from 0.19±0.05 s^{-1} for G93A, to 0.74±0.01 s^{-1} for WT to 0.87±0.15 s^{-1} for A4V mAS-SOD$^{SS}_{Zn}$ (Table 3.1). The effects of the mutations are substantially greater on the unfolding rate constants, which parallel the effects on stability. WT mAS-SOD$^{SS}_{Zn}$ is the slowest to unfold, with a rate constant of 0.23±0.08×10^{-7} s^{-1}, while L106V unfolds the most rapidly, roughly 60-fold faster, with a rate constant of 13.3±3.9×10^{-7} s^{-1}.

These data can be compared with the stabilities of the Zn-free forms of these proteins to yield an apparent Zn affinity for the ALS variants (Table 3.1). A4V and G93A variants bind Zn slightly tighter than WT mAS-SOD1^{SS}, while L38V, L106V and S134N bind Zn more weakly than the WT protein. The corresponding dissociation constants, K_d, for A4V, L38V, G93A and L106V are within a factor of three of the K_d for WT, 100 pM, and, with the exception of S134N, are nearly within the estimated errors of the measurement. The apparent Zn affinity of S134N is reduced by roughly an order-of-magnitude compared to WT. Contrasting with the dramatic effects on stability with the loss of the disulfide bond, Zn has little differential effect on the standard state stability of the A4V, L38V, G93A and L106V variants. Only the apparent Zn affinity of S134N is significantly reduced from WT mAS-SOD1^{SS}.

The apparent Zn affinity of the disulfide-reduced protein is greatly decreased.

The thermodynamic coupling between the disulfide bond and Zn binding was assessed by measuring the Zn affinity of WT and S134N $\mathrm{mAS-SOD1}^{2SH}$ with the kinetic assay described above for the $\mathrm{mAS-SOD}^{SS}$ species. The chevron plot of WT and S134N $\mathrm{mAS-SOD1}^{2SH}_{Apo}$ are shown in Figure 3.7A. In both refolding and unfolding, only a single exponential phase was observed. Neither the denaturant dependence of the refolding rate nor the unfolding rate is significantly affected by the loss of the disulfide-bond. Both

Figure 3.7. Chevron plots of disulfide-reduced WT and S134N.

Observed refolding (open symbols) and unfolding (filled symbols) relaxation times of WT (circles) and S134N (upside-down triangle) (A) $mAS\text{-}SOD1^{2SH}_{Apo}$ and (B) $mAS\text{-}SOD1^{2SH}_{Zn}$ monitored by CD at 230 nm, at pH 7.2 and 20 ºC, and plotted as a function of final denaturant concentration. The data are shown with the best fit line to a two-state folding reaction for WT(solid line) and S134N (dashed line). The protein and Zn concentrations were 10 μM and the buffer used was 20 mM HEPES, 1 mM TCEP pH 7.2.

Figure 3.6. Chevron plots of Zn-bound, disulfide-oxidized variants.

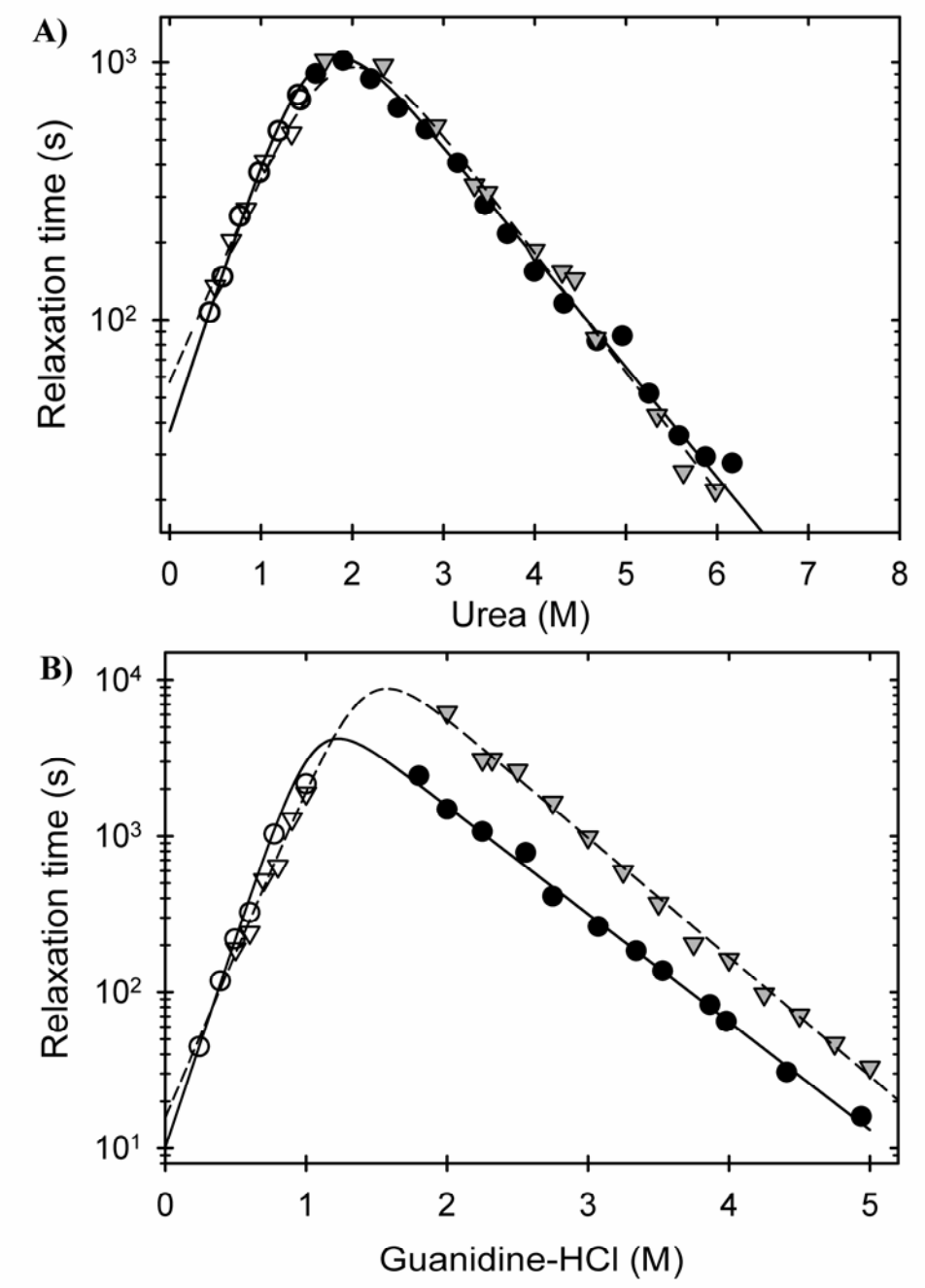

variants exhibit an identical response to disulfide-bond reduction, where the refolding rates are slowed ~3 fold compared to the disulfide-oxidized protein and the unfolding rate is accelerated ~5 fold (Table 3.2).

When Zn was introduced, two phases were observed in refolding and unfolding, comparable to the disulfide-oxidized protein. The slower phase in refolding matched the refolding rate of the metal-free protein. The chevron plot of the slow exponential phase in unfolding and the fast phase in refolding at stoichiometric Zn concentrations for WT and S134N mAS-SOD1$_{Zn}^{2SH}$ are shown in Figure 3.7B and the associated thermodynamic and kinetics parameters are reported in Table 3.2. Although the status of the disulfide bond does not alter the denaturant-dependence of the refolding reaction, the denaturant-dependence of the unfolding reaction is substantially decreased when the disulfide-bond is reduced. This change presumably reflects a less structured native state for mAS-SOD1$_{Zn}^{2SH}$ compared to mAS-SOD1$_{Zn}^{SS}$. The refolding rate in the absence of denaturant for WT mAS-SOD1$_{Zn}^{2SH}$ is nearly 10-fold slower than for mAS-SOD1$_{Zn}^{SS}$, while the unfolding rate constant is nearly 1000-fold faster.

Surprisingly, the disulfide-reduced S134N variant clearly exhibits a ~3-fold slower unfolding rate than the WT protein in the presence of Zn, while the refolding rates for both proteins are comparable. This result suggests that the replacement of serine with

asparagine in the electrostatic loop may actually lead to interactions which stabilize Zn binding compared to the WT protein when the disulfide-bond is reduced and the protein relaxes (see Discussion).

Table 3.2. Thermodynamic parameters, microscopic rate constants and kinetic m‡-values for disulfide-reduced WT and S134N.*

	WT_{apo} [a]	$S134N_{apo}$ [a]	WT_{Zn} [b]	$S134N_{Zn}$ [b]
k_f	0.027±0.006	0.019±0.003	0.099±0.005	0.064±0.014
$m_f^{\ddagger}$	1.43±0.23	1.19±0.12	3.6±0.1	2.87±0.17
k_u	$(1.0\pm0.3)\times10^{-4}$	$(6.6\pm1.7)\times10^{-5}$	$(2.7\pm0.5)\times10^{-5}$	$(5.2\pm0.6)\times10^{-6}$
$m_u^{\ddagger}$	-0.57±0.03	-0.65±0.03	-0.92±0.03	-1.04±0.02
$\Delta G^{\circ}_{(U/M)}$	3.26±0.22	3.30±0.18	4.78±0.11	5.48±0.14
$m_{(U/M)}$ [c]	2.00±0.23	1.84±0.12	4.52±0.1	3.91±0.17
$\Delta\Delta G^{\circ}_{Zn}$	-	-	9.52±0.25	10.2±0.2
K_d [d]	-	-	75±33 nM	25±10 nM

*Units for the U ⇆ M reaction: k_f and k_u, s^{-1}; $m_f^{\ddagger}$, $m_u^{\ddagger}$, and $m_{(U/M)}$, kcal mol^{-1} M^{-1}; $\Delta G^{\circ}_{(U/M)}$, $\Delta\Delta G^{\circ}_{Zn}$, kcal mol^{-1}.

[a] Denaturation was performed with urea.

[b] Denaturation was performed with Gdn-HCl.

[c] Calculated according to $m_{tot} = |m^{\ddagger}_u| + |m^{\ddagger}_f|$

[d] The free energy difference between U+Zn ⇆ N•Zn and the Zn affinity was calculated as described in Kayatekin *et al.* [48]

Discussion

Patients with the five ALS-variants of SOD1 examined in this study, A4V, L38V, G93A, L106V and S134N, exhibit an average life expectancy of less than three years after the onset of disease.[7] Our approach towards testing the potential role of monomeric species in the aggregation hypothesis for toxicity in SOD1-mediated fALS has been to employ classical thermodynamic and kinetic folding experiments to define the folding free energy surface of stable monomeric versions of these variants. The coupling between mutations, disulfide-bond status and Zn binding can be related to the changes in the relative populations of the folded and unfolded states (Figure 3.8). Enhanced populations of marginally-soluble monomeric forms would be expected to increase the propensity for aggregation and, possibly, promote toxicity.

Disulfide-reduced ALS variants are very unstable.

The reduction of the disulfide bond in the stable monomeric models of the A4V, L38V, G93A and L106V variants causes a significant reduction in their stability (Table 3.1) and a corresponding increase in the population of their unfolded states (Figure 3.8). For example G93A $\mathrm{mAS\text{-}SOD1}^{SS}_{Apo}$, the least stable variant, is only 5% unfolded at 20 ºC. Upon reduction of the disulfide bond, the population of unfolded protein increases to 55%. The effect is exacerbated at 37 ºC, where the unfolded populations of A4V, L38V, G93A and L106V exceed 50%, while only 3% of the WT protein is unfolded under these

Figure 3.8. Unfolded state populations.

The fraction of unfolded species populated at equilibrium for each variant, $mAS\text{-}SOD1^{SS}_{Zn}$ (black), $mAS\text{-}SOD1^{SS}_{Apo}$ (light gray), $mAS\text{-}SOD1^{2SH}_{Apo}$ (dark gray) at 10 μM protein concentration, 20 ^{o}C and pH 7.2. The errors for A4V, L38V, G93A and L106V $mAS\text{-}SOD1^{2SH}_{Apo}$ were approximated at 20%. All other errors were determined from the error in the $\Delta G°$.

Figure 3.6. Chevron plots of Zn-bound, disulfide-oxidized variants.

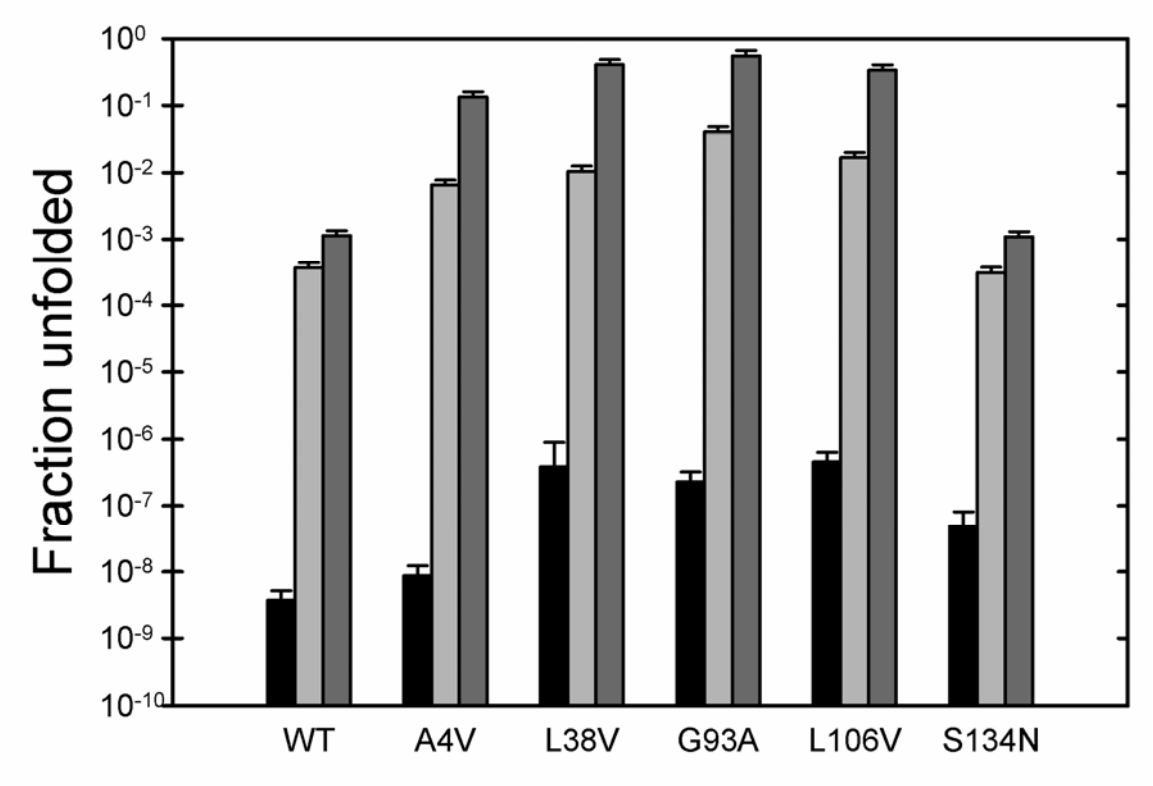

conditions. These results demonstrate that unfolded $mAS\text{-}SOD1^{2SH}_{Apo}$ is prevalent in these ALS variants under physiological conditions and, therefore, could play a critical role in aggregation. A recent report has demonstrated that even WT-$SOD1_{Apo}$ can aggregate under conditions that enhance the unfolded state, such as the addition of reducing agent or the presence of 1M Gdn-HCl, when agitated at 37 ºC.[8] Given that the unfolded thermodynamic state represents a manifold of rapidly-interconverting conformations, it is also possible that a transient population of sub-structure might be more aggregation-prone and, therefore, responsible for the initiation of the aggregation reaction.

Implications for mitochondrial damage.

The dramatic destabilization of the disulfide-reduced forms of the A4V, L38V, G93A and L106V variants may also play a role in mitochondrial damage observed in mouse models of ALS.[166] The transport of SOD1 into yeast mitochondria is greatly favored for the reduced metal-free monomeric form,[30] presumably reflecting the ease of access to an unstructured unfolded state required to traverse the outer membrane. Once inside the intermembrane space, a resident disulfide relay system oxidizes the intra-molecular disulfide bond, which, along with Zn binding and dimer formation, would effectively trap SOD1 inside the mitochondria.[167] The dominant population of the unfolded state for the disulfide-reduced form of the four WT-like variants, A4V, L38V, G93A and L106V, at pH 7.2 and 37 ºC and the unusually slow folding reaction to the disulfide-competent folded state could provide an opportunity for the unfolded state to aggregate or to

associate with other components in the intermembrane space. The observed increased localization of G93A and other ALS variants of SOD1 in mitochondria,[168] especially in the spinal cord of transgenic mice,[169] and their capacity to damage this essential organelle may, therefore, be a manifestation of their thermodynamic and kinetic folding properties.

Zn binding is marginally affected in WT-like ALS variants.

NMR and crystallographic studies have shown that Zn binding has an important role in defining the structure of SOD1 by organizing the Zn binding and electrostatic loops of the WT protein.[35; 36; 49] As shown in the present study, Zn binding to mAS-SOD1^{SS} significantly stabilizes the folded state for all of the variants (Table 3.1). However, the apparent dissociation constants for the WT-like variants, A4V, L38V, G93A and L106V, vary by less than an order of magnitude from the 100 pM apparent K_d for the WT protein and are not consistently decreased. Despite the small differences in the measured Zn affinity, these results correlate well with the observed metal content of the mutant protein when isolated from insect cells.[32]

These results may appear to contradict the findings by Crow *et al.,* [127] who found that the dimeric A4V and L38V SOD1 variants had a 30-fold and 18-fold weakening of the Zn affinity relative to WT protein in 2 M urea; the contradiction can be understood in terms of the increased population of the folded monomeric forms for these variants and their lower zinc affinity relative to the dimeric state.[48] The 66 hours required to extract zinc

from these variants in the Crow *et al.* study would provide ample opportunity for the monomeric form to serve as the conduit for zinc loss.

S134N, a metal-binding variant of SOD1, differs from the β-sandwich variants in that the apparent Zn affinity is significantly reduced. While the S134N variant is not destabilized significantly in its metal-free forms, the weakening in the apparent K_d for Zn binding from 100 pM for WT mAS-SOD1^{SS} to 1.6 nM for S134N mAS-SOD1^{SS} offers the possibility that aggregation of the monomeric forms may still be the source of toxicity. Although this variant can be loaded with Zn and Cu *in vitro,*[94; 95] Hayward and coworkers[83] have observed decreased Zn and Cu content in as-isolated samples of S134N SOD1 expressed in insect cells. The replacement of serine with asparagine in the electrostatic loop may similarly impede full metalation in motor neurons. The potential for aggregation might be further compounded by the spontaneous reduction of the disulfide bond of the metal-free species in the cytoplasm. Thus, even the small fraction of unfolded mAS-SOD1^{2SH} observed for S134N may be sufficient to cause aggregation. Because the predicted metal-free unfolded and folded populations for S134N are nearly identical to WT, the intriguing possibility arises that the loss of Zn even from the WT protein may be sufficient to trigger aggregation.

Zn binding is dramatically decreased by reduction of the disulfide bond.

In contrast to the response to mutations, the reduction of the disulfide bond has a dramatic effect on the Zn affinity of mAS-SOD1, resulting in a ~750-fold weakening in the apparent K_d from 100 pM to 75 nM for the WT protein and a 16-fold weakening in the apparent K_d for the S134N variant from 1.6nM to 25 nM. The 3-fold tighter K_d for disulfide-reduced S134N vs. WT protein contrasts with a 16-fold weaker apparent K_d in the presence of the disulfide bond. This behavior demonstrates thermodynamic coupling between the disulfide bond and Zn binding. Inspection of the crystal structure of SOD1 shows that the disulfide bond is proximal to the Cu site, which shares a ligand with the Zn site. Apparently, the constraints on the structure introduced by the disulfide bond are transmitted to the Zn binding site in a way that reduces the affinity of S134N for Zn. This may be due to the inability of the S134N variant to induce compactness in the electrostatic loop by the formation of the S134 - D125 hydrogen bond.[94] When the protein relaxes in the absence of the disulfide bond, the electrostatic loop may be able to access conformers that form stabilizing electrostatic interactions absent in the WT protein.

These results suggest that disulfide bond oxidation may be the key step in the maturation of SOD1. Because $SOD1^{2SH}_{Apo}$ would not compete effectively for free Zn at ~1 nM concentration *in vivo*, Zn would be expected to bind after the oxidation of the disulfide bond when the apparent K_d decreases to 100 pM. This hypothesis is supported

by the discovery that the presence of Zn does not accelerate the formation of the disulfide bond in SOD1 expressed in rabbit reticulocyte assays [37].

Aggregation following synthesis on the ribosome?

The analysis presented above presumes that the populations of species *in vivo* dictated by the equilibrium free energy surface of SOD1 are those responsible for aggregation and toxicity. Alternately, the aggregation of SOD1 may occur soon after synthesis on the ribosome, prior to its several maturation steps including disulfide bond formation, dimerization and Zn and Cu loading.[37] Disulfide-reduced SOD1 folds surprisingly slowly *in vitro*, requiring ~40 seconds at 20 ^{o}C, nearly four orders of magnitude slower than predicted by its topology.[154] Although the time required for folding is comparable to the length of time required to translate a 153 residue eukaryotic protein, ~30-50 s,[170] co-translational folding of SOD1 is unlikely since the rate-limiting step of folding involves the docking of the first four N-terminal β-strands with the β7 strand near the C-terminus.[124] The observation that the four ALS variants in the β-sandwich structure, A4V, L38V, G93A and L106V, have substantially increased unfolded populations of their disulfide-reduced forms implies an enhanced opportunity for the aggregation of these species prior to their ultimate maturation to their native dimeric forms. The subsequent formation of the disulfide bond increases the stability of the folded monomeric form and drives the dimerization reaction.[40] The high concentration of SOD1 in motor neurons, >10 μM,[104] and its half-life of ~1 day,[171] requires a constant and significant rate of

synthesis on ribosomes. Thus, the aggregation of SOD1 may involve both kinetic, i.e., following synthesis and prior to maturation, and thermodynamic, i.e., at steady-state after maturation,[117] mechanisms.

Materials and Methods

Protein purification.

Recombinant proteins were expressed in and purified from BL21-Gold(DE3) PLysS cells (Stratagene®, Inc. Cedar Creek, TX). The protein was purified using the procedure previously described in Kayatekin *et al.*[48] Protein identity and purity was determined by measuring the molecular weight with LC-ESI mass spectrometry. The protein concentrations were calculated using an extinction coefficient of 5,400 M^{-1} cm^{-1}.

Disulfide-bond reduction.

All variants of mAS-SOD1 were reduced by 24 hour incubation in 1 mM TCEP. The reduction of the disulfide-bond and absence of re-oxidation after the incubation in reducing agent was confirmed by kinetic unfolding or refolding experiments for $mAS\text{-}SOD1_{Apo}$. Fully reduced protein exhibited a single exponential phase with a relaxation time 5-fold faster than the disulfide-oxidized protein in unfolding.

Equilibrium experiments.

All circular dichroism spectroscopy was performed on a Jasco-810 spectropolarimeter (Jasco Inc., Easton, MD) equipped with a water-cooled Peltier temperature control system. The CD spectra of disulfide-reduced protein were an average of 6 spectra

obtained using a 1 mm path length quartz cuvette, a scan rate of 20 nm min^{-1} and a response time of 4 s. The buffer used was 10 mM potassium phosphate, 1 mM ETDA, 1 mM TCEP, pH 7.2. The urea induced unfolding curves were monitored from 220-240 nm in a 0.5 cm path length quartz cuvette using a scan rate of 20 nm min^{-1} and a response time of 8 s. The buffer used was 20 mM HEPES, 1 mM EDTA, 1 mM TCEP for disulfide-reduced and 10 mM KPi, 1 mM EDTA for disulfide-oxidized samples, pH 7.2. Urea concentrations were determined by refractive index on a Leica Mark II refractometer. Titration samples were made from concentration matched stocks of folded protein in standard buffer and unfolded protein at 8 M urea and incubated at the experimental temperature overnight.

Kinetic experiments.

The unfolding and refolding kinetics, initiated by manual mixing, were monitored by CD. For metal-free protein, 10 mM potassium phosphate, 1 mM EDTA, pH 7.2 was used as the buffer. For metal-bound protein the potassium phosphate was replaced with 20 mM HEPES and the 1 mM EDTA was omitted. Data were collected at 230 nm in a 1 cm^2 cuvette under continuous mixing with a solution volume of 1.9 mL. Unfolding jumps were initiated from protein in 0 M urea or Gdn-HCl and refolding jumps were initiated from protein denatured in 4-6 M Gdn-HCl or 8 M urea to various final concentrations. For Zn-loaded samples, the protein was incubated with stoichiometric Zn prior to dilution

in the unfolding/refolding buffer. The final concentration of Gdn-HCl was measured by index of refraction. Protein concentrations were 10 μM for all kinetic experiments.

Acknowledgements

We thank Dr. Osman Bilsel, Sagar V. Kathuria, Steven F. Trueman and Ian M. Love for many helpful discussions, Nicole Washington for purifying S134N mAS-SOD1 and Jessica Adefusika, Graham Dobereiner and Matt Samberg for creating the bacterial constructs. This work was supported by National Institutes of Health grant GM54836, and support for mass spectrometry was provided by NICHD IDDRC Core Grant HD04147.

Chapter IV. Enthalpic barriers associated with desolvation dominate the folding reaction of SOD1 monomers.

Introduction

Amyotrophic lateral sclerosis is a neurodegenerative disease which results in the death of motor neurons. Mutations in the gene encoding for the Cu, Zn superoxide dismutase (SOD1) have been found to cause ALS through a gain-of-function mechanism. To date, over 150 mutations have been discovered in human patients. The overwhelming majority of these are missense mutations, but some deletion mutations and C-terminal truncations also exist (http://alsod.iop.kcl.ac.uk/). These mutations lead to the formation of oligomeric species of SOD1, which, in later stages of the disease, leads to the formation of large aggregates. A variety of mechanisms have been suggested for the toxicity of misfolded and aggregated SOD1,[71] but the exact nature of the toxic species remains unknown.

SOD1 is primarily a cytosolic protein responsible for the dismutation of the highly reactive superoxide anion (O_2^-). The protein is a homodimer with one catalytic copper ion and one structurally important zinc ion bound to each subunit (Figure 4.1). The fold of the protein can be described as a β-sandwich, with eight anti-parallel β-strands supporting two large, catalytically important loops. These loops, the Zn binding loop and the electrostatic loop, are important structurally and for guiding the substrate to the active site, respectively. In the absence of the metals, as in this study, these loops have been

Figure 4.1. Crystal structure and topology of SOD1.

(A) SOD1 is a dimeric β-sandwich protein consisting of eight anti-parallel β-stands supporting two catalytic loops (PDB: 2C9V). The electrostatic loop is depicted in green, while the Zn-binding loop is depicted in cyan. Each monomeric subunit also contains a Zn and Cu ion, which were not present for this study, as well as an intramolecular disulfide bond. The free cysteines, C6/C111 (red), were replaced with alanine and serine respectively. Additionally, a pair of glutamic acid residues was introduced at the dimer interface, replacing F50/G51 (violet), in order to obtain the obligate monomer, mAS-SOD1. (B) The topology of SOD1 immunoglobulin-like. It is made up of two β-sheets, the first consisting of strands 1-3+6 and the second consisting of 4+5+7+8, and contains a Greek-key motif.

Figure 4.1. Crystal structure and topology of SOD1.

A)

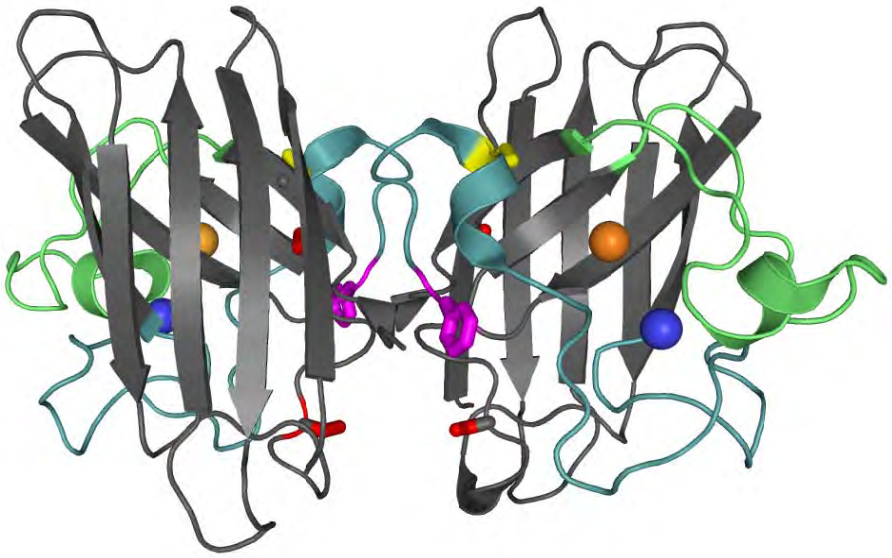

B)

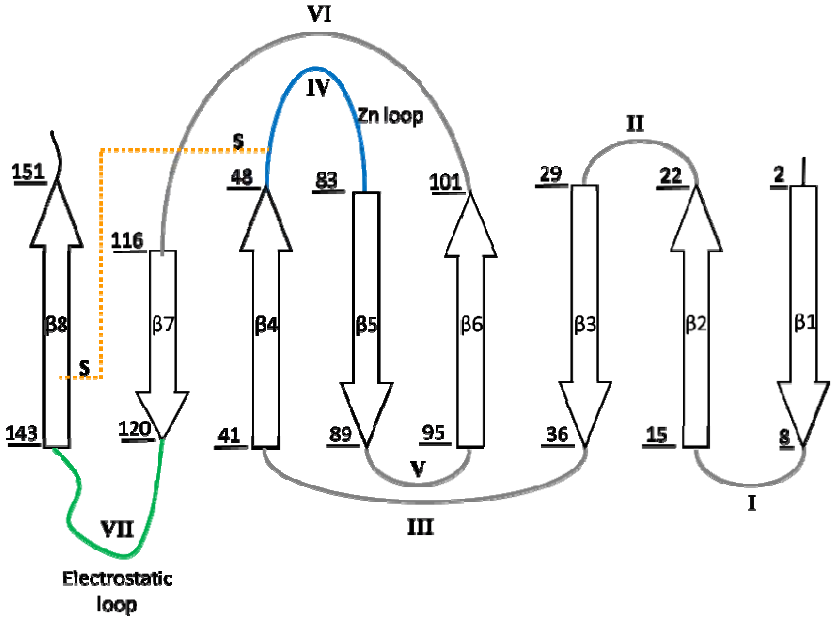

shown to be intrinsically disordered by NMR[35] and x-ray crystallography.[36] Each subunit also features an intramolecular disulfide bond between C57 and C146.

The folding mechanism of SOD1 can be best described as a three-state reaction,[113; 114] $2U \leftrightarrows 2M \leftrightarrows N_2$, in which the rate-limiting monomer folding reaction from the unfolded state, U, to the folded state, M, is followed by their rapid association, contingent upon disulfide-bond oxidation or Zn binding,[40] to form the dimeric native state, N_2. The monomer folding reaction of metal-free SOD1 is of particular interest because the surprisingly slow folding rate constant in the absence of denaturant, $k_f = 0.079\ s^{-1}$,[117] is 3-4 orders of magnitude slower than predictions derived from the complexity of the topology, such as relative contact order[154] or long-range order.[172] The topology of SOD1 is in the family of immunoglobulin-like folds, characterized by two anti-parallel β-sheets with a greek key motif (Figure 4.1B). The formation of long range contacts between hydrophobic residues in the core β-strands are likely the critical step in the formation of the folding transition state.[173] For SOD1, according to the phi analysis performed by Nordlund and co-workers, these residues consist of at least C6, I18, L117, forming a tightly-packed hydrophobic ring similar to those observed for Tnf3 and CAfn2.[174]

Characterization of the transition state between the folded and unfolded forms of the SOD1 monomer can provide insight into the roles of sequence and topology in governing the folding of this molecule. By monitoring the temperature and viscosity dependence of

folding and unfolding reactions, key insights may be obtained on the role of entropy and enthalpy in defining the barriers to folding. These results show that the barriers to folding and unfolding are both enthalpically dominated with large energetic barriers, consistent with slow folding and unfolding reactions. The folding reaction shows unitary dependence with the solvent viscosity, suggesting that chain diffusion and the search for the critical folding nucleus are still contributing to the slow folding reactions. These results combined with the lack of significant global collapse preceding monomer folding,[114] suggest that dehydration of the chain, rather than the breakup of pre-existing structure, is the likely contributor to the enthalpic barrier in refolding.

Materials and methods.

Protein purification.

Recombinant mAS-SOD1 was expressed in BL21-Gold(DE3) cells (Stratagene®, Inc. Cedar Creek, TX) and purified according to the procedure previously described (ref kayatekin 2008). Protein mass and purity were determined by LC-ESI mass spectrometry. Protein concentrations were determined by absorbance measurements performed on a Jasco UV-580 UV/Vis spectrophotometer (Jasco Inc., Easton, MD) using an extinction coefficient of 5,400 M^{-1} cm^{-1} at 280 nm.

Kinetics.

The unfolding and refolding kinetics were all initiated by manual mixing with a dead time of ~3 seconds and monitored by CD utilizing a Jasco J-810 CD spectrophotometer (Jasco Inc., Easton, MD). The data were collected at 230 nm in a 1 cm^2 cuvette with continual mixing and a total volume of 1.9 mL. The standard buffer for all experiments was 20 mM HEPES, 1 mM EDTA, pH 7.2. Refolding jumps were initiated from 5 M Urea for the temperature dependence studies and 4 M Gdn-HCl for the viscosity dependence studies. Unfolding jumps were initiated from the absence of denaturant. The final denaturant concentration for each kinetic point was determined by index of refraction measurements. The final concentration of protein for all experiments was 5-10 μM.

Data analysis.

Individual kinetic traces were fit independently using Savuka 6.2, utilizing the Marquardt-Levenberg non-linear least squares algorithm. The relaxation kinetics were well described by a single exponential:

$$F(t) = F_{\infty} + Ae^{-kt} \tag{1}$$

Where F_{∞} is the CD signal at infinite time and A is the amplitude of the signal change associated with the kinetic phase described by the rate constant, k.

The folding and unfolding data as a function of final denaturant concentration were extrapolated to the absence of denaturant assuming an exponential dependence on the urea concentration:

$$k_{obs} = k_f^0 e^{-m_f[urea]/RT} + k_u^0 e^{-m_u*[urea]/RT} \quad (2)$$

Where k_{obs} is the observed rate at a given denaturant concentration, [urea], k_f^0 and k_u^0 are the folding and unfolding rates in the absence of denaturant, respectively, and m_f and m_u are the denaturant dependence of the folding and unfolding rates, respectively.

Using the rates in the absence of denaturant, the entropic and enthalpic contributions to the activation free energy can be calculated from transition state theory:

$$k_{obs} = k_a \cdot \exp\left(\frac{-\Delta G^{0‡}}{RT}\right) = k_a \cdot \exp\left(\frac{-\Delta H^{0‡}}{RT}\right) \cdot \exp\left(\frac{\Delta S^{0‡}}{R}\right) \quad (3)$$

However, due to the fact that there is a large change in surface area in protein folding and unfolding reactions, the change in heat capacity must also be considered:

$$\Delta H^{0‡} = \Delta H^{0‡}(T_0) + \Delta C_p^{0‡} \cdot (T - T_0) \quad (4)$$

$$\Delta S^{0‡} = \Delta S^{0‡}(T_0) + \Delta C_p^{0‡} \cdot \ln\left(\frac{T}{T_0}\right) \quad (5)$$

Substituting into equation 3, the rate constants in the absence of denaturant at the temperatures studied were then parameterized according to:

$$\ln\left(\frac{k}{T}\right) = \frac{\Delta S^{0^{\ddagger}} - \Delta C_p^{0^{\ddagger}}}{R} + \ln\left(\frac{k_a}{T}\right) + \left(\frac{T}{T^0}\right)\frac{\Delta C_p^{0^{\ddagger}} - \frac{\Delta H^{0^{\ddagger}}}{T^0}}{R} - \frac{\Delta C_p^{0^{\ddagger}}}{R}\ln\frac{T}{T^0} \quad (6)$$

Where k_a is the prefactor, T^0 is 298.15 K, R is the gas constant and $\Delta S^{0^{\ddagger}}$, $\Delta H^{0^{\ddagger}}$, and $\Delta C_p^{0^{\ddagger}}$ are the change in entropy, enthalpy and heat capacity, respectively, at standard state. The choice of the prefactor, k_a, depends on the choice of the Eyring or Kramers formalisms. For the Eyring formalism, $k_a = k_b T/h = 6.2 \times 10^{12}\ s^{-1}$, where k_b is the Boltzmann constant, T is the temperature in Kelvin, and h is Plank's constant. For the Kramers formalism, $k_a = \kappa_0/\eta$, where κ_0 is the rate constant in the absence of a free energy barrier and η is the solvent viscosity. The appropriate value, $k_a = 5 \times 10^8\ s^{-1}$, was chosen based on experiments performed on peptide models.[175; 176]

Results.

Monomer model.

While the dimer dissociation reaction is rate limiting, and therefore the only observable in unfolding reactions, the association reaction proceeds with a rate $>10^6\ s^{-1}$ and is difficult to measure directly because it follows the rate-limiting monomer folding reaction[117]. Alternatively, both the monomer folding and unfolding reactions are amenable to manual mixing techniques in a monomeric variant of SOD1, mAS-SOD1. This variant was created by the replacement of F50 and G51 near the dimer interface with glutamic acid

residues (Figure 4.1).[143] SOD1 with an intact intramolecular disulfide bond was studied specifically to determine whether loop closure plays a significant role in guiding the search process to the native structure. The free cysteines, C6 and C111, were replaced with alanine and serine in order to improve folding reversibility by preventing disulfide interchange in the unfolded state and intermolecular disulfide crosslinking in the native state. Additionally, the removal of the free cysteines, combined with the natural absence of methionine residues, greatly reduces the possibility of oxidative damage associated with experiments performed at higher temperatures.

Temperature dependence of the disulfide-oxidized mAS-SOD1.

The kinetic folding and unfolding reactions for disulfide-oxidized mAS-SOD1 were monitored by circular dichroism spectroscopy at 230 nm and initiated by manual mixing with a dead time of ~2 s. The refolding and unfolding rates were measured as a function of temperature between 10 °C and 40 °C at 2.5 °C intervals. The raw folding and unfolding kinetics were well described by single exponential relaxation kinetics. The chevron plots at every 5 °C are shown in Figure 4.2.

The kinetic data were extrapolated to the absence of denaturant assuming an exponential dependence of the observed rate on the concentration of denaturant (Eq. 2). The free energy of folding, $\Delta G^0 = -RT\ln(k_u / k_f)$, and $m^{\ddagger}$-values as a function of temperature can be seen in Figure 4.3. The free energy increases non-linearly approaching a

Figure 4.2. Temperature dependence of mAS-SOD1 folding kinetics

The folding and unfolding kinetics of disulfide-oxidized mAS-SOD1 are shown as a function of temperature at every 5 °C, ranging from 10 °C (top) to 40 °C (bottom). The solid lines represent the fit to a two-state folding model, N↔U.

Figure 4.2. Temperature dependence of mAS-SOD1 folding kinetics.

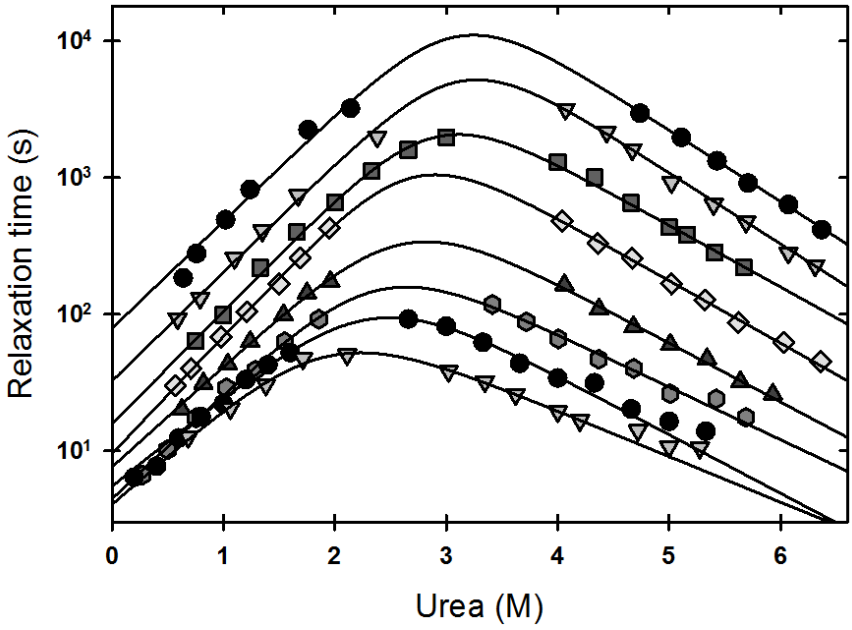

Figure 4.3. Temperature dependence of the ΔG° and the $m^{‡}$-values.

The free energy of folding (A) and the m‡-values (B) of folding (open circles) and unfolding (filled circles) are shown as a function of temperature. The solid line in (A) represents to the best fit to the Gibbs-Helmholtz equation (Eq. 8). The error bars represent the error of the fit.

Figure 4.3. Temperature dependence of the ΔG° and the $m^{\ddagger}$-values.

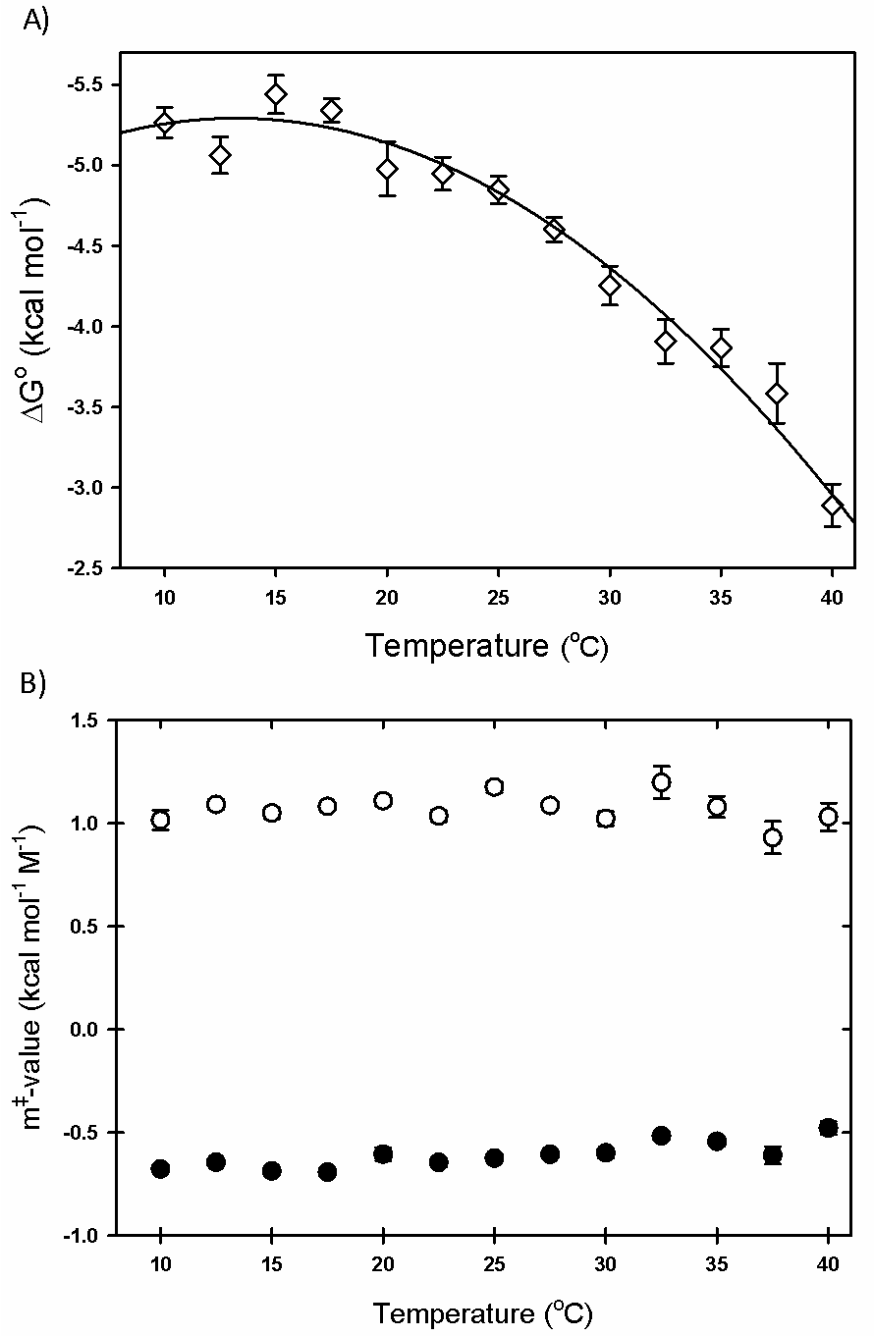

maximum around 10-15 °C. The change in the free energy of folding as a function of temperature, for a two-state process, can be described by the modified Gibbs-Helmholtz equation:[177; 178]

$$\Delta G^{o}(T) = \Delta H_m\left(1-\frac{T}{T_m}\right) - \Delta C_p((T_m - T) + T\ln\left(\frac{T}{T_m}\right) \quad (7)$$

where ΔH_m, T_m, and ΔC_p correspond to the enthalpic change at the midpoint of the transition, the temperature of the midpoint of the transition and the heat capacity change upon unfolding respectively. By this analysis, the unfolding of mAS-SOD1 results in a heat capacity change of 1.93±0.27 kcal mol^{-1} K^{-1}, a change in enthalpy of 28.0±2.2 kcal mol^{-1}, and a change in entropy of 78±7 cal mol^{-1} K^{-1} at 298 K.

Unlike the free energy, the $m^{\ddagger}$-values exhibit a linear dependence on the temperature. The refolding $m^{\ddagger}$-value is relatively unchanged while the unfolding $m^{\ddagger}$-value slightly decreases as a temperature is increased, ranging from -0.67±0.02 kcal mol^{-1} M^{-1} at 10 °C to -0.48±0.03 kcal mol^{-1} M^{-1} at 40 °C. These results suggest that the native state may become less structured at higher temperatures, while the transition state ensemble and the unfolded state are unchanged.

In order to discriminate between the entropic and enthalpic contributions to the free energy of forming the transition state ensemble, the temperature dependence of the rates

Figure 4.4. Eyring plots of the folding and unfolding reactions.

The log of the (A) folding (open circles) and (B) unfolding (filled circles) rates divided by the temperature were plotted as a function of the inverse of the temperature and fit to an Eyring or Kramers model as described in Materials and Methods to obtain the thermodynamic parameters of the transition state, $\Delta S^{0^{\ddagger}}$, $\Delta H^{0^{\ddagger}}$, and $\Delta C_p^{0^{\ddagger}}$.

Figure 4.4 Eyring plots of the folding and unfolding reactions.

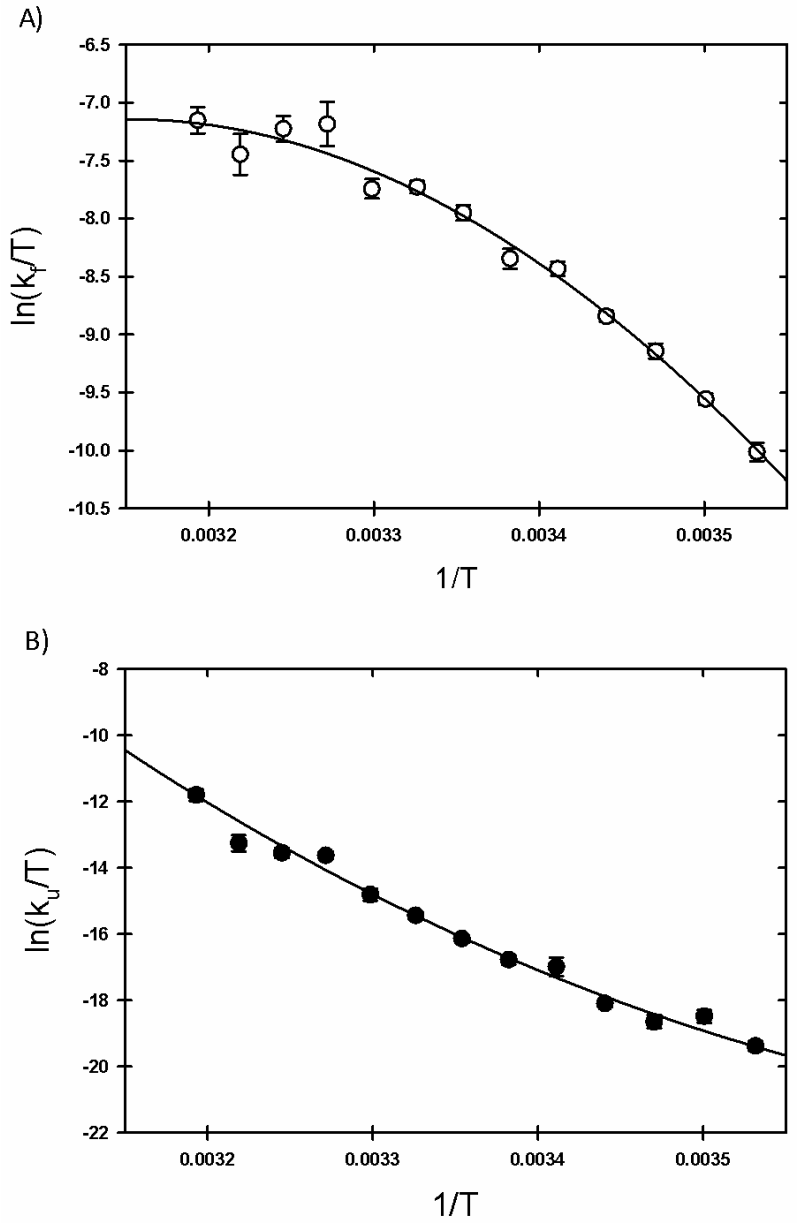

extrapolated to the absence of denaturant (Eq. 3) was evaluated according to equation 6. An Eyring plot of the data can be seen in Figure 4.4. The activation energy parameters for refolding and unfolding, at 298 K, for evaluated with both the Eyring and Kramers formalisms are reported in Table 4.1. This analysis shows that the contribution to the activation energy barrier at 298 K is entirely enthalpic for both unfolding and refolding reactions.. With the exception of the Eyring formalism for the refolding reaction, the entropic contribution is favorable for both the folding and unfolding reactions.

The change in heat capacity and the height of the enthalpic barriers are not unusual for small, single domain proteins characterized as two-state folders,[179] and can be related to the extent of accessible surface area exposure.[147] The change in accessible surface area between the native and unfolded states evaluated by the *m*-value is 12045±364 $Å^2$, while the change in the surface area estimated from the ΔC_p value is 10742±2263 $Å^2$. The good agreement between these numbers instills confidence in the results and further reinforces the two-state nature of mAS-SOD1 folding.

The apparent linear decrease in the activation free energy and activation enthalpy with increasing concentration of denaturant (Figure 4.5) resembles the N→I transition in the α-subunit of tryptophan synthase.[180] A quantitative comparison can be made by fitting the transition state parameters to a denaturant binding model:[180; 181; 182]

Figure 4.5. Urea dependence of the activation energy and enthalpy of unfolding.

The unfolding energy of activation (A) and the enthalpy of activation (B) are shown as a function of urea. The values at each urea concentration were calculated from an interpolation of the measured relaxation times. Solid lines are the best fit to a Tanford urea binding model.[182]

Figure 4.5. Urea dependence of the activation energy and enthalpy of unfolding.

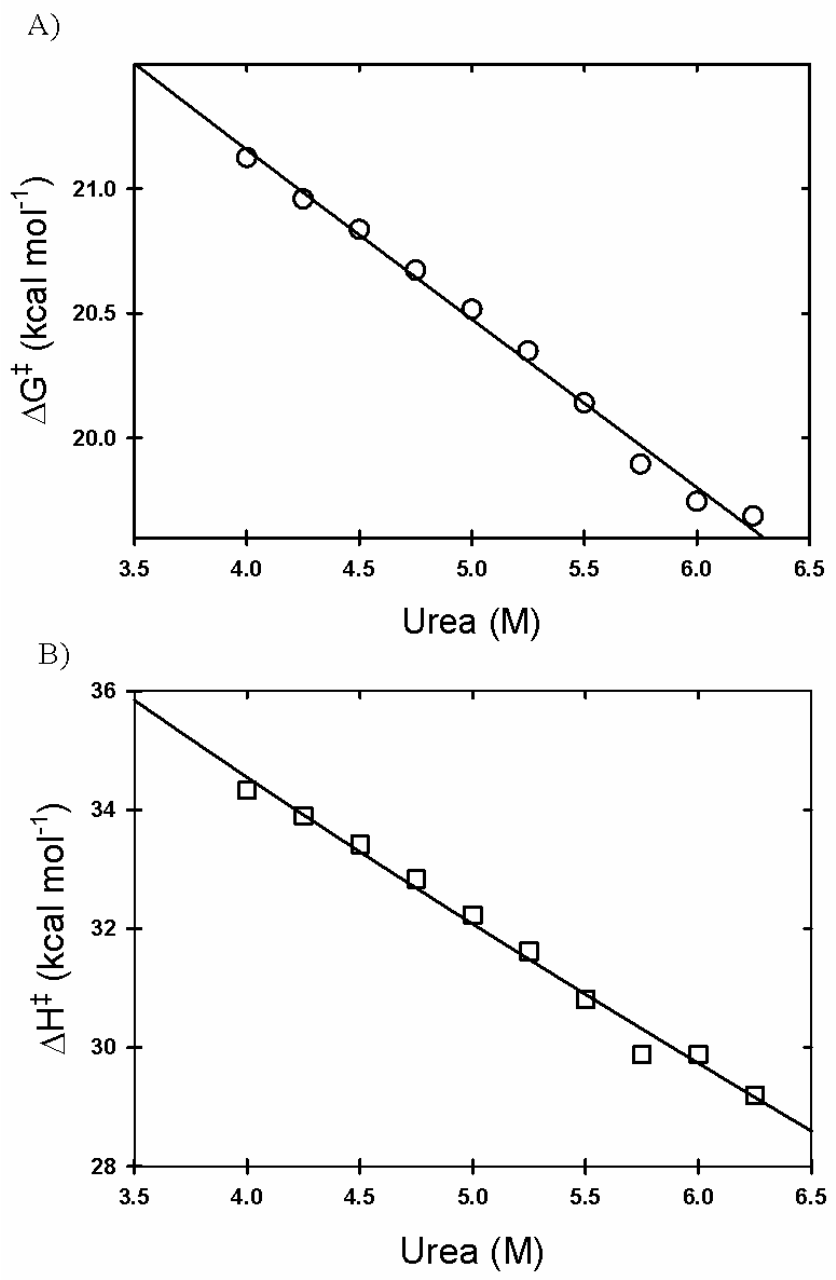

Table 4.1. Thermodynamic parameters of the transition state ensemble of disulfide-oxidized mAS-SOD1.*

	$\Delta H^{\circ\ddagger}$ (kcal mol^{-1})	$\Delta S^{\circ\ddagger}$ (cal mol^{-1})	$\Delta Cp^{\circ\ddagger}$ (kcal mol^{-1} K^{-1})	$\Delta G^{\circ\ddagger}$ (kcal mol^{-1})
Folding				
Eyring	16.1±0.6	-9±2	-0.85±0.12	18.8±0.9
Kramers	16.7±0.6	12±2	-0.85±0.12	13.1±0.6
Unfolding				
Eyring	45.0±1.7	72±6	1.06±0.37	23.5±2.5
Kramers	45.6±1.7	93±6	1.06±0.37	17.9±2.5

* The thermodynamic parameters were calculated by fitting the observed folding rate in the absence of denaturant and are reported at standard temperature, T^{o}=298 K. The choice of prefactor depends on the formalism employed, where $k_a = 6.2\times10^{12}$ s^{-1} for the Eyring formalism and $k_a = 5\times10^{8}$ s^{-1} for the Kramers formalism.

$$\Delta G^{0\ddagger} = \Delta G^{0\ddagger}(\mathrm{H_2O}) - \Delta n^{\ddagger} RT \ln(1 + K \cdot a) \quad (8)$$

$$\Delta H^{0\ddagger} = \Delta H^{0\ddagger}(\mathrm{H_2O}) - \Delta n^{\ddagger} \Delta H_B^{0\ddagger} K \cdot a / (1 + K \cdot a) \quad (9)$$

$$\Delta S^{0\ddagger} = (\Delta H^{0\ddagger} - \Delta G^{0\ddagger}) / T \quad (10)$$

where $\Delta n^{\ddagger}$ represents the number of additional urea binding sites in the TSE compared to the native state, *K* is the binding constant of urea to independent and identical sites on the protein, *a* is the activity of urea, and $\Delta H_B^{0\ddagger}$ is the enthalpy change upon binding urea. The average value of *K* was assumed to resembled values determined for ribonuclease, lysozyme and cytochrome c, 0.061 M^{-1}.[181] The activity of urea was determined using the equation proposed by Pace: a = 0.9815(urea) - 0.02978(urea)^2 + 0.00308(urea)^3. [183]

The activation energy as a function of urea was calculated from an interpolation of the fit to the observed relaxation times, $\tau = 1/k$. As seen in Figure 4.5, equation 8 provides an excellent fit to the observed denaturant dependence of the activation free energy and yields values of $\Delta G^{0\ddagger}(\mathrm{H_2O})$ =24.2±0.1 kcal mol^{-1}, $\Delta n^{\ddagger}$ = 26.1±0.8. These values are held constant to fit the urea dependence of the activation enthalpy (Eq. 9), yielding values: $\Delta H^{0\ddagger}(\mathrm{H_2O})$ = 47.3±0.6 kcal mol^{-1}, $\Delta H_B^{0\ddagger}$ = -2.69±0.10 kcal mol^{-1} M^{-1}. The activation entropy of binding urea to the revealed sites, $\Delta S_B^{0\ddagger}$, can be determined from Equation 10, and has a value of -14.7±0.5 cal mol^{-1} K^{-1} M^{-1}. These values are in good agreement with

those determined urea binding to unfolded proteins obtained from calorimetric experiments: $\Delta H_B^{0\ddagger}$ = -2.2±0.5 kcal mol^{-1} M^{-1}, $\Delta S_B^{0\ddagger}$ =-12.7±1.9 cal mol^{-1} K^{-1} M^{-1}.[181]

Viscosity dependence for the unfolding and refolding rates.

A theoretical explanation for the effect of solvent viscosity on protein folding is provided by the Kramers theory which suggests that the rate of folding should be inversely proportional to the friction.[184] Put in experimental terms, the relaxation time can be interpreted as a function dependent on an adjustable prefactor (C), the internal friction of a system (σ), the height of the energy barrier ($\Delta G^{\ddagger}$) and the viscosity of the solvent (η):

$$k = \frac{1}{\tau} = \frac{C}{\eta + \sigma} \exp\left(\frac{-\Delta G^{\ddagger}}{RT}\right) \qquad (11)$$

For systems in which the internal friction of the protein is negligible relative to the solvent viscosity, the relaxation time should vary linearly with the solvent viscosity with a slope of unity.

We investigated whether internal friction is playing a role in the folding of SOD1 by measuring the folding kinetics of mAS-SOD1 over a range of solvent viscosities. The increased stability of mAS-SOD1 upon the addition of co-solvents led to the choice of guanidine hydrochloride, a more potent denaturant, for these experiments. The chevron plots for mAS-SOD1 folding in the presence of increasing concentrations of glycerol are

shown in Figure 4.6A. The addition of glycerol increases the stability of mAS-SOD1 by both accelerating refolding and slowing unfolding, As a result, glycerol shifts the midpoint of the N↔U reaction from 0.8 M in the absence of glycerol to 1.25 M at 16%, to 1.46 M at 24% and, 1.76 M at 32%. Because neither the unfolding or refolding $m^{\ddagger}$-values are affected by glycerol, the exposure of surface areas of the native, transition state ensemble and the unfolded state do not change in response to the viscogens.

In order to ensure that these results were not the result of some property specific to glycerol but of increased bulk viscosity of the solvent, four concentrations of glucose, one concentration of sucrose, and two concentrations of PEG 8000 were also tested (Figure 4.6A and 4.6B). Both glucose and sucrose exhibit similar behavior to glycerol in that they stabilize mAS-SOD1 by accelerating refolding and slowing unfolding. On the other hand, neither concentration of PEG 8000 shows any effect on the folding kinetics of mAS-SOD1 despite a significant increase in the bulk solvent viscosity.

It may seem counterintuitive that the refolding rates accelerate in a more viscous solvent, but this is a consequence of the increased stability of the protein in the presence of osmolytes.[185; 186; 187] In order to separate the effect on stability from the effect on the folding and unfolding rates, an isostability approach was used.[185] Instead of measuring the rates of folding and unfolding for each viscogens at identical Gdn-HCl concentrations, the rate constants were determined at concentrations of Gdn-HCl where k_f

Figure 4.6. Viscosity dependence of mAS-SOD1 folding and unfolding relaxation times.

The folding and unfolding relaxation times as a function of final denaturant concentration are shown for increasing concentrations of (A) glycerol: 0% (open circles), 16% (light gray), 24% (dark gray), 32% (black); PEG8000: 3% (open diamonds), 6% (gray diamonds); (B) Glucose: 11% (white triangles), 17% (light gray triangles), 20% (dark gray triangles), 26% (black triangles); Sucrose: 18% (white squares). All experiments were performed at 20 °C, in buffer containing 20 mM HEPES, 1 mM EDTA pH 7.2.

Figure 4.6. Viscosity dependence of mAS-SOD1 folding and unfolding relaxation times.

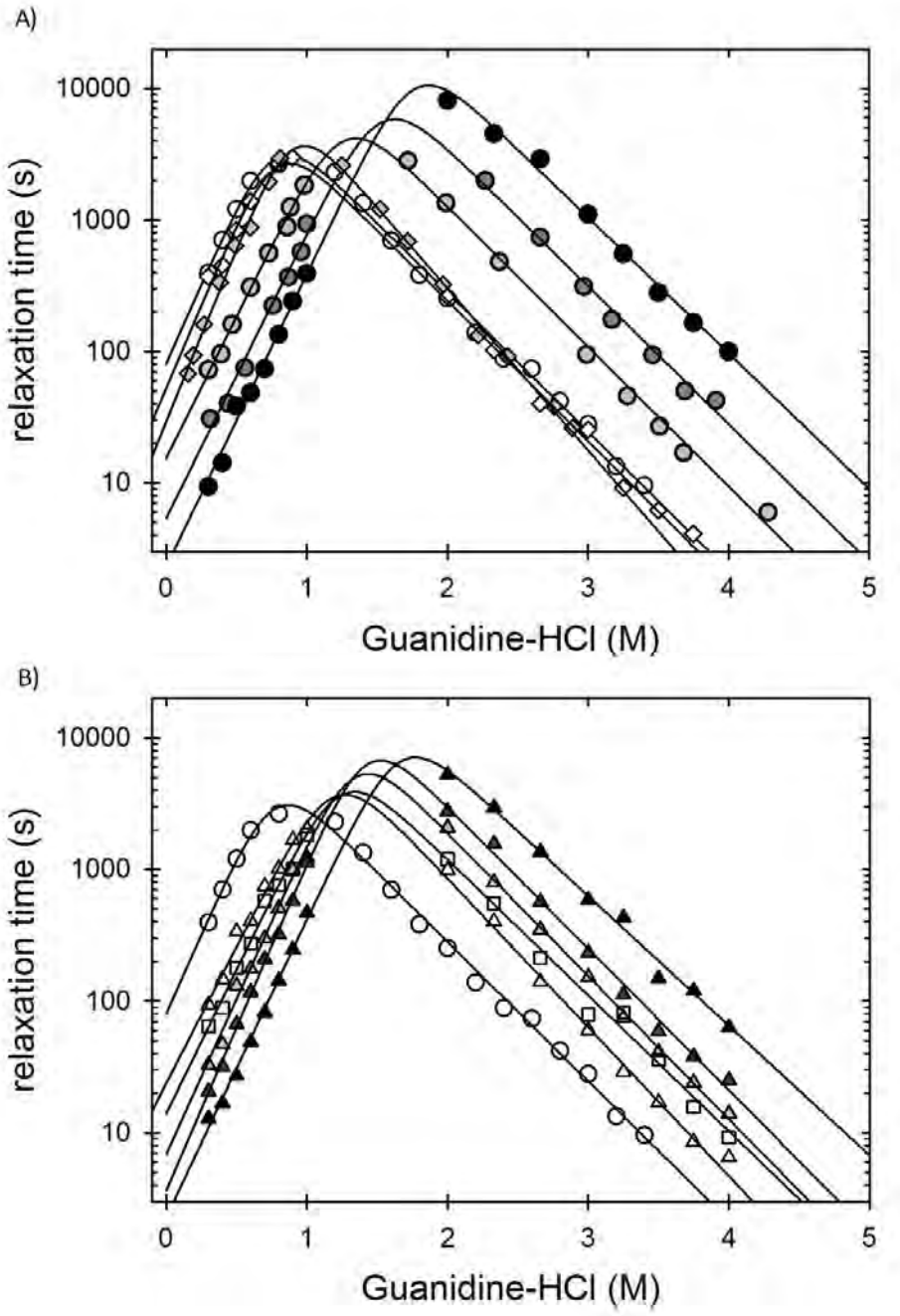

= 1000 k_u and k_u = 1000 k_f respectively. A plot of the observed relaxation time in the presence of a viscogen under isostability conditions relative to the relaxation time in buffer versus the relative viscosity of the solvent is shown in Figure 4.7. For a protein with little or no internal friction, a unitary dependence on the solvent viscosity is expected. The best-fit line to relative relaxation time versus relative viscosity for folding and unfolding yields a slope of 1.34±0.26 and 1.32±0.27 respectively. Within the uncertainly of these data, the results suggest a diffusion-limited process for both unfolding and refolding.

Figure 4.7. The increase in the relative relaxation time of mAS-SOD1 folding and unfolding reactions with increasing solvent viscosity.

The relative relaxation time (τ/τ_o) for mAS-SOD1 in the presence of glycerol (circle), glucose (diamond), sucrose (triangle) and PEG 8000 (square) are plotted as a function of the solvent viscosity. Open circles represent refolding data while the closed circles represent unfolding. The solid line represents a linear relationship between the relaxation time and solvent viscosity with a slope of unity. The dotted line represents a viscosity independent relative relaxation time, the behavior exhibited in the presence of PEG 8000.

Figure 4.7. The increase in the relative relaxation time of mAS-SOD1 folding and unfolding reactions with increasing solvent viscosity.

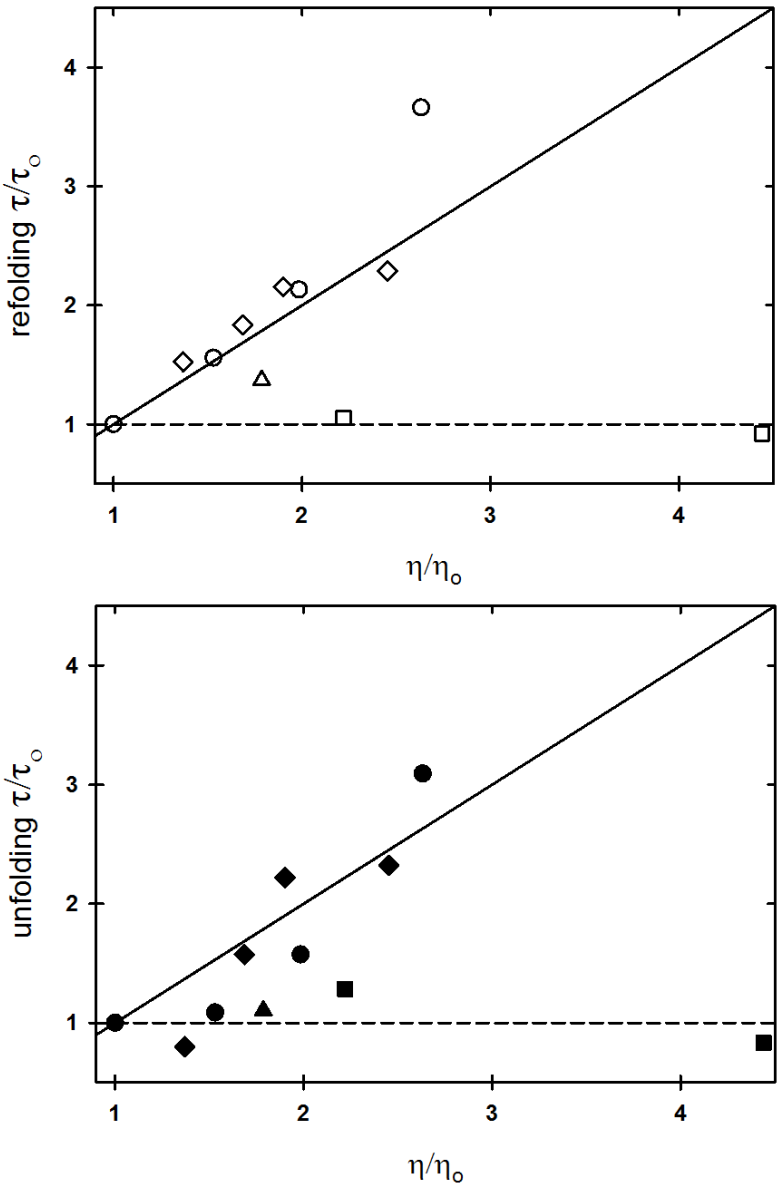

Discussion

The slow folding reaction of SOD1 monomers and its potential relationship to aggregation motivated the study of the temperature and viscosity dependence of the folding and unfolding rates of disulfide-oxidized mAS-SOD1. The refolding relaxation time of SOD1 under physiological conditions, $\tau \sim 1$ s, is much slower than folding reactions observed for α-helical proteins, which can fold in milliseconds or even microseconds.[188; 189] This 4-5 orders of magnitude difference in timescales may partially explain the aggregation propensity of this protein. Both the unfolding and refolding activation energy barriers were found to be dominated by unfavorable enthalpic contributions. Depending on the choice of formalism, all or all but the refolding reaction are partially offset by favorable entropic contributions. SOD1 exhibited the expected slowing of the folding and unfolding rates with solvent viscosity, consistent with a diffusive process, suggesting that internal friction is not playing a role in the slow folding reaction.

The nature of the transition state.

Insights into the relative position of the transition state ensemble with respect to the native and unfolded states can be obtained by comparing the ratio of the refolding $m^{\ddagger}$-value and $\Delta C_p^{0\ddagger}$ values to the total *m*-value and ΔC_p^0. This parameter, designated α, can be related to the surface area buried upon formation of the transition state:

$$\alpha = \frac{X_{UN}^{\ddagger}}{X_{UN}^{\ddagger} - X_{NU}^{\ddagger}} \qquad (12)$$

where $X^{\ddagger}$ is either the $m^{\ddagger}$ or $\Delta C_p^{0\ddagger}$ value. An α-value near 1 suggests a very native-like transition state, whereas an α-value near 0 suggests an unfolded-like transition state. While the net value of both the *m*-value and ΔC_p^0 are dominated by the exposure of hydrophobic residues, the value of ΔC_p^0 reflects the nature of the exposed surface. The contributions to the *m*-value, which is a measurement of the exposure of the polypeptide backbone, are positive regardless of the nature of the side chain. In contrast, the exposure of hydrophobic residues contributes positively to ΔC_p^0, whereas the exposure of hydrophilic or polar residues results in a slight negative contribution.[181; 190]

The α-value obtained from $\Delta C_p^{0\ddagger}$ is 0.44±0.11, whereas the α-value obtained from the $m^{\ddagger}$-values is considerably higher, 0.65±0.02. These results suggest that for the disulfide-oxidized protein, the burial of hydrophobic residues does not entirely dominate the refolding reaction. This is supported by evidence obtained from the phi analysis which shows that many hydrophobic residues in the core of the protein were found to have phi values of less than 0.3.[124] While the TSE is not entirely hydrophobic in character, the amino acids with the highest phi values, with the exception of C6 are branched aliphatic amino acids - specifically I18, I35, L117. The combination of a few residues with very high phi values (>0.5) surrounded by many residues with much lower phi values (<0.3)

implies a TSE with a very tightly packed core, surrounded by loosely packed residues. It is interesting to note that the A4V substitution has an accelerating effect on the refolding rate.[44; 117] The additional van der Waals interactions provided by the larger valine side chain compared to alanine may stabilize the loosely formed region of the transition state ensemble. Beyond the transition state, due to the increased packing density in the native state, this and other bulkier substitutions, such as C6F, are severely destabilizing.

This model is also supported by the interpretation of the urea dependence of the activation energy and activation enthalpy of the barrier to unfolding.[180] These thermodynamic parameters represent the nature of the urea binding sites revealed upon unfolding to the TSE from the native state. Since the energetics of urea binding to the exposed sites in the TSE of mAS-SOD1 resembles the energetics of urea binding to the unfolded state,[181] it is reasonable to postulate that the formation of the TSE involves the complete unfolding of parts of the protein, rather than loose packing of the entire structure, and may reflect the unfolding of the loosely packed secondary shell of residues around the tight core formed by C6, I18, I35, and L117.

Comparisons with contact order predictions.

Baker and co-workers, studying proteins which exhibit two-state folding behavior have demonstrated a correlation between the rate constant of folding and the topological complexity of the protein.[154] One metric by which the complexity is quantified, absolute

contact order (ACO), is the average sequence distance between all pairs of contacting residues.[191] Apo-SOD1 was determined to have a ACO of 20.6 (using PDB: 1RK7) and is shown in relation to other studied proteins in Figure 4.8.

When considering the entire set of proteins used to determine the correlation of rate constant and ACO, much variation in the data is observed. Istomin and colleagues have shown that separating the proteins by secondary structure content, all α, all β, and mixed α/β, leads to much improved correlations.[192] Indeed, when considering only all-β proteins, SOD1 seems to lie well within the expected refolding rate constant range (Figure 4.8).

An enthalpic barrier associated with desolvation.

Important energetic and structural information about the TSE for SOD1 can be obtained by the analysis of the change in heat capacity, enthalpy, and entropy for the folding and unfolding reactions. The entropic contributions to the energy barriers, the quantification of the net gain or loss of degrees of freedom in the system, represent the sum of contributions from the chain entropy and the solvent entropy. The loss of chain entropy upon folding is counterbalanced by the increase in solvent entropy by the desolvation of side chains, freeing water molecules into the bulk water.

Figure 4.8. Correlations of folding rate constants and a measure of topological complexity.

The log of the refolding rate is plotted as a function of the absolute contact order determined from the structure of the protein. Circles represent a combination of all-β, all-α, and mixtures of α/β topologies, while filled circles represent solely the all-β. The open square represents mAS-SOD1. The data for proteins other than SOD1 were adapted from Istomin *et al.*[192]

Figure 4.8. Correlations of folding rate constants and a measure of topological complexity.

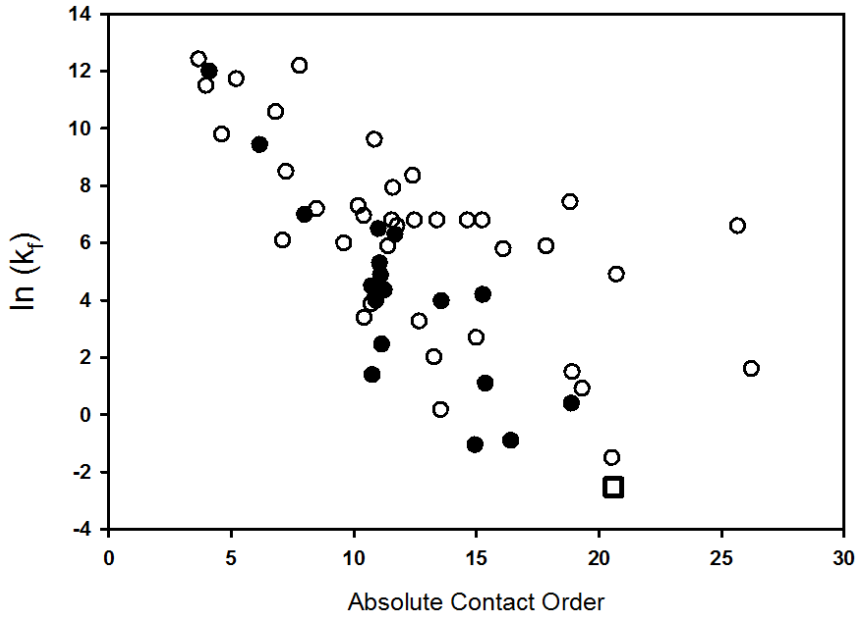

In unfolding, the increase in chain entropy is often compensated by a comparable and unfavorable contribution from the solvent entropy. The entropic contribution to the formation of the TSE is favorable regardless of the choice of formalism, consistent with a partial unfolding of the native state which remains desolvated. Because the activation enthalpy is independent of the entropic effects of the conformational search, it provides a more direct structural reflection of the intermolecular interactions in the amino acid chain. Furthermore, unlike the activation entropy, it is not convoluted by the uncertainties in the choice of appropriate prefactor to accurately measure the value. The large enthalpic barrier to unfolding implies a loss of hydrogen bonding and packing in the TSE, consistent with the analysis of the α-values above. The combination of these results suggests the TSE becomes loosely packed relative to the native state in unfolding but likely remains desolvated.

In refolding, the barrier is once again dominated by the enthalpic term. The entropic contribution to $\Delta G^{\ddagger}$ is very slightly unfavorable according to the Eyring formalism or contributes favorably to the energy barrier according to the Kramers formalism. These results suggest that the loss of chain entropy is almost entirely, or entirely compensated by the increase in solvent entropy, consistent with a highly desolvated TSE. Furthermore, mAS-SOD1 folds highly cooperatively by a two-state mechanism, as evidenced by the lack of curvature in the chevron plots,[44; 113; 117; 119] and an absence of collapse prior to the rate-limiting folding reaction as measured by small angle x-ray scattering.[114] These

observations indicate that breakup of existing structure prior to the formation of the TSE cannot contribute to the enthalpic barrier observed in refolding and further reinforces the role of desolvation.

It has been suggested that desolvation may play a critical role in the formation of large enthalpic barriers in folding. The requirement for a desolvated TSE may also explain different correlations of the $\ln(k_f)$ and the ACO for all-α, all-β, and mixed α/β proteins. All-β proteins show a much steeper dependence on the ACO, perhaps due to the non-local interactions required to form the extensive β-sheets. This would lead to the requirement of the cooperative desolvation of many water molecules, which may give rise to this high enthalpic barrier, as opposed to the desolvation of a few water molecules, such as in the formation of an α-helix, which may be overcome by thermal fluctuations.

Chapter V. Structural characterization of the native and higher energy states of SOD1.

Section I. Native State Hydrogen Exchange.

Background and Rationale

Though the presence of SOD1 containing aggregates has been a hallmark of SOD1 mediated ALS, the nature of the aggregation prone species of SOD1 is not well understood. One potential pathway is through higher energy species of the dimeric state, as observed for S134N.[95] Furthermore, the detection of higher energy species accessible to the apo-SOD1 monomer suggest that these species may also be potential candidates for aggregation.[163] Native state hydrogen exchange techniques provide a structural probe to map the differences in the features of these hypothesized higher energy states and the native structure of SOD1.

Hydrogen exchange is a powerful tool for obtaining insights into the extent of secondary structure formation in a protein or an ensemble of proteins. These methods exploit the fact that amide protons engaged in secondary structure formation, either by the formation of hydrogen bonds or by burial in the core of the protein, are less accessible to exchange with protons from the solvent. Hydrogen exchange methods, coupled with either NMR or mass spectroscopy, have been used ubiquitously to probe the secondary structure and dynamics of proteins and more recently in efforts to obtain structural information on aggregate formation.[193; 194] In mass spectroscopy, the exchange is monitored by either a gain or loss of mass, as the exchange of hydrogen with deuterium leads to a change in

mass. In NMR, the loss of peaks arising from hydrogen atoms are monitored because deuterium has no net nuclear spin.

Shaw and colleagues[165] have used this approach to analyze the effects of the A4V mutation, finding protection throughout the sequence for both the WT and A4V proteins. The only differences in exchange kinetics were observed for the sequence near the disulfide bond, where A4V showed enhanced exchange. Additionally, for the disulfide-reduced protein, little or no protection from exchange was observed for the A4V variant, consistent with the thermodynamic results presented in Chapter III, demonstrating that this variant is partially unfolded at 37 °C when disulfide reduced. Furthermore, studies in the Agar lab on as-isolated SOD1 variants have suggested that the destabilization of the electrostatic loop may be a common feature of ALS variants.[96] Nevertheless, the partial metalation of the samples in this particular study makes the results difficult to interpret as the exchange may be arising from a sub-population of metal-free species.

Native state hydrogen exchange experiments were performed on the monomeric and dimeric SOD1 in an effort to elucidate the structural determinants of SOD1 aggregation. Considering the implication of monomeric species in the aggregation pathway, structural or dynamic differences should be evident between the monomeric and dimeric constructs. The common regions of protection against hydrogen exchange should reveal the core of

SOD1 stability. The regions of missing protection in the monomer, if any, could reveal protective structural features which must be unfolded to allow aggregation.

Materials and Methods

Native state hydrogen exchange.

Hydrogen exchange of all samples was initiated by a 10:1 dilution of protonated protein into deuterated buffer consisting of 20 mM HEPES, 1 mM EDTA, pD 7.2. The fully deuterated sample was prepared by incubating the protein in deuterated buffer containing 6 M urea. Aliquots for each time point were quenched by another 10:1 dilution into quench buffer consisting of 1 mM TCEP, 0.025% TFA, 5% acetonitrile, pH 2.4. Samples were frozen in liquid nitrogen immediately following the quench and stored at −80 °C.

Preparation of peptides.

Pepsin digestion of AS-SOD1 was performed with immobilized pepsin at an enzyme to substrate ratio of 1:1 w/w. Deuterated mAS-SOD1 was diluted 10:1 into 100 μL of prewashed immobilized pepsin incubated in 100 μL of quench buffer. Digestion was carried out for 4 minutes on ice with occasional mixing. The digested samples were then centrifuged for <10 s at 14,000 g and frozen in liquid nitrogen for storage at −80 °C.

Liquid chromatography-Electrospray ionization mass spectrometry (ESI-MS).

The extent of hydrogen/deuterium exchange of full length mAS-SOD1 variants was determined by HPLC ESI-MS. 20μL of protein was loaded on to a reverse phase Vydac C4 column, 1 mm x 10 mm, and eluted with a 10 minute gradient of 2% - 98% acetonitrile, 0.05% TFA, with a flow rate of 20 μL/min. The column and the tubing leading into the HPLC were all kept on ice to minimize back exchange. The mass spectrometry was performed on an ion trap LCQ ESI mass spectrometer.

Matrix-assisted laser desorption ionization mass spectroscopy (MALDI-MS).

Samples for MALDI-MS analysis were prepared in a 4°C cold room to limit back exchange. Samples were thawed and run through a C18 ZipTip™ according to the standard procedure provided by Millipore. 0.2-0.5 μL of samples was plated with 0.5 μL of 10 mg ml-1 α-cyano-4-hydroxycinnamic acid, which served as the matrix. Spots were dried at room temperature in 1-2 min under a vacuum. MALDI time-of-flight (MALDI-TOF) mass spectra were obtained with a Micromass MALDI-LR instrument in reflectron mode. An average of 50-100 laser shots were used to generate each mass spectrum. Peptides were identified using the software package PAWS with a maximum error of ±100 ppm.

Results and discussion

Full length hydrogen exchange of SOD1 monomers.

The hydrogen exchange kinetics of full length WT and A4V mAS-SOD1 were measured in an effort to ascertain the presence of intermediate species which may exist in the folding free energy surface of SOD1 monomers but are otherwise not observed by traditional kinetic and equilibrium studies. The number of exchanged protons as a function of time can be seen in Figure 5.1. It should be noted that the back exchange control was not performed for these experiments, and the number of exchanged protons represents a number smaller than the actual number of exchanged protons. Similar experiments performed in the lab on other proteins have found that a minimum of 20-25% back exchange occurs in these LC-MS experiments.[195]

The evidence for exchange from partially folded intermediates would be revealed by multiple exponential phases of hydrogen deuterium exchange. The characteristic signature of multiphasic exchange in a plot of the number of exchanged protons as a function of the log of the time of exchange is the presence of plateaus in the curve. Neither WT nor A4V exhibit any such plateaus until the proteins appear fully exchanged after a more than 10^5 s for A4V and 6×10^6 s for WT. These results are consistent with a two-state model for mAS-SOD1 folding between the folded and the unfolded state. Previous HX studies on the full length protein were performed over a much shorter time

Figure 5.1. Hydrogen exchange kinetics on full length WT and A4V mAS-SOD1.

The extent of hydrogen exchange in full-length WT (black squares) and A4V (red circles) mAS-SOD1 was monitored by ESI-MS and the number of exchange protons are plotted as a function of the log of time allowed to exchange with the deuterated buffer. Both proteins exhibit exchange kinetics consistent with a single exponential phase, where the number of exchanged protons for the A4V variant reaches a maximum at 10^5 s, while the exchange for the WT protein reaches a maximum at 6×10^6 s.

Figure 5.1. Hydrogen exchange kinetics on full length WT and A4V mAS-SOD1.

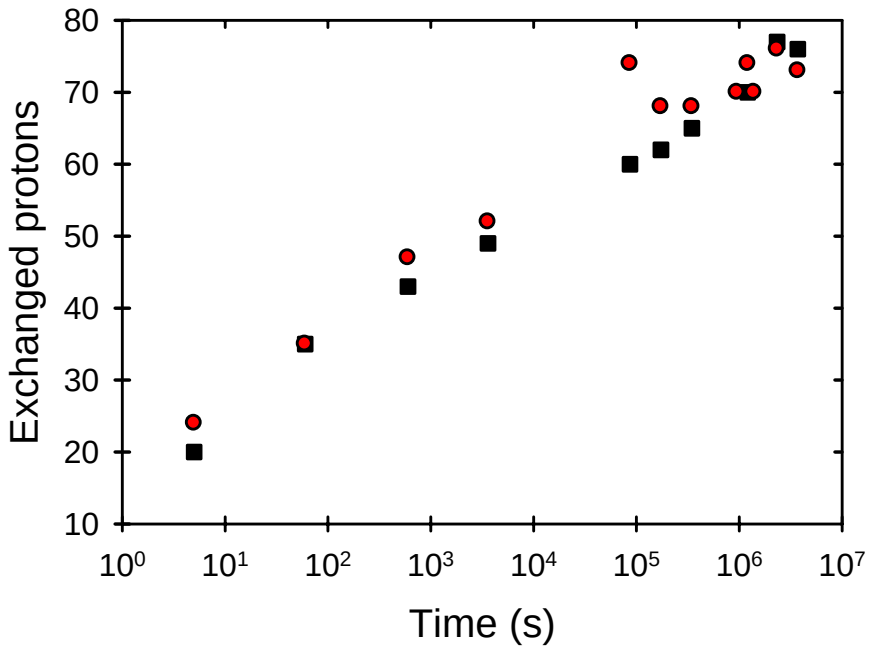

course making comparisons difficult.[165] However, the time-scale for hydrogen-deuterium exchange observed for both of these variants, which must be controlled by the unfolding rate of the protein, is inconsistent with the unfolding relaxation time measured by kinetic folding experiments, τ = 50000 s for WT, and τ = 833 s for A4V. These results may suggest that some compact structure in the unfolded state may be preventing the exchange of these amides with solvent.

Peptide specific detection of hydrogen exchange in the SOD1 dimer.

The sequence coverage of immobilized pepsin digested apo-AS-SOD1 is shown in Figure 5.2A. Only the highest signal peptides are shown, but more peptides are present in the far N and C termini providing increased overlap but not increased coverage. Peptide digests were performed at six time points: 5 s, 60 s, 2 min, 1 hour, 2 hours, 1 day, 2 days. Digests were also performed on the unexchanged and fully exchanged peptides in order to define the start and endpoints of the exchange.

The protection against hydrogen exchange was ranked qualitatively based on the observed exchange over 2 days. Unprotected peptides, depicted in red, show immediate and full exchange at the earliest time points. Not surprisingly this peptide maps to the Zn-binding loop (Figure 5.2B), which is unstructured in these experiments due to the absence of metals.

Figure 5.2. Sequence coverage and peptide specific resistance against hydrogen exchange.

The sequence, secondary structure map, and sequence coverage of apo-AS-SOD1 by immobilized pepsin digestion is shown in (A). The peptide coverage is shown by the blue, yellow and red solid lines, which represent the length of the observed peptides. The color coding is based on the resistance to hydrogen exchange, which can be mapped on the crystal structure of SOD1 (PDB: 2C9V), where blue peptides are strongly resistant, yellow peptides show intermediate resistance, and the red peptide shows little or no resistance (B).

Figure 5.2. Sequence coverage and peptide specific resistance against hydrogen exchange.

A)

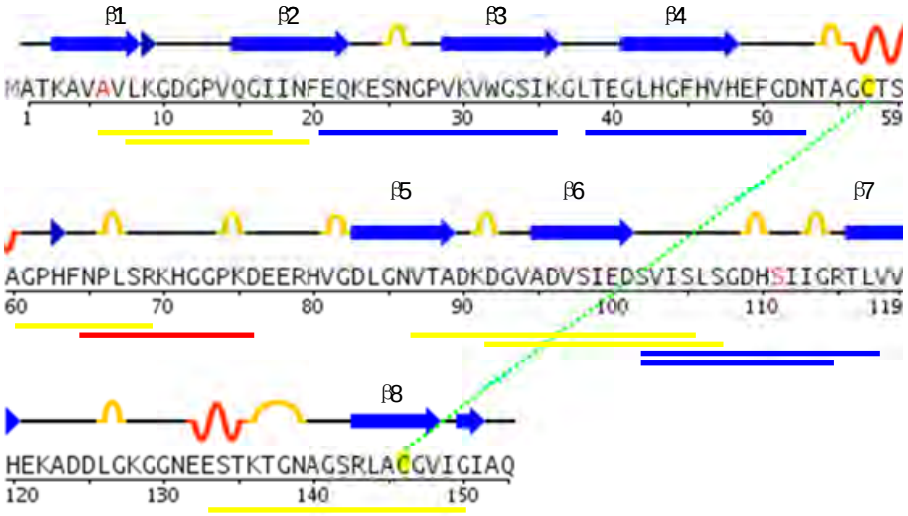

B)

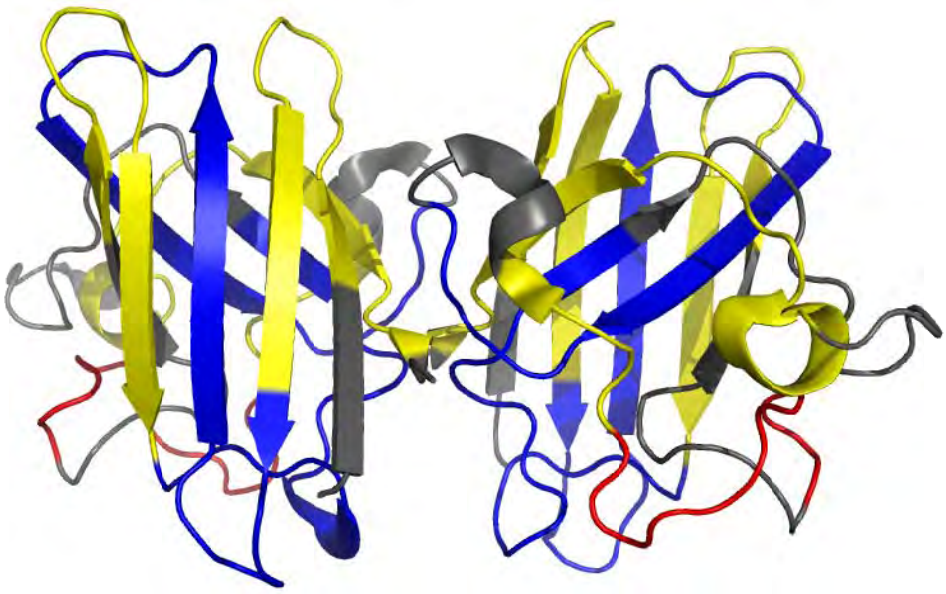

Weakly protected peptides, highlighted in yellow, show exchange kinetics between the 5 s and 2 hour time points and are protected after that. These peptides are found in the dimer interface, in the edge β-strands, β5 and β6, as well as the electrostatic loop (Figure 5.2B). The time constant for these exchange reactions, while not quantitatively measured, is consistent with the relaxation time of dimer dissociation, τ = 1351 s.[117] It is interesting that the exchange in the electrostatic loop is not as rapid as the exchange observed for the Zn-binding loop. It is possible that the electrostatic loop is more compact in the apo-state than previously thought based on NMR and x-ray scattering experiments, which suggested that it is completely disordered. Furthermore, the electrostatic loop and β5-β6 are considered gatekeepers against the exposure of the hydrophobic core of SOD1.[123; 124] The exchange observed in these regions of the apo-protein may serve to explain the observed increased aggregation potential of disulfide-reduced, and therefore monomeric, proteins.[8]

Strongly protected peptides exhibit no increased exchange between 5 seconds and 2 days, and closely resemble the mass of the unexchanged peptide. These peptides are solely found in the hydrophobic core of the SOD1 monomer, in β2-β4 and β7 (Figure 5.2B). This is identical to the critical folding nucleus determined by the phi analysis performed by Nordlund and co-workers, suggesting that these peptides likely exchange only from the unfolded state.[124]

Future directions

The ultimate goal of these experiments is to obtain structural insights into aggregation prone species of SOD1.[193] This will be facilitated by a comparison of the hydrogen exchange profile of soluble SOD1 and aggregated SOD1. Hydrogen exchange of SOD1 in aggregates can be performed by incubating *in vitro* aggregated SOD1 in deuterated buffer followed by disaggregation in high concentrations of denaturant and then digestion by immobilized pepsin, identical to the treatment of the soluble protein. Similar studies utilizing HX-MS or HX-NMR have been performed previously to gain insight into the structure of aggregated α-synuclein,[194] which is natively disordered in solution, and β2-microglobulin.[196]

Section II. Small-angle x-ray scattering

Background and Rationale

Numerous structural studies, both by x-ray crystallography and by NMR have been performed on SOD1 and ALS-inducing variants of SOD1. X-ray crystal structures have been primarily reported for the fully metalated, or partially metalated proteins, revealing little or no structural perturbations of the native state of the protein for the disease variants, even for a highly destabilizing mutation such as A4V.[97; 98] Similar structural insights were obtained for the holo-G37R SOD1 by NMR, suggesting that this is not simply an artifact of crystallization. For this particular variant, it was shown that the addition of metals to the apo-G37R SOD1 restored the ALS variant to the dynamic properties of the WT protein, despite being more dynamic in the apo-state.[99] These results are consistent with the high catalytic activity observed for many ALS variants, suggesting that the native structure of the protein is likely intact.[171] Considering the high thermodynamic stability of holo-SOD1 and the observation that many ALS-variants of SOD1 can lead to the destabilization of their metal-free[44; 115; 117; 120; 121] or metal-bound states,[32; 44; 116; 127] it is possible that the addition of metals obscure structural differences that may exist in immature species of SOD1, which may be important for inducing aggregation.

Immature species of SOD1, such as the apo-protein, show significant differences in the dynamics of the loops and the extent of hydrogen bonding in the β-sheet architecture, reflecting the significant loss of stability upon the loss of the metals.[35] One might expect that this more loosely structured protein may be able to better accommodate changes to the amino acid sequence, yet studies on the apo, disulfide-reduced ALS variants suggests that amino acid replacements in the β-sandwich lead to considerable destabilization even in immature species.[43; 44] For these reasons, structural differences in the immature species of SOD1 may explain the aggregation propensity of ALS variants. Small angle x-ray scattering provides a straightforward, but low resolution probe of solution structure that can be performed at relatively low concentrations and is amenable to destabilized variants, which may be prone to aggregation at the concentrations required for crystallization or NMR. Furthermore, data acquisition is relatively rapid, potentially allowing for the screening of dozens of variants.

Materials and Methods.

Data acquisition.

Small angle x-ray scattering data were collected at the BioCAT beamline at the Advanced Photon Source at Argonne National Labs. Samples, at a concentration of 1-2 mg/ml were flowed continuously through a 1 mm capillary during data acquisition. This procedure reduces the effective exposure time of the protein to the x-ray beam to 10 ms,

greatly reducing the possibility for radiation damage. A matched buffer sample was also collected for each sample to ensure appropriate blank subtraction. The scattering data were acquired with an exposure time of 1 s and an average of 6-10 exposures were used in the analysis. The samples were equilibrated and measured at the ambient temperature of the BioCAT beamline, ~25 °C.

Data analysis.

The data were analyzed using IGOR Pro (Wavemetrics, Inc, Lake Oswego, OR) macros written at BioCAT. The radius of gyration, R_g, was obtained using the Guinier approximation in the range where $R_gQ < 1.3$. The bead modeling was performed using the simulated annealing program GASBOR[197] using the default parameters and a maximum length of 45 Å and then superimposed on a monomeric subunit of the crystal structure of SOD1 (PDB: 2C9V) using SUPCOMB.[198] Repeated simulations of the bead modeling led to visually similar structures but a consensus structure of multiple bead models was not generated. Due to the statistical nature of the output of these programs, a more rigorous analysis may be required to gauge the accuracy of the results.

Results and discussion.

In order to specifically monitor differences in immature species of SOD1, the pseudo-WT monomeric and variant C6A/F50E/G51E/C111S SOD1, mAS-SOD1, was used. This model has been repeatedly used in our lab and others as a faithful representation of the native SOD1 monomer. Small angle x-ray scattering spectra on the WT and five ALS-variants of SOD1 were measured in order to obtain structural insights into the conformations of the protein in solution.

Guinier analysis.

The radii of gyration determined by the Guinier approximation and are reported in Figure 5.3. Measurements reported with error bars represent the average of two or more independent measurements. The largest differences in the radii of gyration are observed for the disulfide-reduced β-sandwich variants compared to the WT protein. These variants are destabilized to such an extent that the unfolded state is partially populated under these conditions.[44] The small angle x-ray scattering intensity increases non-linearly with the size of a molecule and significant populations of the larger unfolded state should inflate the apparent radius of gyration. Therefore, these measurements likely represent an overestimate of the size of the folded, disulfide-reduced protein. Interestingly, the S134N variant also appears larger than WT, despite exhibiting no difference in thermodynamic stability.[44; 117] Upon oxidation of the disulfide bond, all β-sandwich variants exhibit

increased compactness. Once again, this is likely due to the increased fraction of folded protein and may not reflect a significant change in the native structure. Furthermore, addition of Zn leads to a significant compaction for the A4V variant, while all other variants either compact very slightly or remain unchanged. Surprisingly, the S134N variant shows no change with respect to either Zn binding or disulfide-bond oxidation, suggesting that this protein may have structural differences compared to the WT protein in both the apo and Zn-bound states.

Kratky analysis.

The Kratky plots, a plot of $I(q)q^2$ *vs* q, for the same scattering data are shown in Fig. 5.4. The sharp peak observed near q = 0.1 $Å^{-1}$ is indicative of a globular species and can be compared to the unfolded spectra taken at 6 M urea. Interestingly, a difference can be observed between the reduced and oxidized unfolded spectra, suggesting that simply circularization of the chain can contribute to the peak. Similar observations have been noted for circular DHFR in which the N- and C-termini were linked by an engineered disulfide bond.[199] Since contributions to the scattering intensity from the unfolded state for disulfide-reduced variants make it difficult to deconvolute an appropriate spectrum for the native species, only the disulfide-oxidized apo and Zn-bound proteins were compared in their Kratky spectra. Analysis of the Kratky spectra parallels the Guinier analysis. The addition of Zn leads to small changes in the spectrum relative to WT, where the Zn-bound proteins more closely resemble WT. On the other hand, the spectrum for

Figure 5.3. Guinier analysis of ALS variants.

Guinier analysis of the WT (black), A4V (red), L38V (cyan), G93A (green), L106V (yellow), and S134N (blue) mAS-SOD1 scattering data, obtained by fitting data where $R_g \cdot q_{max} < 1.3$, reveals differences in the size of ALS variants of SOD1. Though the greatest differences are observed for the disulfide-reduced protein, this result is partially exaggerated due to the contribution from the unfolded state for these proteins. Introduction of post-translational modifications lessens structural differences between the variants and the WT protein. Error bars reflect the standard deviation of the mean between measurements of two or more identically prepared samples.

Figure 5.3. Guinier analysis of ALS variants.

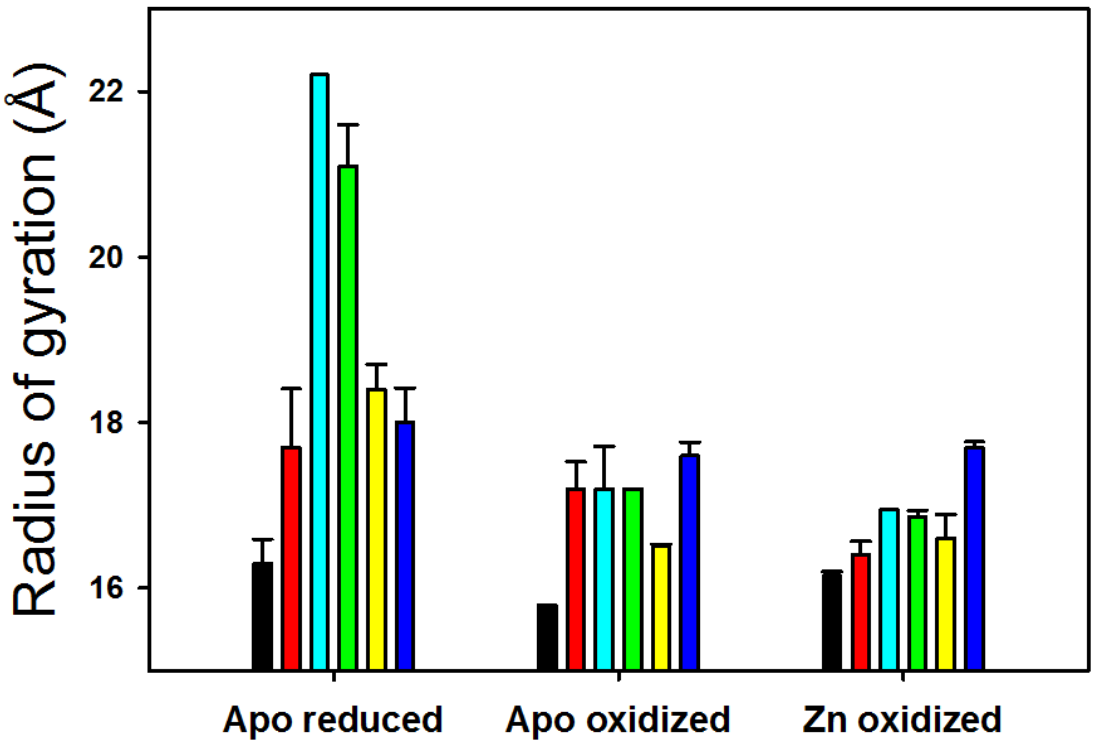

S134N remains unchanged regardless of the presence of Zn. The increased intensity in the high q region for the L38V variant is likely due to the aggregation of the sample prior to data acquisition.

Bead modeling.

In order to visualize structural differences that may be present in the apo, disulfide-oxidized state of the SOD1 variants, the SAXS data were bead modeled using the simulated annealing program GASBOR.[197] A comparison of bead models generated for each of the ALS variants and the WT protein, superimposed on the crystal structure of the WT holo-SOD1, can be seen in Figure 5.5. While the ALS variants seem to be slightly larger than the WT protein, consistent with the increased R_g, no specific structural difference stands out. It is possible that this low resolution technique is not sufficiently sensitive to determine the structural differences between these variants. Surprisingly, the most different protein is the S134N variant, which shows a loss of scattering density in the center of the protein. This result, in combination with the Kratky and Guinier analyses suggest that this particular variant exhibits structural defects even in the absence of metals.

Conclusions and future directions

Overall, these results suggest that many ALS variants destabilize SOD1, increasing the population of the unfolded state, rather than significantly altering the native structure. This is consistent with little or no differences in the native CD spectrum of the disulfide-

Figure 5.4. Kratky analysis of ALS variants.

Kratky of plots of WT (black), A4V (red), L38V (green), G93A (brown), L106V (teal), and S134N (blue) reflect the globularity of the protein. The magnitude of $q^2I(q)$ has been normalized by I(0) to correct for concentration differences between the samples. (A) Disulfide-oxidized (solid lines) and disulfide-reduced (dotted lines) folded (black) and unfolded (cyan) WT mAS-SOD1 are shown. (B) In the apo-state, both A4V and L106V resemble the WT protein, while the reduced amplitude at q=0.1 for L38V, G93A and S134N indicates that these proteins are less globular. (C) The addition of Zn alleviates some of these differences for the β-barrel variants but S134N remains largely unchanged. This may reflect the inability of Zn to structure the electrostatic loop for this variant and also suggests that the electrostatic loop may be compact in the apo-state. The increased amplitude at high q for L38V may be indicative of some aggregation in this sample.

Figure 5.4. Kratky analysis of ALS variants.

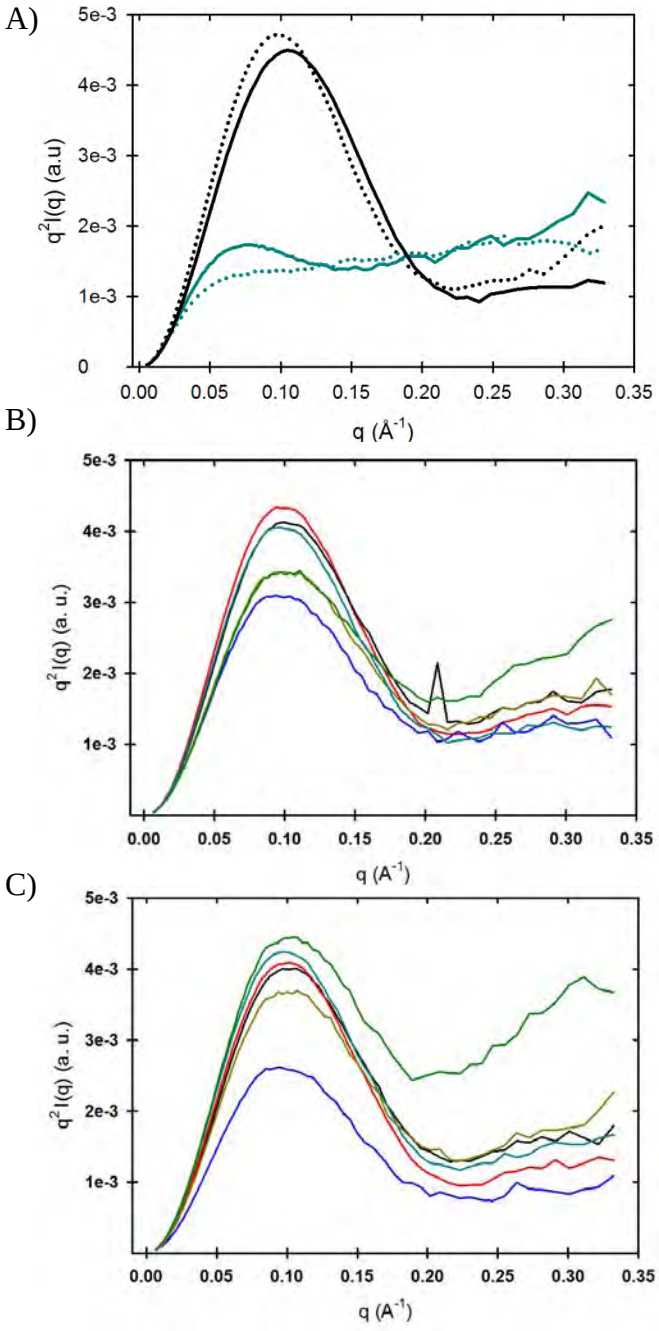

Figure 5.5. Bead models of disulfide-oxidized mAS-SOD1 variants.

Bead modeling of the scattering data was performed to visualize differences observed in the Kratky plots and the R_g. Bead modeling of the WT data is represented by the gray spheres, while the ALS variants are in color. The bead models were generated by the simulated annealing program GASBOR and overlaid on the crystal structure (PDB: 2C9V) using SUPCOMB. While some clear differences are visible for the S134N variant, the four β-barrel variants fill the expected density of the protein fairly similarly to WT.

Figure 5.5. Bead models of disulfide-oxidized mAS-SOD1 variants.

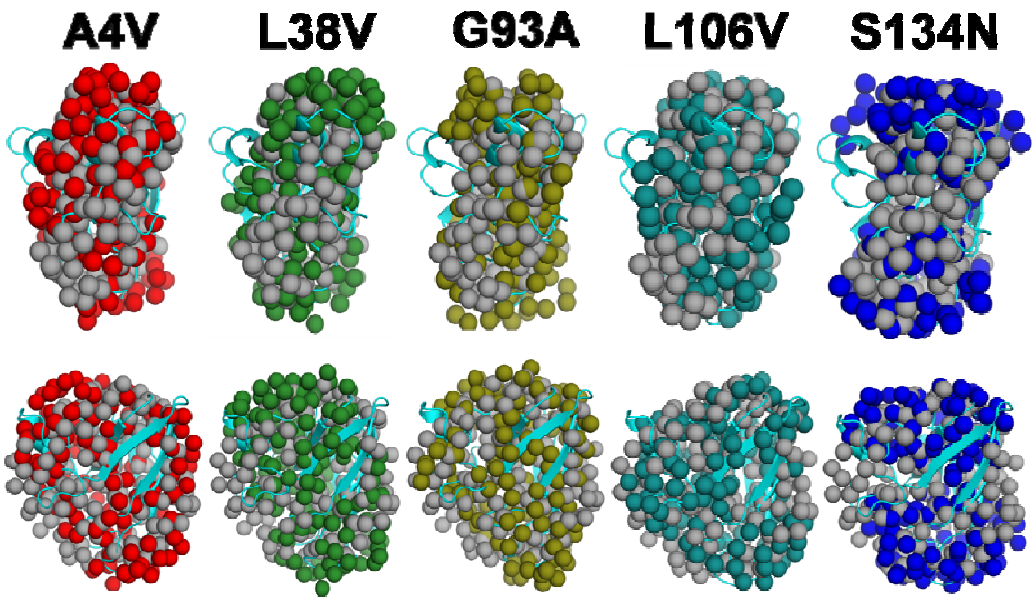

oxidized ALS variants studied here.[44; 117] Previous SAXS studies on the native dimeric I113T and A4V SOD1 had revealed structural differences inconsistent with the crystal structures determined from the same protein.[98] While it is not stated explicitly in the paper, it appears that the authors used as-isolated protein samples which contain a variable amount of metals.[83] Therefore, while the crystals may have formed from the least dynamic, fully metalated species, the SAXS data represent an average of the various metalation states of the protein. Since apo- SOD1 is more dynamic and extended than the holo-protein,[35] it is possible that the differences observed are due to the differences in the populations of metal-bound and metal-free SOD1 species. Alternatively, it is possible that dimerization induces structural constraints on the SOD1 monomer, exacerbating the deleterious effects of the amino acid replacement. A comparison of the SAXS spectra of monomeric and dimeric versions of these variants is required to test this hypothesis.

Even with these low resolution experiments, the apo-state of the monomeric ALS variants seems different than WT, though the magnitude of these differences may be small. Measurements with increased sensitivity, either using a variety of protein concentrations and/or repeated measurements, should allow more accurate measurements of the structural differences. Additionally, the ability to access the unfolded state by modulating the populations of highly destabilized, disulfide-reduced ALS variants with temperature allows for a unique opportunity to study the unfolded state in the absence of denaturant. A systematic survey of the scattering intensity as a function of temperature

should allow for the deconvolution of the native and unfolded spectra since the populations of the folded and unfolded species as a function of temperature have been measured.

Chapter VI. Future Directions and Summary

Future directions

Our continued interest in SOD1 as a model system arises from both a desire to further understand the role of amino acid sequence in defining the folding pathway and native structure of a protein and to discover the molecular mechanism underlying the link between mutations in SOD1 and ALS. Therefore, future studies can be divided into two specific categories: (1) studies of structural elements that may play a role in aggregation, which studies the link between SOD1 and ALS, and (2) the study of the nature of the slow folding reaction of SOD1, which explores the question of how proteins fold into their native structure.

Aggregation arising from residual structure in the unfolded state.

Currently, the consensus of the SOD1 field is that mutations in SOD1 lead to a gain-of-function toxicity, which is lethal to motor neurons due to some unknown susceptibility, and that this lethality may be linked to the formation of soluble or insoluble aggregates. The thermodynamic destabilization of the SOD1 is a consequence of a majority of SOD1 mutations identified in patients, raising the possibility that the aggregation prone species exists naturally in the folding pathway of SOD1 and that ALS variants simply increase the populations of this species. Based on our results, a likely candidate for this aggregation prone species is the unfolded state. Thus, we propose a kinetic mechanism for SOD1 aggregation, where the combination of increased turnover and high populations

of the unfolded state for ALS variants of SOD1 lead to increased opportunities for off-pathway folding reactions leading to aggregation (Figure 6.1).

The observed increase in unfolded state populations (Chapter III) motivates the study of the unfolded state as a relevant aggregation prone species. The intrinsic aggregation propensity of the unfolded state may be due to compact, possibly non-native structure in the unfolded state. A phi analysis performed by the Oliveberg group suggests that the formation of long-range contracts between β2-4 and β7 are likely critical in the transition state to productive folding.[124] On the other hand, more sequence-local residues may be involved in the formation of structure in the unfolded state. The two most likely candidates are the β1-3 hairpin module and β5+β6 - the most sequence local of the secondary structural elements that make up the native structure of SOD1. The other connected β strands, β4+β5 and β7+β8, are separated by the long Zn binding and electrostatic loops, respectively. These loops are unstructured in the absence of metals, and given the relatively low affinity of the unfolded state for Zn, it is unlikely that they would form stable structures in the unfolded state *in vivo*.

While it seems reasonable that these sequence local elements could form compact structures, evidence demonstrating the existence of such structures in the unfolded state is currently lacking. No global compaction was observed in refolding studies probed by small angle x-ray scattering, nor is there a significant burst phase in refolding reactions monitored by circular dichroism.[114]

Figure 6.1. Proposed pathway for SOD1 aggregation.

ALS variants lead to increased populations of unfolded species after synthesis, either by significantly destabilizing the apo, disulfide-reduced state or by partially inhibiting Zn binding. Combined with the relatively low Zn affinity of disulfide-reduced SOD1, these premature species may persist for significant amount of time and represent a likely candidate for aggregation. While chaperones may compensate for the low stability of some ALS variants and aid in folding them, the diminished activity of these pathways with age will eventually result in a buildup of misfolded and aggregated protein.

Figure 6.1. Proposed pathway for SOD1 aggregation.

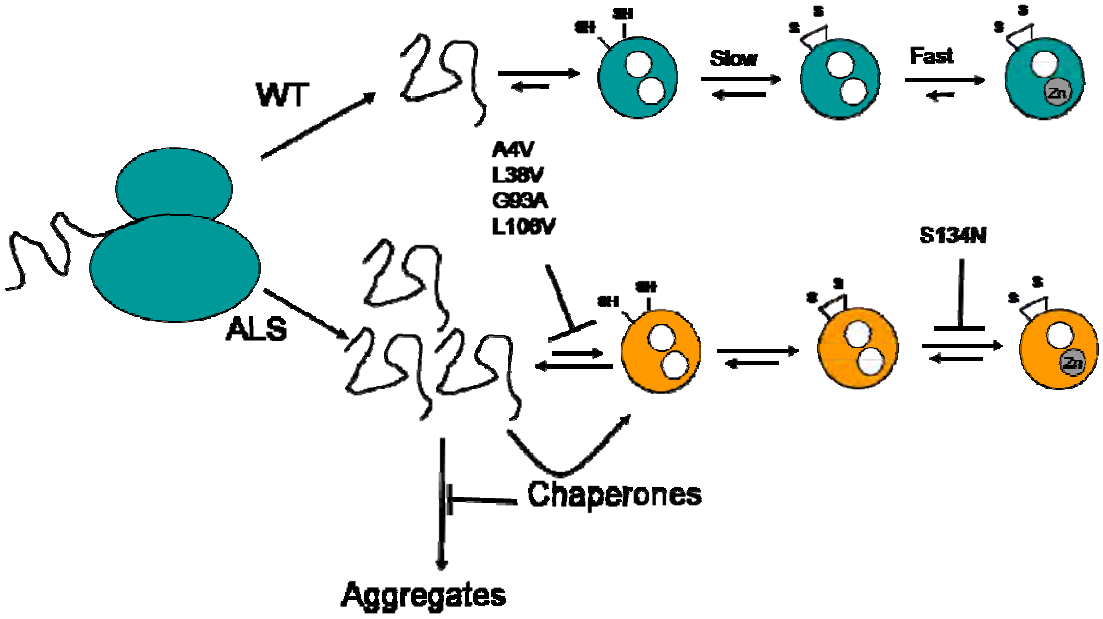

It is possible that these spectroscopic probes are simply insensitive to structures in the unfolded state. Therefore, more sensitive fluorescence spectroscopic techniques will be employed, utilizing Förster resonance energy transfer between the intrinsic tryptophan, W32, and EDANS, a fluorescent dye. The EDANS moiety can be covalently attached to judiciously positioned cysteine residues using maleimide chemistry, creating probes of local and/or global structure (Table 6.1 and Figure 6.2). In these experiments, the pairs D11C-W32 (Figure 6.2A) and T2C-W32 serve as probes of local structure, while T88C-W32 serves as a probe of global structure. If the β1-β3 module is in fact compact in the unfolded state, then energy transfer from the donor to the acceptor should be observed for the D11C-W32 and T2C-W32 FRET pairs, but not for T88C-W32. The use of multiple independent FRET pairs may also help rule out false positive results arising from structure induced by the dye itself, or minimize the consequences of perturbations to the native structure from the dye modification.

Another drawback of the existing studies was the requirement of denaturants to access the unfolded state, which can disrupt weakly formed structures in the unfolded state. In order to avoid the requirement for denaturants, future experiments can be performed on the disulfide-reduced protein containing one of the highly destabilizing mutations, such as G93A, which is >90% unfolded at 37 °C in the absence of denaturant. Alternatively, peptides can be utilized in order to monitor local structures in the absence of the entire protein. One such peptide, consisting of the N-terminal 37 residues of SOD1 with an

Figure 6.2. D11C-W32 and E0-W32 peptide FRET pairs.

Two probes for structure in the unfolded state were created by utilizing FRET between the intrinsic W32 and EDANS molecules covalently attached to cysteine at position 11 (A) or glutamic acid residue added to the N-terminus (B) (zeroth position). Both these constructs probe for residual structure in the sequence local β1-β3 module.

Figure 6.2. D11C-W32 and E0-W32 peptide FRET pairs.

A)

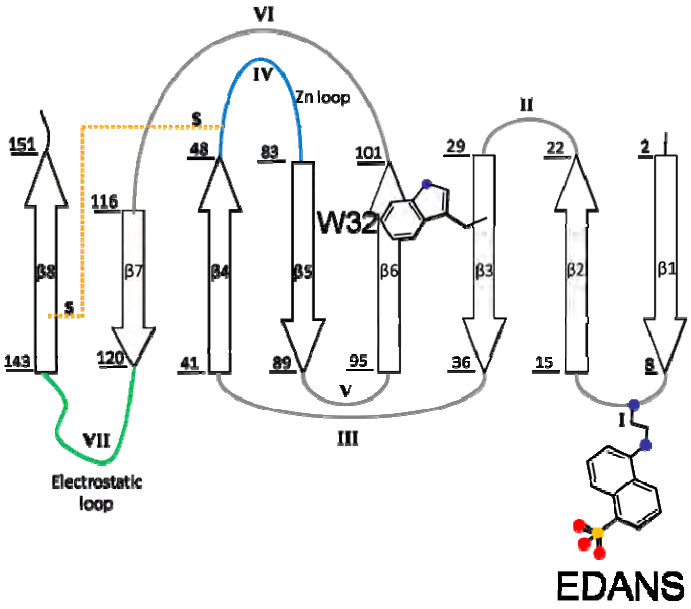

B)

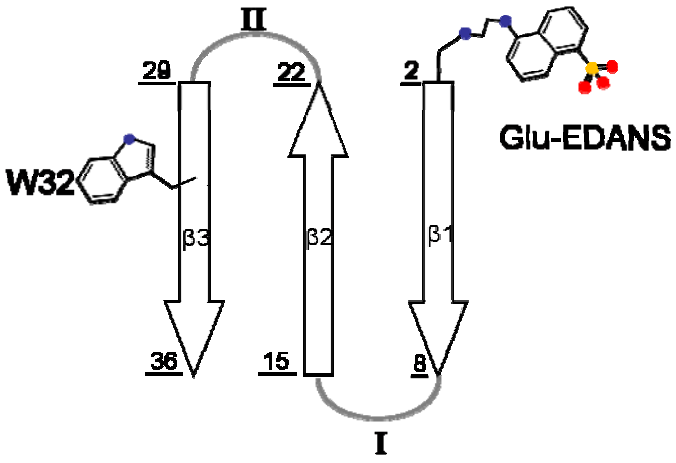

additional glutamate residue modified with an EDANS moiety at the N-terminus is shown in Figure 6.2B.

Preliminary data on the labeled D11C-W32 pair can be seen in Figure 6.3A. Titrations in urea and Gdn-HCl, and monitored by tryptophan fluorescence, show shorter lifetimes in the absence of denaturant, characteristic of energy transfer between the donor tryptophan and the acceptor EDANS. Upon unfolding, the average tryptophan lifetime increases, consistent with the increase in the donor-acceptor distance and concomitant loss of energy transfer. Compactness in the unfolded state is evident from a comparison of the N-terminal peptide with free tryptophan and EDANS (Figure 6.3B). The increased fluorescence from the acceptor EDANS in the absence of denaturant is likely due to energy transfer from a compact structure in this peptide, as an unfolded peptide of the same length would be expected to exhibit only 2% energy transfer (Table 6.1).

In order to measure the distance between the donor and acceptor molecules for these FRET pairs, a comparison of the labeled and unlabeled molecules is required, and these experiments are currently under way. Small angle x-ray scattering may also be used as a complementary technique to measure the radius of gyration for the peptide, as demonstrated for the full length protein in Chapter V. In working with this peptide, it is clearly soluble enough to reach the concentration requirements for these experiments, ~1-2 mg/ml. These experiments have the added advantage of not requiring the additional

Table 6.1. Distances and expected FRET efficiencies of the unfolded state probes.*

Donor-Acceptor Pair	Structural element	Unfolded distance	FRET efficiency	Folded distance	FRET efficiency
W32 – T88C	Global	59 Å	0.2%	13.7 Å	94%
D11C – W32	β1-β3	33.5 Å	2%	25.1 Å	31%
T2C – W32	β1-β3	41.3 Å	7%	14.3 Å	93%
E0-W32 (Peptide)	β1-β3	43.6 Å	2%	14.4 Å	93%

*Distances in the folded state were measured from the crystal structure of the holo-SOD1 (PDB: 2C9V). Distances in the unfolded state were calculated from predictions based on a space filling random coil.[200] Expected FRET efficiency was calculated using: $E = 1/(1+D/R_o)^6$), where R_o is the distance for 50% energy transfer, 22 Å for Trp-EDANS, and D is the donor-acceptor distance.[188]

Figure 6.3. Evidence for energy transfer between tryptophan and EDANS.

(A) Urea (white squares and solid line) and Gdn-HCl (blue circles) titrations were performed to determine the stability and observe the change in FRET efficiency between the folded and unfolded states. The addition of the fluorophore did not significantly affect the stability of the protein. (B) Energy transfer between Trp32 and the N-terminal EDANS moiety was confirmed by an increase in EDANS fluorescence (blue line) above that measured for free tryptophan and EDANS (black line).

Figure 6.3. Evidence for energy transfer between tryptophan and EDANS

A)

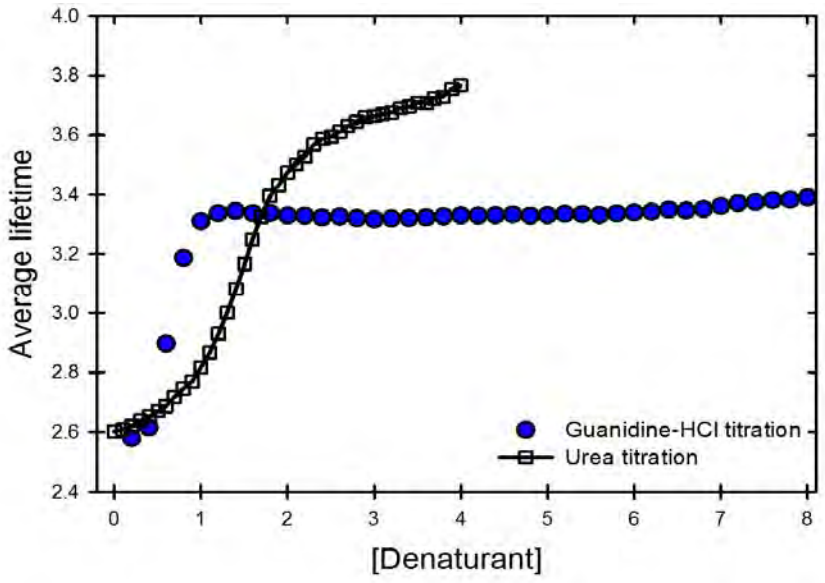

B)

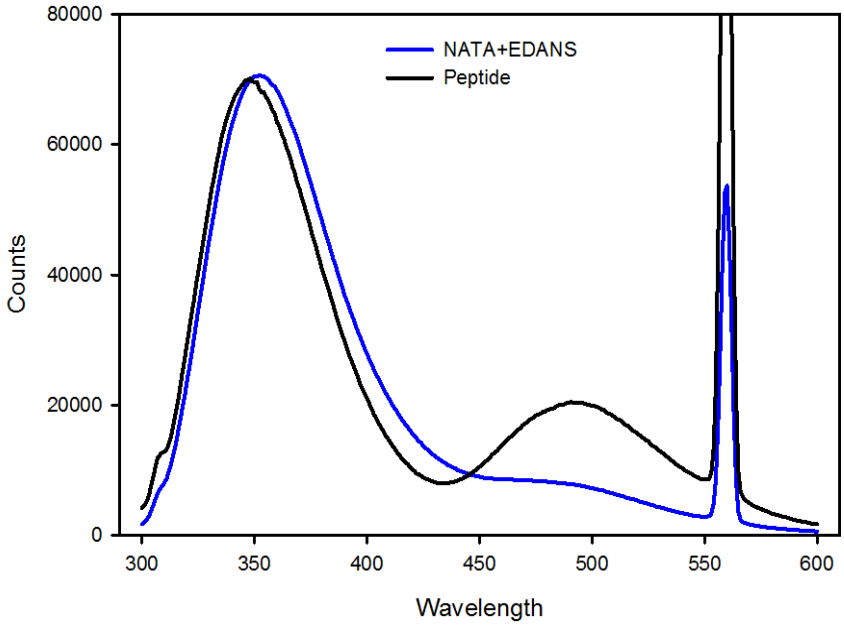

glutamic acid residue and the covalently attached fluorophore, more accurately recapitulating the unfolded state of SOD1.

Aggregation from higher energy folded states of SOD1.

These increased populations of the unfolded state observed in Chapter III do not entirely rule out a role for folded species in aggregation. The S134N variant shows no destabilization relative to WT in the apo-states[44; 117] and the x-ray scattering studies presented in Chapter V suggest that structural differences may exist in the disulfide-reduced and oxidized Zn-free states of the SOD1 monomer. These results are consistent with the native-state hydrogen exchange studies, which show that the regions of structure flanking the hydrophobic core of the SOD1 monomer undergo exchange, while the core remains protected (Chapter V). In combination, these results imply that the folded SOD1 monomer may also be aggregation prone. This is likely due to the exposure of the hydrophobic core, which becomes less protected when the dimer is dissociated, increasing the potential for intermolecular interactions.[123; 124] This property may be further exacerbated by ALS variants which alter the native fold of the SOD1 monomer.

A comparison of the hydrogen exchange profile of soluble SOD1 and aggregated SOD1 may give insights into the structural differences between soluble and aggregated SOD1, thereby discriminating between whether an unfolded state or a folded state is giving rise to aggregation. Similar studies utilizing HX-MS or HX-NMR have been performed

previously to gain insight into the structure of aggregated α-synuclein and β2-microglobulin.[194; 196] The differences in protection patterns can be directly related to the structure of the aggregation prone species. If most of the β-sandwich structure of SOD1 is participating in aggregation, one would expect most of the β-strands to be protected in the aggregate, as they are in the soluble dimer. If a partially unfolded, higher energy state of the protein is the source of the aggregate, then the fraying and loss of protection in the edges of the β-sheet may be observed. Alternatively, if the unfolded state of SOD1 is giving rise to aggregation through some entirely non-native structure, then altered protection patterns throughout the sequence should be observed.

Small molecule screen to stabilize SOD1 monomers.

While the determination of the molecular mechanism of aggregation may lead to important discoveries in preventing it, knowledge of the mechanism is not a strict requirement in developing therapeutic strategies. Work in the Lansbury group have demonstrated that stabilizing the native dimer of SOD1 by engineering and intermolecular disulfide bond in the dimer interface can prevent aggregation.[201] Taking this a step further, utilizing *in silico* screening, they were able to identify small molecules which stabilize the native dimer of SOD1, thereby lowering its aggregation propensity.[202] These studies essentially mimic the effect of Zn and reduce the populations of monomeric species.

If monomeric species are prone to aggregation due to increased dynamics of the native fold, or due to their propensity to sample the unfolded state, could stabilizing the native fold of the SOD1 monomer also reduce aggregation? As stated above, the large fraction of unfolded species observed for the disulfide-reduced G93A under physiological conditions make this variant an excellent candidate to study the unfolded state in the absence of denaturant via the FRET pairs in Table 6.1. The large change in tryptophan lifetimes between the folded and unfolded states, ~0.8 ns, as seen in Figure 6.3A, allow for the rapid determination of the relative folded/unfolded populations of a sample by fluorescence. These properties can be utilized for a small molecule screen for stabilizers of SOD1 monomeric folding (Figure 6.4).

This assay will utilize the cysteine free variant, C6A/C57A/C111S/C146A SOD1, mimicking the disulfide-reduced protein, without the requirement for reducing agents. The removal of the cysteines also enables site specific labeling with introduced cysteines without complications of disulfide-interchange in the unfolded state. Furthermore, intermolecular crosslinking is no longer a problem because reducing agent can be present without concern for breaking the native disulfide bond. Also, since the disulfide-reduced SOD1, in the absence of metals, is natively monomeric, the F50E/G51E mutations are no longer required. This experiment will likely utilize T88C-EDANS-W32 FRET pair, as this combination results in the highest difference in FRET efficiency between the folded and unfolded states. Since the donor and acceptor sites are not local in sequence, this pair

Figure 6.4. A small molecule screen for SOD1 monomer stabilizers.

The naturally low thermodynamic stability of the disulfide-reduced β-sandwich variants of SOD1 (Chapter III) allow for a small molecule screen to be constructed for stabilizers of the native fold. In this assay, an increase in temperature will reduce folded populations, while small molecule stabilizers will increase them. Utilizing the large change in average tryptophan lifetimes between the folded and unfolded populations of EDANS labeled molecules, fluorescent screening can be used to rapidly determine whether molecules have successfully folded the protein.

Figure 6.4. A small molecule screen for SOD1 monomer stabilizers.

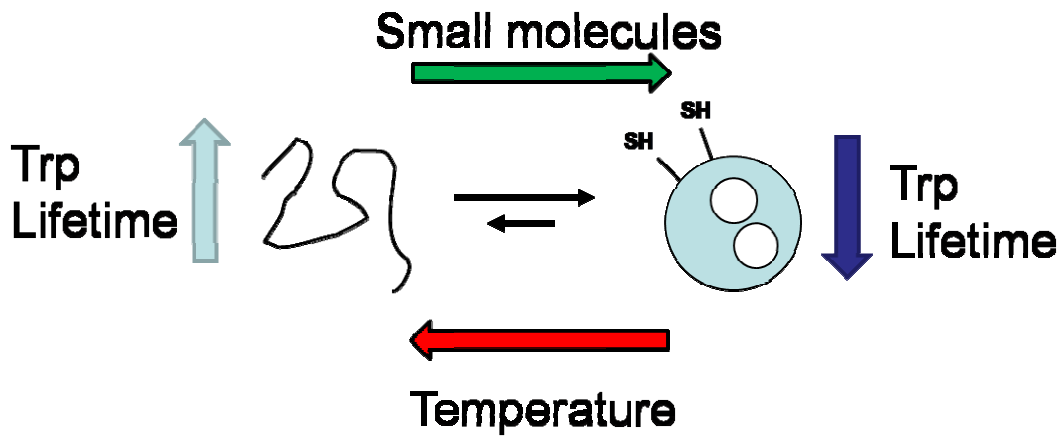

also provides a measurement of the global structure of the protein. Unpublished results in the Matthews lab suggest that labeling at T88C with EDANS, or even a much larger fluorophore like Alexa-488 does not significantly perturb the stability of SOD1 (AM, JAZ, CRM unpublished).

The role of dehydration in the enthalpic barrier to folding of SOD1 monomers.

As described in Chapter IV, enthalpic barriers dominate both the folding and unfolding of SOD1. In unfolding, this can be explained by the disruption of existing structure in the native state. In refolding, since no significant structure is thought to exist in the unfolded state, dehydration of the chain presents a plausible model. The β-sandwich of SOD1 is comprised of a pair of 4-stranded sheets. 28 isoleucines, leucines and valines, present in these sheets, form a large hydrophobic cluster in the core of the sandwich. The improbability of locally organizing, dehydrating and then docking these two sheets may be the underlying reason for the slow folding reaction of SOD1.

The dehydration hypothesis can be tested by replacing selected buried valines and leucines in the core of SOD1 with their isosteric and polar counterparts, threonine and glutamine. If removal of water is playing a role in the activation energy of SOD1 folding, then the presence of more polar residues will make desolvation more difficult, thereby increasing the observed activation energy in refolding. This technique has been previously used to map out the extent of solvation in the folding pathway of Im7.[203]

For SOD1, which exhibits two-state behavior, these experiments provide an analytical tool to measure the extent of solvation in the TSE. In effect, if the TSE buries the residue of interest, the replacement with the polar amino acid serves to stabilize the unfolded state relative to the TSE. Amino acids that are highly desolvated in the TSE will significantly slow the refolding rate and diminish the global stability. On the other hand, residues which become desolvated in the native state or remain exposed to solvent will only affect the global stability or show no affect on the stability, respectively. If large-scale desolvation of the sheets is playing a significant role in defining the barrier to folding in SOD1, then these studies should identify a significant number of polar substitutions which perturb the refolding rate.

Summary

This project has advanced the SOD1 folding field by the detailed study of the monomer folding reaction of SOD1 and by quantitatively measuring the thermodynamic and structural consequences of SOD1 mutations on a variety of post-translational states of SOD1. The thermodynamic analysis of SOD1 folding has revealed that a large enthalpic barrier, potentially due to the desolvation of the chain, is playing a significant role in the activation energy of refolding. The involvement of a large fraction of the amino acids which make up the core of the β-sandwich may serve to explain the slow folding reaction of SOD1, as well as the higher dependence of the observed folding rates of β-sheet rich proteins on the topological complexity as compared to the α-helix rich counterparts.

The study of the coupling between post-translational modifications and amino acid replacements and their effects on the folding free energy surface of SOD1 revealed insights into the properties of this protein and has significant implications for ALS. Zn was found to bind progressively tighter along the folding pathway of SOD1, thereby shifting the equilibrium towards natively folded dimers. Studies on the monomeric species of SOD1 revealed that ALS variants greatly increased the population of the unfolded state, a potentially aggregation prone species. These detailed analyses pave the way for future experiments to identify the regions involved in aggregation and to develop small molecule screening assays for stabilizers of SOD1 monomers.

References

1. Soto, C. (2003). Unfolding the role of protein misfolding in neurodegenerative diseases. *Nat Rev Neurosci* **4**, 49-60.
2. Chiti, F. & Dobson, C. M. (2006). Protein misfolding, functional amyloid, and human disease. *Annu Rev Biochem* **75**, 333-66.
3. Balch, W. E., Morimoto, R. I., Dillin, A. & Kelly, J. W. (2008). Adapting proteostasis for disease intervention. *Science* **319**, 916-9.
4. Massey, A. C., Kiffin, R. & Cuervo, A. M. (2006). Autophagic defects in aging: looking for an "emergency exit"? *Cell Cycle* **5**, 1292-6.
5. Bruijn, L. I., Miller, T. M. & Cleveland, D. W. (2004). Unraveling the mechanisms involved in motor neuron degeneration in ALS. *Annu Rev Neurosci* **27**, 723-49.
6. Andersen, P. M. (2006). Amyotrophic lateral sclerosis associated with mutations in the CuZn superoxide dismutase gene. *Curr Neurol Neurosci Rep* **6**, 37-46.
7. Wang, Q., Johnson, J. L., Agar, N. Y. & Agar, J. N. (2008). Protein aggregation and protein instability govern familial amyotrophic lateral sclerosis patient survival. *PLoS Biol* **6**, e170.
8. Chattopadhyay, M., Durazo, A., Sohn, S. H., Strong, C. D., Gralla, E. B., Whitelegge, J. P. & Valentine, J. S. (2008). Initiation and elongation in fibrillation of ALS-linked superoxide dismutase. *Proc Natl Acad Sci U S A* **105**, 18663-8.
9. Yang, Y., Hentati, A., Deng, H. X., Dabbagh, O., Sasaki, T., Hirano, M., Hung, W. Y., Ouahchi, K., Yan, J., Azim, A. C., Cole, N., Gascon, G., Yagmour, A., Ben-Hamida, M., Pericak-Vance, M., Hentati, F. & Siddique, T. (2001). The gene encoding alsin, a protein with three guanine-nucleotide exchange factor domains, is mutated in a form of recessive amyotrophic lateral sclerosis. *Nat Genet* **29**, 160-5.
10. Hadano, S., Hand, C. K., Osuga, H., Yanagisawa, Y., Otomo, A., Devon, R. S., Miyamoto, N., Showguchi-Miyata, J., Okada, Y., Singaraja, R., Figlewicz, D. A., Kwiatkowski, T., Hosler, B. A., Sagie, T., Skaug, J., Nasir, J., Brown, R. H., Jr., Scherer, S. W., Rouleau, G. A., Hayden, M. R. & Ikeda, J. E. (2001). A gene encoding a putative GTPase regulator is mutated in familial amyotrophic lateral sclerosis 2. *Nat Genet* **29**, 166-73.
11. Chen, Y. Z., Bennett, C. L., Huynh, H. M., Blair, I. P., Puls, I., Irobi, J., Dierick, I., Abel, A., Kennerson, M. L., Rabin, B. A., Nicholson, G. A., Auer-Grumbach, M., Wagner, K., De Jonghe, P., Griffin, J. W., Fischbeck, K. H., Timmerman, V., Cornblath, D. R. & Chance, P. F. (2004). DNA/RNA helicase gene mutations in a form of juvenile amyotrophic lateral sclerosis (ALS4). *Am J Hum Genet* **74**, 1128-35.
12. Nishimura, A. L., Mitne-Neto, M., Silva, H. C., Richieri-Costa, A., Middleton, S., Cascio, D., Kok, F., Oliveira, J. R., Gillingwater, T., Webb, J., Skehel, P. & Zatz, M. (2004). A mutation in the vesicle-trafficking protein VAPB causes late-onset

spinal muscular atrophy and amyotrophic lateral sclerosis. *Am J Hum Genet* **75**, 822-31.

13. Puls, I., Jonnakuty, C., LaMonte, B. H., Holzbaur, E. L., Tokito, M., Mann, E., Floeter, M. K., Bidus, K., Drayna, D., Oh, S. J., Brown, R. H., Jr., Ludlow, C. L. & Fischbeck, K. H. (2003). Mutant dynactin in motor neuron disease. *Nat Genet* **33**, 455-6.
14. Rosen, D. R., Siddique, T., Patterson, D., Figlewicz, D. A., Sapp, P., Hentati, A., Donaldson, D., Goto, J., O'Regan, J. P., Deng, H. X. & et al. (1993). Mutations in Cu/Zn superoxide dismutase gene are associated with familial amyotrophic lateral sclerosis. *Nature* **362**, 59-62.
15. Kwiatkowski, T. J., Jr., Bosco, D. A., Leclerc, A. L., Tamrazian, E., Vanderburg, C. R., Russ, C., Davis, A., Gilchrist, J., Kasarskis, E. J., Munsat, T., Valdmanis, P., Rouleau, G. A., Hosler, B. A., Cortelli, P., de Jong, P. J., Yoshinaga, Y., Haines, J. L., Pericak-Vance, M. A., Yan, J., Ticozzi, N., Siddique, T., McKenna-Yasek, D., Sapp, P. C., Horvitz, H. R., Landers, J. E. & Brown, R. H., Jr. (2009). Mutations in the FUS/TLS gene on chromosome 16 cause familial amyotrophic lateral sclerosis. *Science* **323**, 1205-8.
16. Sreedharan, J., Blair, I. P., Tripathi, V. B., Hu, X., Vance, C., Rogelj, B., Ackerley, S., Durnall, J. C., Williams, K. L., Buratti, E., Baralle, F., de Belleroche, J., Mitchell, J. D., Leigh, P. N., Al-Chalabi, A., Miller, C. C., Nicholson, G. & Shaw, C. E. (2008). TDP-43 mutations in familial and sporadic amyotrophic lateral sclerosis. *Science* **319**, 1668-72.
17. Ripps, M. E., Huntley, G. W., Hof, P. R., Morrison, J. H. & Gordon, J. W. (1995). Transgenic mice expressing an altered murine superoxide dismutase gene provide an animal model of amyotrophic lateral sclerosis. *Proc Natl Acad Sci U S A* **92**, 689-93.
18. Morrison, B. M., Janssen, W. G., Gordon, J. W. & Morrison, J. H. (1998). Time course of neuropathology in the spinal cord of G86R superoxide dismutase transgenic mice. *J Comp Neurol* **391**, 64-77.
19. Awano, T., Johnson, G. S., Wade, C. M., Katz, M. L., Johnson, G. C., Taylor, J. F., Perloski, M., Biagi, T., Baranowska, I., Long, S., March, P. A., Olby, N. J., Shelton, G. D., Khan, S., O'Brien, D. P., Lindblad-Toh, K. & Coates, J. R. (2009). Genome-wide association analysis reveals a SOD1 mutation in canine degenerative myelopathy that resembles amyotrophic lateral sclerosis. *Proc Natl Acad Sci U S A* **106**, 2794-9.
20. Wang, J., Xu, G. & Borchelt, D. R. (2006). Mapping superoxide dismutase 1 domains of non-native interaction: roles of intra- and intermolecular disulfide bonding in aggregation. *J Neurochem* **96**, 1277-88.
21. McCord, J. M. & Fridovich, I. (1969). Superoxide dismutase. An enzymic function for erythrocuprein (hemocuprein). *J Biol Chem* **244**, 6049-55.
22. Bordo, D., Djinovic, K. & Bolognesi, M. (1994). Conserved patterns in the Cu,Zn superoxide dismutase family. *J Mol Biol* **238**, 366-86.
23. Bruijn, L. I., Houseweart, M. K., Kato, S., Anderson, K. L., Anderson, S. D., Ohama, E., Reaume, A. G., Scott, R. W. & Cleveland, D. W. (1998). Aggregation

and motor neuron toxicity of an ALS-linked SOD1 mutant independent from wild-type SOD1. *Science* **281**, 1851-4.

24. Li, Y., Huang, T. T., Carlson, E. J., Melov, S., Ursell, P. C., Olson, J. L., Noble, L. J., Yoshimura, M. P., Berger, C., Chan, P. H., Wallace, D. C. & Epstein, C. J. (1995). Dilated cardiomyopathy and neonatal lethality in mutant mice lacking manganese superoxide dismutase. *Nat Genet* **11**, 376-81.
25. Shefner, J. M., Reaume, A. G., Flood, D. G., Scott, R. W., Kowall, N. W., Ferrante, R. J., Siwek, D. F., Upton-Rice, M. & Brown, R. H., Jr. (1999). Mice lacking cytosolic copper/zinc superoxide dismutase display a distinctive motor axonopathy. *Neurology* **53**, 1239-46.
26. Ho, Y. S., Gargano, M., Cao, J., Bronson, R. T., Heimler, I. & Hutz, R. J. (1998). Reduced fertility in female mice lacking copper-zinc superoxide dismutase. *J Biol Chem* **273**, 7765-9.
27. Kurobe, N., Suzuki, F., Okajima, K. & Kato, K. (1990). Sensitive enzyme immunoassay for human Cu/Zn superoxide dismutase. *Clin Chim Acta* **187**, 11-20.
28. Lindenau, J., Noack, H., Possel, H., Asayama, K. & Wolf, G. (2000). Cellular distribution of superoxide dismutases in the rat CNS. *Glia* **29**, 25-34.
29. Sturtz, L. A., Diekert, K., Jensen, L. T., Lill, R. & Culotta, V. C. (2001). A fraction of yeast Cu,Zn-superoxide dismutase and its metallochaperone, CCS, localize to the intermembrane space of mitochondria. A physiological role for SOD1 in guarding against mitochondrial oxidative damage. *J Biol Chem* **276**, 38084-9.
30. Field, L. S., Furukawa, Y., O'Halloran, T. V. & Culotta, V. C. (2003). Factors controlling the uptake of yeast copper/zinc superoxide dismutase into mitochondria. *J Biol Chem* **278**, 28052-9.
31. Chang, L. Y., Slot, J. W., Geuze, H. J. & Crapo, J. D. (1988). Molecular immunocytochemistry of the CuZn superoxide dismutase in rat hepatocytes. *J Cell Biol* **107**, 2169-79.
32. Rodriguez, J. A., Valentine, J. S., Eggers, D. K., Roe, J. A., Tiwari, A., Brown, R. H., Jr. & Hayward, L. J. (2002). Familial amyotrophic lateral sclerosis-associated mutations decrease the thermal stability of distinctly metallated species of human copper/zinc superoxide dismutase. *J Biol Chem* **277**, 15932-7.
33. Roe, J. A., Butler, A., Scholler, D. M., Valentine, J. S., Marky, L. & Breslauer, K. J. (1988). Differential scanning calorimetry of Cu,Zn-superoxide dismutase, the apoprotein, and its zinc-substituted derivatives. *Biochemistry* **27**, 950-8.
34. Lyons, T. J., Gralla, E. B. & Valentine, J. S. (1999). Biological chemistry of copper-zinc superoxide dismutase and its link to amyotrophic lateral sclerosis. *Met Ions Biol Syst* **36**, 125-77.
35. Banci, L., Bertini, I., Cramaro, F., Del Conte, R. & Viezzoli, M. S. (2003). Solution structure of Apo Cu,Zn superoxide dismutase: role of metal ions in protein folding. *Biochemistry* **42**, 9543-53.
36. Strange, R. W., Antonyuk, S., Hough, M. A., Doucette, P. A., Rodriguez, J. A., Hart, P. J., Hayward, L. J., Valentine, J. S. & Hasnain, S. S. (2003). The structure

of holo and metal-deficient wild-type human Cu, Zn superoxide dismutase and its relevance to familial amyotrophic lateral sclerosis. *J Mol Biol* **328**, 877-91.

37. Bruns, C. K. & Kopito, R. R. (2007). Impaired post-translational folding of familial ALS-linked Cu, Zn superoxide dismutase mutants. *Embo J* **26**, 855-66.
38. Doucette, P. A., Whitson, L. J., Cao, X., Schirf, V., Demeler, B., Valentine, J. S., Hansen, J. C. & Hart, P. J. (2004). Dissociation of human copper-zinc superoxide dismutase dimers using chaotrope and reductant. Insights into the molecular basis for dimer stability. *J Biol Chem* **279**, 54558-66.
39. Kawamata, H. & Manfredi, G. Import, maturation, and function of SOD1 and its copper chaperone CCS in the mitochondrial intermembrane space. *Antioxid Redox Signal*.
40. Arnesano, F., Banci, L., Bertini, I., Martinelli, M., Furukawa, Y. & O'Halloran, T. V. (2004). The unusually stable quaternary structure of human Cu,Zn-superoxide dismutase 1 is controlled by both metal occupancy and disulfide status. *J Biol Chem* **279**, 47998-8003.
41. Lamb, A. L., Torres, A. S., O'Halloran, T. V. & Rosenzweig, A. C. (2001). Heterodimeric structure of superoxide dismutase in complex with its metallochaperone. *Nat Struct Biol* **8**, 751-5.
42. Furukawa, Y., Torres, A. S. & O'Halloran, T. V. (2004). Oxygen-induced maturation of SOD1: a key role for disulfide formation by the copper chaperone CCS. *Embo J* **23**, 2872-81.
43. Furukawa, Y. & O'Halloran, T. V. (2005). Amyotrophic lateral sclerosis mutations have the greatest destabilizing effect on the apo- and reduced form of SOD1, leading to unfolding and oxidative aggregation. *J Biol Chem* **280**, 17266-74.
44. Kayatekin, C., Zitzewitz, J. A. & Matthews, C. R. (2010). Disulfide-reduced ALS variants of Cu, Zn superoxide dismutase exhibit increased populations of unfolded species. *J Mol Biol* **398**, 320-31.
45. Leitch, J. M., Jensen, L. T., Bouldin, S. D., Outten, C. E., Hart, P. J. & Culotta, V. C. (2009). Activation of Cu,Zn-superoxide dismutase in the absence of oxygen and the copper chaperone CCS. *J Biol Chem* **284**, 21863-71.
46. Carroll, M. C., Girouard, J. B., Ulloa, J. L., Subramaniam, J. R., Wong, P. C., Valentine, J. S. & Culotta, V. C. (2004). Mechanisms for activating Cu- and Zn-containing superoxide dismutase in the absence of the CCS Cu chaperone. *Proc Natl Acad Sci U S A* **101**, 5964-9.
47. Tiwari, A., Xu, Z. & Hayward, L. J. (2005). Aberrantly increased hydrophobicity shared by mutants of Cu,Zn-superoxide dismutase in familial amyotrophic lateral sclerosis. *J Biol Chem* **280**, 29771-9.
48. Kayatekin, C., Zitzewitz, J. A. & Matthews, C. R. (2008). Zinc binding modulates the entire folding free energy surface of human Cu,Zn superoxide dismutase. *J Mol Biol* **384**, 540-55.
49. Banci, L., Bertini, I., Cantini, F., D'Onofrio, M. & Viezzoli, M. S. (2002). Structure and dynamics of copper-free SOD: The protein before binding copper. *Protein Sci* **11**, 2479-2492.

50. Roberts, B. R., Tainer, J. A., Getzoff, E. D., Malencik, D. A., Anderson, S. R., Bomben, V. C., Meyers, K. R., Karplus, P. A. & Beckman, J. S. (2007). Structural characterization of zinc-deficient human superoxide dismutase and implications for ALS. *J Mol Biol* **373**, 877-90.
51. Banci, L., Benedetto, M., Bertini, I., Del Conte, R., Piccioli, M. & Viezzoli, M. S. (1998). Solution structure of reduced monomeric Q133M2 copper, zinc superoxide dismutase (SOD). Why is SOD a dimeric enzyme? *Biochemistry* **37**, 11780-91.
52. Leitch, J. M., Yick, P. J. & Culotta, V. C. (2009). The right to choose: multiple pathways for activating copper,zinc superoxide dismutase. *J Biol Chem* **284**, 24679-83.
53. Jensen, L. T. & Culotta, V. C. (2005). Activation of CuZn superoxide dismutases from Caenorhabditis elegans does not require the copper chaperone CCS. *J Biol Chem* **280**, 41373-9.
54. Rae, T. D., Torres, A. S., Pufahl, R. A. & O'Halloran, T. V. (2001). Mechanism of Cu,Zn-superoxide dismutase activation by the human metallochaperone hCCS. *J Biol Chem* **276**, 5166-76.
55. Brown, N. M., Torres, A. S., Doan, P. E. & O'Halloran, T. V. (2004). Oxygen and the copper chaperone CCS regulate posttranslational activation of Cu,Zn superoxide dismutase. *Proc Natl Acad Sci U S A* **101**, 5518-23.
56. Stathopulos, P. B., Rumfeldt, J. A., Karbassi, F., Siddall, C. A., Lepock, J. R. & Meiering, E. M. (2006). Calorimetric analysis of thermodynamic stability and aggregation for apo and holo amyotrophic lateral sclerosis-associated Gly-93 mutants of superoxide dismutase. *J Biol Chem* **281**, 6184-93.
57. Lynch, S. M. & Colon, W. (2006). Dominant role of copper in the kinetic stability of Cu/Zn superoxide dismutase. *Biochem Biophys Res Commun* **340**, 457-61.
58. Cleveland, D. W., Bruijn, L. I., Wong, P. C., Marszalek, J. R., Vechio, J. D., Lee, M. K., Xu, X. S., Borchelt, D. R., Sisodia, S. S. & Price, D. L. (1996). Mechanisms of selective motor neuron death in transgenic mouse models of motor neuron disease. *Neurology* **47**, S54-61; discussion S61-2.
59. Gurney, M. E., Pu, H., Chiu, A. Y., Dal Canto, M. C., Polchow, C. Y., Alexander, D. D., Caliendo, J., Hentati, A., Kwon, Y. W., Deng, H. X. & et al. (1994). Motor neuron degeneration in mice that express a human Cu,Zn superoxide dismutase mutation. *Science* **264**, 1772-5.
60. Nagai, M., Aoki, M., Miyoshi, I., Kato, M., Pasinelli, P., Kasai, N., Brown, R. H., Jr. & Itoyama, Y. (2001). Rats expressing human cytosolic copper-zinc superoxide dismutase transgenes with amyotrophic lateral sclerosis: associated mutations develop motor neuron disease. *J Neurosci* **21**, 9246-54.
61. Howland, D. S., Liu, J., She, Y., Goad, B., Maragakis, N. J., Kim, B., Erickson, J., Kulik, J., DeVito, L., Psaltis, G., DeGennaro, L. J., Cleveland, D. W. & Rothstein, J. D. (2002). Focal loss of the glutamate transporter EAAT2 in a transgenic rat model of SOD1 mutant-mediated amyotrophic lateral sclerosis (ALS). *Proc Natl Acad Sci U S A* **99**, 1604-9.

62. Deng, H. X., Shi, Y., Furukawa, Y., Zhai, H., Fu, R., Liu, E., Gorrie, G. H., Khan, M. S., Hung, W. Y., Bigio, E. H., Lukas, T., Dal Canto, M. C., O'Halloran, T. V. & Siddique, T. (2006). Conversion to the amyotrophic lateral sclerosis phenotype is associated with intermolecular linked insoluble aggregates of SOD1 in mitochondria. *Proc Natl Acad Sci U S A* **103**, 7142-7.
63. Reaume, A. G., Elliott, J. L., Hoffman, E. K., Kowall, N. W., Ferrante, R. J., Siwek, D. F., Wilcox, H. M., Flood, D. G., Beal, M. F., Brown, R. H., Jr., Scott, R. W. & Snider, W. D. (1996). Motor neurons in Cu/Zn superoxide dismutase-deficient mice develop normally but exhibit enhanced cell death after axonal injury. *Nat Genet* **13**, 43-7.
64. Wang, J., Xu, G., Gonzales, V., Coonfield, M., Fromholt, D., Copeland, N. G., Jenkins, N. A. & Borchelt, D. R. (2002). Fibrillar inclusions and motor neuron degeneration in transgenic mice expressing superoxide dismutase 1 with a disrupted copper-binding site. *Neurobiol Dis* **10**, 128-38.
65. Wang, J., Slunt, H., Gonzales, V., Fromholt, D., Coonfield, M., Copeland, N. G., Jenkins, N. A. & Borchelt, D. R. (2003). Copper-binding-site-null SOD1 causes ALS in transgenic mice: aggregates of non-native SOD1 delineate a common feature. *Hum Mol Genet* **12**, 2753-64.
66. Subramaniam, J. R., Lyons, W. E., Liu, J., Bartnikas, T. B., Rothstein, J., Price, D. L., Cleveland, D. W., Gitlin, J. D. & Wong, P. C. (2002). Mutant SOD1 causes motor neuron disease independent of copper chaperone-mediated copper loading. *Nat Neurosci* **5**, 301-7.
67. Son, M., Fu, Q., Puttaparthi, K., Matthews, C. M. & Elliott, J. L. (2009). Redox susceptibility of SOD1 mutants is associated with the differential response to CCS over-expression in vivo. *Neurobiol Dis* **34**, 155-62.
68. Julien, J. P. & Kriz, J. (2006). Transgenic mouse models of amyotrophic lateral sclerosis. *Biochim Biophys Acta* **1762**, 1013-24.
69. Jonsson, P. A., Graffmo, K. S., Andersen, P. M., Brannstrom, T., Lindberg, M., Oliveberg, M. & Marklund, S. L. (2006). Disulphide-reduced superoxide dismutase-1 in CNS of transgenic amyotrophic lateral sclerosis models. *Brain* **129**, 451-64.
70. Zetterstrom, P., Stewart, H. G., Bergemalm, D., Jonsson, P. A., Graffmo, K. S., Andersen, P. M., Brannstrom, T., Oliveberg, M. & Marklund, S. L. (2007). Soluble misfolded subfractions of mutant superoxide dismutase-1s are enriched in spinal cords throughout life in murine ALS models. *Proc Natl Acad Sci U S A* **104**, 14157-62.
71. Ilieva, H., Polymenidou, M. & Cleveland, D. W. (2009). Non-cell autonomous toxicity in neurodegenerative disorders: ALS and beyond. *J Cell Biol* **187**, 761-72.
72. Durham, H. D., Roy, J., Dong, L. & Figlewicz, D. A. (1997). Aggregation of mutant Cu/Zn superoxide dismutase proteins in a culture model of ALS. *J Neuropathol Exp Neurol* **56**, 523-30.

73. Pramatarova, A., Laganiere, J., Roussel, J., Brisebois, K. & Rouleau, G. A. (2001). Neuron-specific expression of mutant superoxide dismutase 1 in transgenic mice does not lead to motor impairment. *J Neurosci* **21**, 3369-74.
74. Lino, M. M., Schneider, C. & Caroni, P. (2002). Accumulation of SOD1 mutants in postnatal motoneurons does not cause motoneuron pathology or motoneuron disease. *J Neurosci* **22**, 4825-32.
75. Jaarsma, D., Teuling, E., Haasdijk, E. D., De Zeeuw, C. I. & Hoogenraad, C. C. (2008). Neuron-specific expression of mutant superoxide dismutase is sufficient to induce amyotrophic lateral sclerosis in transgenic mice. *J Neurosci* **28**, 2075-88.
76. Boillee, S., Yamanaka, K., Lobsiger, C. S., Copeland, N. G., Jenkins, N. A., Kassiotis, G., Kollias, G. & Cleveland, D. W. (2006). Onset and progression in inherited ALS determined by motor neurons and microglia. *Science* **312**, 1389-92.
77. Wang, L., Sharma, K., Grisotti, G. & Roos, R. P. (2009). The effect of mutant SOD1 dismutase activity on non-cell autonomous degeneration in familial amyotrophic lateral sclerosis. *Neurobiol Dis* **35**, 234-40.
78. Liochev, S. I. & Fridovich, I. (2000). Copper- and zinc-containing superoxide dismutase can act as a superoxide reductase and a superoxide oxidase. *J Biol Chem* **275**, 38482-5.
79. Estevez, A. G., Crow, J. P., Sampson, J. B., Reiter, C., Zhuang, Y., Richardson, G. J., Tarpey, M. M., Barbeito, L. & Beckman, J. S. (1999). Induction of nitric oxide-dependent apoptosis in motor neurons by zinc-deficient superoxide dismutase. *Science* **286**, 2498-500.
80. Wiedau-Pazos, M., Goto, J. J., Rabizadeh, S., Gralla, E. B., Roe, J. A., Lee, M. K., Valentine, J. S. & Bredesen, D. E. (1996). Altered reactivity of superoxide dismutase in familial amyotrophic lateral sclerosis. *Science* **271**, 515-8.
81. Beal, M. F., Ferrante, R. J., Browne, S. E., Matthews, R. T., Kowall, N. W. & Brown, R. H., Jr. (1997). Increased 3-nitrotyrosine in both sporadic and familial amyotrophic lateral sclerosis. *Ann Neurol* **42**, 644-54.
82. Bruijn, L. I., Beal, M. F., Becher, M. W., Schulz, J. B., Wong, P. C., Price, D. L. & Cleveland, D. W. (1997). Elevated free nitrotyrosine levels, but not protein-bound nitrotyrosine or hydroxyl radicals, throughout amyotrophic lateral sclerosis (ALS)-like disease implicate tyrosine nitration as an aberrant in vivo property of one familial ALS-linked superoxide dismutase 1 mutant. *Proc Natl Acad Sci U S A* **94**, 7606-11.
83. Hayward, L. J., Rodriguez, J. A., Kim, J. W., Tiwari, A., Goto, J. J., Cabelli, D. E., Valentine, J. S. & Brown, R. H., Jr. (2002). Decreased metallation and activity in subsets of mutant superoxide dismutases associated with familial amyotrophic lateral sclerosis. *J Biol Chem* **277**, 15923-31.
84. Watanabe, S., Nagano, S., Duce, J., Kiaei, M., Li, Q. X., Tucker, S. M., Tiwari, A., Brown, R. H., Jr., Beal, M. F., Hayward, L. J., Culotta, V. C., Yoshihara, S., Sakoda, S. & Bush, A. I. (2007). Increased affinity for copper mediated by cysteine 111 in forms of mutant superoxide dismutase 1 linked to amyotrophic lateral sclerosis. *Free Radic Biol Med* **42**, 1534-42.

85. Matsumoto, G., Stojanovic, A., Holmberg, C. I., Kim, S. & Morimoto, R. I. (2005). Structural properties and neuronal toxicity of amyotrophic lateral sclerosis-associated Cu/Zn superoxide dismutase 1 aggregates. *J Cell Biol* **171**, 75-85.
86. Johnston, J. A., Dalton, M. J., Gurney, M. E. & Kopito, R. R. (2000). Formation of high molecular weight complexes of mutant Cu, Zn-superoxide dismutase in a mouse model for familial amyotrophic lateral sclerosis. *Proc Natl Acad Sci U S A* **97**, 12571-6.
87. Wang, J., Xu, G. & Borchelt, D. R. (2002). High molecular weight complexes of mutant superoxide dismutase 1: age-dependent and tissue-specific accumulation. *Neurobiol Dis* **9**, 139-48.
88. Lashuel, H. A., Wurth, C., Woo, L. & Kelly, J. W. (1999). The most pathogenic transthyretin variant, L55P, forms amyloid fibrils under acidic conditions and protofilaments under physiological conditions. *Biochemistry* **38**, 13560-73.
89. Cappai, R., Leck, S. L., Tew, D. J., Williamson, N. A., Smith, D. P., Galatis, D., Sharples, R. A., Curtain, C. C., Ali, F. E., Cherny, R. A., Culvenor, J. G., Bottomley, S. P., Masters, C. L., Barnham, K. J. & Hill, A. F. (2005). Dopamine promotes alpha-synuclein aggregation into SDS-resistant soluble oligomers via a distinct folding pathway. *Faseb J* **19**, 1377-9.
90. Bucciantini, M., Giannoni, E., Chiti, F., Baroni, F., Formigli, L., Zurdo, J., Taddei, N., Ramponi, G., Dobson, C. M. & Stefani, M. (2002). Inherent toxicity of aggregates implies a common mechanism for protein misfolding diseases. *Nature* **416**, 507-11.
91. Sirangelo, I., Malmo, C., Iannuzzi, C., Mezzogiorno, A., Bianco, M. R., Papa, M. & Irace, G. (2004). Fibrillogenesis and cytotoxic activity of the amyloid-forming apomyoglobin mutant W7FW14F. *J Biol Chem* **279**, 13183-9.
92. Malisauskas, M., Ostman, J., Darinskas, A., Zamotin, V., Liutkevicius, E., Lundgren, E. & Morozova-Roche, L. A. (2005). Does the cytotoxic effect of transient amyloid oligomers from common equine lysozyme in vitro imply innate amyloid toxicity? *J Biol Chem* **280**, 6269-75.
93. Glabe, C. G. (2008). Structural classification of toxic amyloid oligomers. *J Biol Chem* **283**, 29639-43.
94. Banci, L., Bertini, I., D'Amelio, N., Gaggelli, E., Libralesso, E., Matecko, I., Turano, P. & Valentine, J. S. (2005). Fully metallated S134N Cu,Zn-superoxide dismutase displays abnormal mobility and intermolecular contacts in solution. *J Biol Chem* **280**, 35815-21.
95. Elam, J. S., Taylor, A. B., Strange, R., Antonyuk, S., Doucette, P. A., Rodriguez, J. A., Hasnain, S. S., Hayward, L. J., Valentine, J. S., Yeates, T. O. & Hart, P. J. (2003). Amyloid-like filaments and water-filled nanotubes formed by SOD1 mutant proteins linked to familial ALS. *Nat Struct Biol* **10**, 461-7.
96. Molnar, K. S., Karabacak, N. M., Johnson, J. L., Wang, Q., Tiwari, A., Hayward, L. J., Coales, S. J., Hamuro, Y. & Agar, J. N. (2009). A common property of amyotrophic lateral sclerosis-associated variants: destabilization of the copper/zinc superoxide dismutase electrostatic loop. *J Biol Chem* **284**, 30965-73.

97. Cardoso, R. M., Thayer, M. M., DiDonato, M., Lo, T. P., Bruns, C. K., Getzoff, E. D. & Tainer, J. A. (2002). Insights into Lou Gehrig's disease from the structure and instability of the A4V mutant of human Cu,Zn superoxide dismutase. *J Mol Biol* **324**, 247-56.
98. Hough, M. A., Grossmann, J. G., Antonyuk, S. V., Strange, R. W., Doucette, P. A., Rodriguez, J. A., Whitson, L. J., Hart, P. J., Hayward, L. J., Valentine, J. S. & Hasnain, S. S. (2004). Dimer destabilization in superoxide dismutase may result in disease-causing properties: structures of motor neuron disease mutants. *Proc Natl Acad Sci U S A* **101**, 5976-81.
99. Banci, L., Bertini, I., D'Amelio, N., Libralesso, E., Turano, P. & Valentine, J. S. (2007). Metalation of the Amyotrophic Lateral Sclerosis Mutant Glycine 37 to Arginine Superoxide Dismutase (SOD1) Apoprotein Restores Its Structural and Dynamical Properties in Solution to Those of Metalated Wild-Type SOD1. *Biochemistry* **46**, 9953-9962.
100. Shipp, E. L., Cantini, F., Bertini, I., Valentine, J. S. & Banci, L. (2003). Dynamic properties of the G93A mutant of copper-zinc superoxide dismutase as detected by NMR spectroscopy: implications for the pathology of familial amyotrophic lateral sclerosis. *Biochemistry* **42**, 1890-9.
101. Banci, L., Bertini, I., Durazo, A., Girotto, S., Gralla, E. B., Martinelli, M., Valentine, J. S., Vieru, M. & Whitelegge, J. P. (2007). Metal-free superoxide dismutase forms soluble oligomers under physiological conditions: a possible general mechanism for familial ALS. *Proc Natl Acad Sci U S A* **104**, 11263-7.
102. Banci, L., Bertini, I., Boca, M., Girotto, S., Martinelli, M., Valentine, J. S. & Vieru, M. (2008). SOD1 and amyotrophic lateral sclerosis: mutations and oligomerization. *PLoS ONE* **3**, e1677.
103. Karch, C. M. & Borchelt, D. R. (2008). A limited role for disulfide cross-linking in the aggregation of mutant SOD1 linked to familial amyotrophic lateral sclerosis. *J Biol Chem* **283**, 13528-37.
104. Rakhit, R., Crow, J. P., Lepock, J. R., Kondejewski, L. H., Cashman, N. R. & Chakrabartty, A. (2004). Monomeric Cu,Zn-superoxide dismutase is a common misfolding intermediate in the oxidation models of sporadic and familial amyotrophic lateral sclerosis. *J Biol Chem* **279**, 15499-504.
105. Rakhit, R., Robertson, J., Vande Velde, C., Horne, P., Ruth, D. M., Griffin, J., Cleveland, D. W., Cashman, N. R. & Chakrabartty, A. (2007). An immunological epitope selective for pathological monomer-misfolded SOD1 in ALS. *Nat Med* **13**, 754-9.
106. Di Noto, L., Whitson, L. J., Cao, X., Hart, P. J. & Levine, R. L. (2005). Proteasomal degradation of mutant superoxide dismutases linked to amyotrophic lateral sclerosis. *J Biol Chem* **280**, 39907-13.
107. Puttaparthi, K., Wojcik, C., Rajendran, B., DeMartino, G. N. & Elliott, J. L. (2003). Aggregate formation in the spinal cord of mutant SOD1 transgenic mice is reversible and mediated by proteasomes. *J Neurochem* **87**, 851-60.
108. Jonsson, P. A., Ernhill, K., Andersen, P. M., Bergemalm, D., Brannstrom, T., Gredal, O., Nilsson, P. & Marklund, S. L. (2004). Minute quantities of misfolded

mutant superoxide dismutase-1 cause amyotrophic lateral sclerosis. *Brain* **127**, 73-88.

109. Prakash, S., Tian, L., Ratliff, K. S., Lehotzky, R. E. & Matouschek, A. (2004). An unstructured initiation site is required for efficient proteasome-mediated degradation. *Nat Struct Mol Biol* **11**, 830-7.
110. Khare, S. D., Caplow, M. & Dokholyan, N. V. (2004). The rate and equilibrium constants for a multistep reaction sequence for the aggregation of superoxide dismutase in amyotrophic lateral sclerosis. *Proc Natl Acad Sci U S A* **101**, 15094-9.
111. Mulligan, V. K., Kerman, A., Ho, S. & Chakrabartty, A. (2008). Denaturational Stress Induces Formation of Zinc-Deficient Monomers of Cu,Zn Superoxide Dismutase: Implications for Pathogenesis in Amyotrophic Lateral Sclerosis. *J Mol Biol*.
112. Rumfeldt, J. A., Lepock, J. R. & Meiering, E. M. (2009). Unfolding and folding kinetics of amyotrophic lateral sclerosis-associated mutant Cu,Zn superoxide dismutases. *J Mol Biol* **385**, 278-98.
113. Lindberg, M. J., Normark, J., Holmgren, A. & Oliveberg, M. (2004). Folding of human superoxide dismutase: disulfide reduction prevents dimerization and produces marginally stable monomers. *Proc Natl Acad Sci U S A* **101**, 15893-8.
114. Svensson, A. K., Bilsel, O., Kondrashkina, E., Zitzewitz, J. A. & Matthews, C. R. (2006). Mapping the folding free energy surface for metal-free human Cu,Zn superoxide dismutase. *J Mol Biol* **364**, 1084-102.
115. Vassall, K. A., Stathopulos, P. B., Rumfeldt, J. A., Lepock, J. R. & Meiering, E. M. (2006). Equilibrium thermodynamic analysis of amyotrophic lateral sclerosis-associated mutant apo Cu,Zn superoxide dismutases. *Biochemistry* **45**, 7366-79.
116. Rumfeldt, J. A., Stathopulos, P. B., Chakrabarrty, A., Lepock, J. R. & Meiering, E. M. (2006). Mechanism and thermodynamics of guanidinium chloride-induced denaturation of ALS-associated mutant Cu,Zn superoxide dismutases. *J Mol Biol* **355**, 106-23.
117. Svensson, A. K., Bilsel, O., Kayatekin, C., Adefusika, J. A., Zitzewitz, J. A. & Matthews, C. R. (2010). Metal-free ALS-Variants of Dimeric Human Cu,Zn-Superoxide Dismutase Have Enhanced Populations of Monomeric Species. *PloS One*.
118. Parge, H. E., Hallewell, R. A. & Tainer, J. A. (1992). Atomic structures of wild-type and thermostable mutant recombinant human Cu,Zn superoxide dismutase. *Proc Natl Acad Sci U S A* **89**, 6109-13.
119. Lindberg, M. J., Bystrom, R., Boknas, N., Andersen, P. M. & Oliveberg, M. (2005). Systematically perturbed folding patterns of amyotrophic lateral sclerosis (ALS)-associated SOD1 mutants. *Proc Natl Acad Sci U S A* **102**, 9754-9.
120. Lindberg, M. J., Tibell, L. & Oliveberg, M. (2002). Common denominator of Cu/Zn superoxide dismutase mutants associated with amyotrophic lateral sclerosis: decreased stability of the apo state. *Proc Natl Acad Sci U S A* **99**, 16607-12.

121. Rodriguez, J. A., Shaw, B. F., Durazo, A., Sohn, S. H., Doucette, P. A., Nersissian, A. M., Faull, K. F., Eggers, D. K., Tiwari, A., Hayward, L. J. & Valentine, J. S. (2005). Destabilization of apoprotein is insufficient to explain Cu,Zn-superoxide dismutase-linked ALS pathogenesis. *Proc Natl Acad Sci U S A* **102**, 10516-21.
122. Felbecker, A., Camu, W., Valdmanis, P. N., Sperfeld, A. D., Waibel, S., Steinbach, P., Rouleau, G. A., Ludolph, A. C. & Andersen, P. M. Four familial ALS pedigrees discordant for two SOD1 mutations: are all SOD1 mutations pathogenic? *J Neurol Neurosurg Psychiatry* **81**, 572-7.
123. Richardson, J. S. & Richardson, D. C. (2002). Natural beta-sheet proteins use negative design to avoid edge-to-edge aggregation. *Proc Natl Acad Sci U S A* **99**, 2754-9.
124. Nordlund, A. & Oliveberg, M. (2006). Folding of Cu/Zn superoxide dismutase suggests structural hotspots for gain of neurotoxic function in ALS: parallels to precursors in amyloid disease. *Proc Natl Acad Sci U S A* **103**, 10218-23.
125. Shaw, B. F. & Valentine, J. S. (2007). How do ALS-associated mutations in superoxide dismutase 1 promote aggregation of the protein? *Trends Biochem Sci* **32**, 78-85.
126. Furukawa, Y. & O'Halloran, T. V. (2006). Posttranslational modifications in Cu,Zn-superoxide dismutase and mutations associated with amyotrophic lateral sclerosis. *Antioxid Redox Signal* **8**, 847-67.
127. Crow, J. P., Sampson, J. B., Zhuang, Y., Thompson, J. A. & Beckman, J. S. (1997). Decreased zinc affinity of amyotrophic lateral sclerosis-associated superoxide dismutase mutants leads to enhanced catalysis of tyrosine nitration by peroxynitrite. *J Neurochem* **69**, 1936-44.
128. Rowland, L. P. & Shneider, N. A. (2001). Amyotrophic lateral sclerosis. *N Engl J Med* **344**, 1688-700.
129. Andersen, P. M., Sims, K. B., Xin, W. W., Kiely, R., O'Neill, G., Ravits, J., Pioro, E., Harati, Y., Brower, R. D., Levine, J. S., Heinicke, H. U., Seltzer, W., Boss, M. & Brown, R. H., Jr. (2003). Sixteen novel mutations in the Cu/Zn superoxide dismutase gene in amyotrophic lateral sclerosis: a decade of discoveries, defects and disputes. *Amyotroph Lateral Scler Other Motor Neuron Disord* **4**, 62-73.
130. Strange, R. W., Antonyuk, S. V., Hough, M. A., Doucette, P. A., Valentine, J. S. & Hasnain, S. S. (2006). Variable metallation of human superoxide dismutase: atomic resolution crystal structures of Cu-Zn, Zn-Zn and as-isolated wild-type enzymes. *J Mol Biol* **356**, 1152-62.
131. Potter, S. Z., Zhu, H., Shaw, B. F., Rodriguez, J. A., Doucette, P. A., Sohn, S. H., Durazo, A., Faull, K. F., Gralla, E. B., Nersissian, A. M. & Valentine, J. S. (2007). Binding of a single zinc ion to one subunit of copper-zinc superoxide dismutase apoprotein substantially influences the structure and stability of the entire homodimeric protein. *J Am Chem Soc* **129**, 4575-83.
132. Valentine, J. S. & Hart, P. J. (2003). Misfolded CuZnSOD and amyotrophic lateral sclerosis. *Proc Natl Acad Sci U S A* **100**, 3617-22.

133. Cleveland, D. W. & Rothstein, J. D. (2001). From Charcot to Lou Gehrig: deciphering selective motor neuron death in ALS. *Nat Rev Neurosci* **2**, 806-19.
134. Wood, J. D., Beaujeux, T. P. & Shaw, P. J. (2003). Protein aggregation in motor neurone disorders. *Neuropathol Appl Neurobiol* **29**, 529-45.
135. Caughey, B. & Lansbury, P. T. (2003). Protofibrils, pores, fibrils, and neurodegeneration: separating the responsible protein aggregates from the innocent bystanders. *Annu Rev Neurosci* **26**, 267-98.
136. Stefani, M. & Dobson, C. M. (2003). Protein aggregation and aggregate toxicity: new insights into protein folding, misfolding diseases and biological evolution. *J Mol Med* **81**, 678-99.
137. Valentine, J. S., Doucette, P. A. & Zittin Potter, S. (2005). Copper-zinc superoxide dismutase and amyotrophic lateral sclerosis. *Annu Rev Biochem* **74**, 563-93.
138. Ross, C. A. & Poirier, M. A. (2004). Protein aggregation and neurodegenerative disease. *Nat Med* **10 Suppl**, S10-7.
139. Hart, P. J. (2006). Pathogenic superoxide dismutase structure, folding, aggregation and turnover. *Curr Opin Chem Biol* **10**, 131-8.
140. Cao, X., Antonyuk, S., Seetharaman, S. V., Whitson, L. J., Taylor, A. B., Holloway, S. P., Strange, R. W., Doucette, P. A., Valentine, J. S., Tiwari, A., Hayward, L. J., Padua, S., Cohlberg, J. A., Hasnain, S. S. & Hart, P. J. (2008). Structures of the G85R variant of SOD1 in Familial ALS. *J Biol Chem*.
141. Hornberg, A., Logan, D. T., Marklund, S. L. & Oliveberg, M. (2007). The coupling between disulphide status, metallation and dimer interface strength in Cu/Zn superoxide dismutase. *J Mol Biol* **365**, 333-42.
142. Hallewell, R. A., Imlay, K. C., Lee, P., Fong, N. M., Gallegos, C., Getzoff, E. D., Tainer, J. A., Cabelli, D. E., Tekamp-Olson, P., Mullenbach, G. T. & et al. (1991). Thermostabilization of recombinant human and bovine CuZn superoxide dismutases by replacement of free cysteines. *Biochem Biophys Res Commun* **181**, 474-80.
143. Bertini, I., Piccioli, M., Viezzoli, M. S., Chiu, C. Y. & Mullenbach, G. T. (1994). A spectroscopic characterization of a monomeric analog of copper, zinc superoxide dismutase. *Eur Biophys J* **23**, 167-76.
144. Lyons, T. J., Nersissian, A., Huang, H., Yeom, H., Nishida, C. R., Graden, J. A., Gralla, E. B. & Valentine, J. S. (2000). The metal binding properties of the zinc site of yeast copper-zinc superoxide dismutase: implications for amyotrophic lateral sclerosis. *J Biol Inorg Chem* **5**, 189-203.
145. Pozdnyakova, I., Guidry, J. & Wittung-Stafshede, P. (2001). Probing copper ligands in denatured Pseudomonas aeruginosa azurin: unfolding His117Gly and His46Gly mutants. *J Biol Inorg Chem* **6**, 182-8.
146. Wittung-Stafshede, P. (2002). Role of cofactors in protein folding. *Acc Chem Res* **35**, 201-8.
147. Myers, J. K., Pace, C. N. & Scholtz, J. M. (1995). Denaturant m values and heat capacity changes: relation to changes in accessible surface areas of protein unfolding. *Protein Sci* **4**, 2138-48.

148. Matthews, C. R. (1987). Effect of point mutations on the folding of globular proteins. *Methods Enzymol* **154**, 498-511.
149. Pace, C. N., Shirley, B. A. & Thompson, J. A. (1990). *Measuring the conformational stability of a protein*. Protein Structure, a Practical Approach., IRL Press, Oxford University press.
150. Bodenreider, C. & Kiefhaber, T. (2005). Interpretation of protein folding psi values. *J Mol Biol* **351**, 393-401.
151. Choi, D. W. & Koh, J. Y. (1998). Zinc and brain injury. *Annu Rev Neurosci* **21**, 347-75.
152. Khare, S. D. & Dokholyan, N. V. (2006). Common dynamical signatures of familial amyotrophic lateral sclerosis-associated structurally diverse Cu, Zn superoxide dismutase mutants. *Proc Natl Acad Sci U S A* **103**, 3147-52.
153. Jahn, T. R. & Radford, S. E. (2008). Folding versus aggregation: polypeptide conformations on competing pathways. *Arch Biochem Biophys* **469**, 100-17.
154. Plaxco, K. W., Simons, K. T. & Baker, D. (1998). Contact order, transition state placement and the refolding rates of single domain proteins. *J Mol Biol* **277**, 985-94.
155. Romero, P., Obradovic, Z., Li, X., Garner, E. C., Brown, C. J. & Dunker, A. K. (2001). Sequence complexity of disordered protein. *Proteins* **42**, 38-48.
156. Khare, S. D., Caplow, M. & Dokholyan, N. V. (2006). FALS mutations in Cu, Zn superoxide dismutase destabilize the dimer and increase dimer dissociation propensity: a large-scale thermodynamic analysis. *Amyloid* **13**, 226-35.
157. Tiwari, A. & Hayward, L. J. (2003). Familial amyotrophic lateral sclerosis mutants of copper/zinc superoxide dismutase are susceptible to disulfide reduction. *J Biol Chem* **278**, 5984-92.
158. Zhang, Q., Powers, E. T., Nieva, J., Huff, M. E., Dendle, M. A., Bieschke, J., Glabe, C. G., Eschenmoser, A., Wentworth, P., Jr., Lerner, R. A. & Kelly, J. W. (2004). Metabolite-initiated protein misfolding may trigger Alzheimer's disease. *Proc Natl Acad Sci U S A* **101**, 4752-7.
159. Derham, B. K. & Harding, J. J. (1997). Effect of aging on the chaperone-like function of human alpha-crystallin assessed by three methods. *Biochem J* **328 (Pt 3)**, 763-8.
160. Thomson, J. A., Shirley, B. A., Grimsley, G. R. & Pace, C. N. (1989). Conformational stability and mechanism of folding of ribonuclease T1. *J Biol Chem* **264**, 11614-20.
161. Bilsel, O., Zitzewitz, J. A., Bowers, K. E. & Matthews, C. R. (1999). Folding mechanism of the alpha-subunit of tryptophan synthase, an alpha/beta barrel protein: global analysis highlights the interconversion of multiple native, intermediate, and unfolded forms through parallel channels. *Biochemistry* **38**, 1018-29.
162. Seetharaman, S. V., Prudencio, M., Karch, C., Holloway, S. P., Borchelt, D. R. & Hart, P. J. (2009). Immature Copper-zinc Superoxide Dismutase and Familial Amyotrophic Lateral Sclerosis. *Exp Biol Med (Maywood)*.

163. Teilum, K., Smith, M. H., Schulz, E., Christensen, L. C., Solomentsev, G., Oliveberg, M. & Akke, M. (2009). Transient structural distortion of metal-free Cu/Zn superoxide dismutase triggers aberrant oligomerization. *Proc Natl Acad Sci U S A* **106**, 18273-8.
164. Ionescu, R. M., Smith, V. F., O'Neill, J. C., Jr. & Matthews, C. R. (2000). Multistate equilibrium unfolding of Escherichia coli dihydrofolate reductase: thermodynamic and spectroscopic description of the native, intermediate, and unfolded ensembles. *Biochemistry* **39**, 9540-50.
165. Shaw, B. F., Durazo, A., Nersissian, A. M., Whitelegge, J. P., Faull, K. F. & Valentine, J. S. (2006). Local unfolding in a destabilized, pathogenic variant of superoxide dismutase 1 observed with H/D exchange and mass spectrometry. *J Biol Chem* **281**, 18167-76.
166. Hervias, I., Beal, M. F. & Manfredi, G. (2006). Mitochondrial dysfunction and amyotrophic lateral sclerosis. *Muscle Nerve* **33**, 598-608.
167. Hell, K. (2008). The Erv1-Mia40 disulfide relay system in the intermembrane space of mitochondria. *Biochim Biophys Acta* **1783**, 601-9.
168. Kawamata, H. & Manfredi, G. (2008). Different regulation of wild-type and mutant Cu,Zn superoxide dismutase localization in mammalian mitochondria. *Hum Mol Genet* **17**, 3303-17.
169. Liu, J., Lillo, C., Jonsson, P. A., Vande Velde, C., Ward, C. M., Miller, T. M., Subramaniam, J. R., Rothstein, J. D., Marklund, S., Andersen, P. M., Brannstrom, T., Gredal, O., Wong, P. C., Williams, D. S. & Cleveland, D. W. (2004). Toxicity of familial ALS-linked SOD1 mutants from selective recruitment to spinal mitochondria. *Neuron* **43**, 5-17.
170. Hershey, J. W. (1991). Translational control in mammalian cells. *Annu Rev Biochem* **60**, 717-55.
171. Borchelt, D. R., Lee, M. K., Slunt, H. S., Guarnieri, M., Xu, Z. S., Wong, P. C., Brown, R. H., Jr., Price, D. L., Sisodia, S. S. & Cleveland, D. W. (1994). Superoxide dismutase 1 with mutations linked to familial amyotrophic lateral sclerosis possesses significant activity. *Proc Natl Acad Sci U S A* **91**, 8292-6.
172. Gromiha, M. M. & Selvaraj, S. (2001). Comparison between long-range interactions and contact order in determining the folding rate of two-state proteins: application of long-range order to folding rate prediction. *J Mol Biol* **310**, 27-32.
173. Geierhaas, C. D., Paci, E., Vendruscolo, M. & Clarke, J. (2004). Comparison of the transition states for folding of two Ig-like proteins from different superfamilies. *J Mol Biol* **343**, 1111-23.
174. Lappalainen, I., Hurley, M. G. & Clarke, J. (2008). Plasticity within the obligatory folding nucleus of an immunoglobulin-like domain. *J Mol Biol* **375**, 547-59.
175. Thompson, P. A., Eaton, W. A. & Hofrichter, J. (1997). Laser temperature jump study of the helix<==>coil kinetics of an alanine peptide interpreted with a 'kinetic zipper' model. *Biochemistry* **36**, 9200-10.

176. Munoz, V., Henry, E. R., Hofrichter, J. & Eaton, W. A. (1998). A statistical mechanical model for beta-hairpin kinetics. *Proc Natl Acad Sci U S A* **95**, 5872-9.
177. Brorsson, A. C., Kjellson, A., Aronsson, G., Sethson, I., Hambraeus, C. & Jonsson, B. H. (2004). The "two-state folder" MerP forms partially unfolded structures that show temperature dependent hydrogen exchange. *J Mol Biol* **340**, 333-44.
178. Mohan, P. M., Chakraborty, S. & Hosur, R. V. (2009). NMR investigations on residue level unfolding thermodynamics in DLC8 dimer by temperature dependent native state hydrogen exchange. *J Biomol NMR* **44**, 1-11.
179. Makhatadze, G. I. & Privalov, P. L. (1995). Energetics of protein structure. *Adv Protein Chem* **47**, 307-425.
180. Chen, X. & Matthews, C. R. (1994). Thermodynamic properties of the transition state for the rate-limiting step in the folding of the alpha subunit of tryptophan synthase. *Biochemistry* **33**, 6356-62.
181. Makhatadze, G. I. & Privalov, P. L. (1992). Protein interactions with urea and guanidinium chloride. A calorimetric study. *J Mol Biol* **226**, 491-505.
182. Tanford, C. (1970). Protein denaturation. C. Theoretical models for the mechanism of denaturation. *Adv Protein Chem* **24**, 1-95.
183. Pace, C. N. (1986). Determination and analysis of urea and guanidine hydrochloride denaturation curves. *Methods Enzymol* **131**, 266-80.
184. Jacob, M. & Schmid, F. X. (1999). Protein folding as a diffusional process. *Biochemistry* **38**, 13773-9.
185. Chrunyk, B. A. & Matthews, C. R. (1990). Role of diffusion in the folding of the alpha subunit of tryptophan synthase from Escherichia coli. *Biochemistry* **29**, 2149-54.
186. Bhattacharyya, R. P. & Sosnick, T. R. (1999). Viscosity dependence of the folding kinetics of a dimeric and monomeric coiled coil. *Biochemistry* **38**, 2601-9.
187. Jacob, M., Schindler, T., Balbach, J. & Schmid, F. X. (1997). Diffusion control in an elementary protein folding reaction. *Proc Natl Acad Sci U S A* **94**, 5622-7.
188. Wu, Y., Kondrashkina, E., Kayatekin, C., Matthews, C. R. & Bilsel, O. (2008). Microsecond acquisition of heterogeneous structure in the folding of a TIM barrel protein. *Proc Natl Acad Sci U S A* **105**, 13367-72.
189. Shastry, M. C. & Roder, H. (1998). Evidence for barrier-limited protein folding kinetics on the microsecond time scale. *Nat Struct Biol* **5**, 385-92.
190. Dunbar, J., Yennawar, H. P., Banerjee, S., Luo, J. & Farber, G. K. (1997). The effect of denaturants on protein structure. *Protein Sci* **6**, 1727-33.
191. Ivankov, D. N., Garbuzynskiy, S. O., Alm, E., Plaxco, K. W., Baker, D. & Finkelstein, A. V. (2003). Contact order revisited: influence of protein size on the folding rate. *Protein Sci* **12**, 2057-62.
192. Istomin, A. Y., Jacobs, D. J. & Livesay, D. R. (2007). On the role of structural class of a protein with two-state folding kinetics in determining correlations between its size, topology, and folding rate. *Protein Sci* **16**, 2564-9.
193. Kheterpal, I. & Wetzel, R. (2006). Hydrogen/deuterium exchange mass spectrometry--a window into amyloid structure. *Acc Chem Res* **39**, 584-93.

194. Del Mar, C., Greenbaum, E. A., Mayne, L., Englander, S. W. & Woods, V. L., Jr. (2005). Structure and properties of alpha-synuclein and other amyloids determined at the amino acid level. *Proc Natl Acad Sci U S A* **102**, 15477-82.
195. Gu, Z., Rao, M. K., Forsyth, W. R., Finke, J. M. & Matthews, C. R. (2007). Structural analysis of kinetic folding intermediates for a TIM barrel protein, indole-3-glycerol phosphate synthase, by hydrogen exchange mass spectrometry and Go model simulation. *J Mol Biol* **374**, 528-46.
196. Hoshino, M., Katou, H., Hagihara, Y., Hasegawa, K., Naiki, H. & Goto, Y. (2002). Mapping the core of the beta(2)-microglobulin amyloid fibril by H/D exchange. *Nat Struct Biol* **9**, 332-6.
197. Svergun, D. I., Petoukhov, M. V. & Koch, M. H. (2001). Determination of domain structure of proteins from X-ray solution scattering. *Biophys J* **80**, 2946-53.
198. Kozin, M. B. & Svergun, D. I. (2001). Automated matching of high- and low-resolution structural models. *Journal of Applied Crystallography* **34**, 33-41.
199. Arai, M., Kataoka, M., Kuwajima, K., Matthews, C. R. & Iwakura, M. (2003). Effects of the difference in the unfolded-state ensemble on the folding of Escherichia coli dihydrofolate reductase. *J Mol Biol* **329**, 779-91.
200. Goldenberg, D. P. (2003). Computational simulation of the statistical properties of unfolded proteins. *J Mol Biol* **326**, 1615-33.
201. Ray, S. S., Nowak, R. J., Strokovich, K., Brown, R. H., Jr., Walz, T. & Lansbury, P. T., Jr. (2004). An intersubunit disulfide bond prevents in vitro aggregation of a superoxide dismutase-1 mutant linked to familial amytrophic lateral sclerosis. *Biochemistry* **43**, 4899-905.
202. Ray, S. S., Nowak, R. J., Brown, R. H., Jr. & Lansbury, P. T., Jr. (2005). Small-molecule-mediated stabilization of familial amyotrophic lateral sclerosis-linked superoxide dismutase mutants against unfolding and aggregation. *Proc Natl Acad Sci U S A* **102**, 3639-44.
203. Bartlett, A. I. & Radford, S. E. Desolvation and development of specific hydrophobic core packing during Im7 folding. *J Mol Biol* **396**, 1329-45.